The Chemical, Physical, and Microbial Origins of Pleistocene Cherts at Lake Magadi, Kenya Rift Valley

A thesis submitted to the
College of Graduate Studies and Research
in partial fulfilment of the requirements
for the Degree of Master of Science
in the Department of Geological Sciences
University of Saskatchewan
Saskatoon

by

BRITNI LAUREN BRENNA

PERMISSION TO USE

In presenting this thesis in partial fulfillment of the requirements for a Postgraduate degree from the University of Saskatchewan, I agree that the Libraries of this University may make it freely available for inspection. I further agree that permission for copying of this thesis in any manner, in whole or in part, for scholarly purposes may be granted by the professor or professors who supervised my thesis work or, in their absence, by the Head of the Department or the Dean of the College in which my thesis work was done. It is understood that any copying or publication or use of this thesis or parts thereof for financial gain shall not be allowed without my written permission. It is also understood that due recognition shall be given to me and to the University of Saskatchewan in any scholarly use which may be made of any material in my thesis.

Requests for permission to copy or to make other use of material in this thesis, in whole or part, should be addressed to:

The Head of the Department of Geological Sciences
University of Saskatchewan
114 Science Place
Saskatoon, Saskatchewan S7N 5E2 Canada

OR

The Dean
College of Graduate Studies and Research
University of Saskatchewan
107 Administration Place
Saskatoon, Saskatchewan S7N 5A2 Canada

ABSTRACT

The cherts in the Magadi basin have long been considered to be a product of the diagenesis of the rare, inorganically-precipitated, soft sodium-silicate mineral, magadiite (forming "Magadi-type chert"). While this process is known to have occurred in the basin, not all chert necessarily formed from diagenetic conversion of this mineral, as there are several features to suggest other mechanisms of silica deposition alternative to that of magadiite.

Lake Magadi, in the southern Kenya rift, shows a highly geochemically evolved closed-lake system rich in dissolved Na-CO_3-Cl, that has produced many unique sedimentary deposits throughout its geological history. Sediments deposited in the Magadi Basin from the mid- to late Pleistocene host many distinct varieties of lacustrine chert, which formed as a result of tectonic, climatic, microbial, and geochemical processes. The form, distribution, morphology, and abundance of cherts in the Magadi basin has drawn many researchers to consider their origin and diagenesis. The aim of this study is to reassess ideas about the origins of the siliceous sediments and rocks exposed in the Magadi basin.

Of the four recognized sedimentary units in the Magadi Basin, chert occurs in three of them. The oldest cherts, found in the Oloronga Beds (800 to 300 ka), are diatomaceous in composition, and were excluded from this study. A staggering amount of the chert in the Magadi Basin (95%) belongs to the Green Beds (98 to 40 ka), a recently defined sedimentary unit. Features in many of the Green Beds cherts imply a potential microbial influence during precipitation of the precursor material, and also a possible relationship with hot springs. The High Magadi Beds (24 to 9 ka) are host to definitive Magadi-type cherts, with distinct macro- and microscopic features allowing for their identification (reticulate patterning, and "grid-like" precipitation of chalcedony, respectively).

The Green Beds cherts have not been studied in detail since the introduction of this previously undefined sedimentary unit (Behr & Röhricht, 2000; Behr 2002). Microscopic evidence of preserved microbial remains in Magadi chert is indistinct, but macroscopic evidence of microbial influence is extensive (e.g., petee and tepee structures in chert;

couplets and triplets of thin, banded chert layers). Extensive bedded chert layers crop out in a few locations around the basin, displaying evidence of a shallow, evaporative environment (e.g., preserved salt crystal casts on chert surfaces).

Geothermal influence at the time of silica precipitation is inferred by macroscopic, geochemical, and analogous observations (e.g., a possible hot spring vent mound composed of chert; geochemical signatures; modern Na-Al-Si gels precipitating near hot spring inflow in Nasikie Engida). Perennial lagoons, sustained by warm springs issuing along the faulted margins of the basin, are observable to this day. Spring activity is locally observable, as perennial peripheral lagoons, and can also be inferred as a past process. Geothermal activity occurs along long-lived fault lines, and the surface expression of these tectonic features is distinctly discernible across the modern landscape (horsts and graben tectonism that can be playfully referred to as a "piano key landscape").

Whereas "Magadi-type chert" was once used to describe all chert in the basin, and was also thought to form in a deep, stratified lake, many lines of evidence exist to suggest siliceous-gel-like precursors, and a shallow, evaporative, and geothermally-influenced environment.

ACKNOWLEDGEMENTS

I would like to thank my supervisor, Robin Renaut, for giving me an opportunity to travel to and study the East African Rift, and for introducing me to many unique landscapes, as well as an international community of researchers. I would like to also thank my committee members, Luis Buatois and Chris Holmden, for their thoughtful comments throughout my degree program. Tom Bonli and Blaine Novakoski provided assistance and guidance in executing laboratory analyses. Tim Prokopiuk and Fina Nelson provided much needed support on numerous occasions. Alec Aitken kindly acted as an external examiner in my defence, and his feedback was invaluable.

I would also like to thank my friends, family, and fellow graduate students for their unique perspectives, and their ongoing support as I worked towards my degree.

TABLE OF CONTENTS

LIST OF TABLES

LIST OF FIGURES

LIST OF PLATES

CHAPTER 1: INTRODUCTION

1.1 Overview

Chert is a rock composed of micro- to cryptocrystalline quartz (SiO_2), often occurring as a replacement of precursor materials (Knauth, 1992). It occurs in a variety of sedimentary environments, including both marine and continental.

Most research on chert origins has focused on Phanerozoic marine cherts derived from skeletal remains (as opal-A: hydrated amorphous silica ($SiO_2 – nH_2O$)) – radiolaria, sponges, then much later, diatoms (Knauth, 1992). Chert nodules (flint) also commonly formed in Phanerozoic marine chalk, especially during the Late Cretaceous (Knauth, 1979), from diagenetic dissolution and re-precipitation of opaline silica, derived from sponges, as quartz.

Continental cherts have received much less attention. These cherts include accumulations of diatoms, mainly in freshwater systems (Owen, 2002), as well as inorganically-precipitated silica in more extreme environments (Eugster, 1969). Chemical precipitation of silica is uncommon, notably in modern settings, and is found in either hot spring or shallow lacustrine environments. Some examples of chemical cherts (though often biologically influenced) include hydrothermal sinters (i.e. Jones & Renaut, 2003; Renaut & Jones, 2003), silcretes (i.e. Wopfner, 1983), lacustrine cherts derived from opal (ie: Renaut & Owen, 1988), silica gels (i.e. Eugster & Jones, 1968), and sodium silicates (and Magadi-type chert (i.e. Hay, 1968)). Evidence of siliceous or silicified bioherms are quite uncommon, with only a few modern examples described in the literature, often in relation to hot spring activity (Berelson *et al.*, 2011; Cangemi *et al.*, 2010; Pepe-Ranney *et al.*, 2012).

Precambrian cherts often belong in a category of their own. Precambrian banded-iron formations (BIFs) are predominantly considered to be the result of chemical precipitation of SiO_2 and Fe_3O_4 on the sea floor (Mel'nik, 1982). Some (non-BIF) Precambrian cherts have been interpreted as a product of siliceous (or silicified) bioherms, and host some of the earliest forms of life (e.g., unicellular organisms; Brasier *et al*., 2005).

The many distinctive occurrences of chert in the rock record show the depositional versatility of silica, and many sedimentological factors must be considered when determining the origins of cherts. Many previous studies have shown that the Magadi Basin has the geochemical and environmental characteristics favourable for silica accumulation, but the mechanisms for precipitation and the timing of chert formation remain uncertain.

This thesis focuses on the origin of the many types of chert in the Lake Magadi basin in the southern Kenya Rift Valley. Since the late 1950s, geologists such as Baker (1958) have examined the morphology, sedimentary context, distribution, and geochemistry of those cherts, and have tried to determine their origin and ages (Baker, 1958; Eugster, 1969; Behr & Röhricht, 2000; Behr 2002). The cherts at Lake Magadi are unusual in morphology, texture, mineralogy, and stratigraphic context, and differ from most other types of continental chert. Superficially, some resemble Archean cherts.

1.2 Aims and scope of research

The aims of this research are to:

1. Re-evaluate the origins of the cherts at Lake Magadi;
2. Outline the major sedimentological and geochemical differences between the different chert types;
3. Use observations from field and laboratory analyses to define depositional parameters for the Green Beds unit;
4. Incorporate findings into the depositional history of the Magadi basin;
5. Discern if Green Beds cherts are analogous to chert found elsewhere in the rock record.

1.3 Previous work on Magadi cherts

Hydrological and sedimentological investigations in the Magadi Basin began in the early-to-mid 1900s (Stevens, 1932; Stevens & Spink, 1946; Temperley, 1951). Lake Magadi today usually desiccates annually to form a saline pan during the dry season. Its surface is underlain by > 40 m of bedded trona ($Na_3(CO_3)(HCO_3)•2H_2O$) that has accumulated during the last 9,000 years (Eugster, 1980). Defining the extent of the evaporites became of interest to the resource extraction industry (Temperley, 1951), and several boreholes were drilled by the mining company, before any investigations by the Kenya Government Geological Survey (Baker, 1958; Baker, 1963). The hypersaline alkaline brines of Lake Magadi are pumped into artificial solar ponds to produce the evaporite minerals trona and halite (NaCl) for industry (Stevens, 1932; Baker, 1958).

Baker (1958, 1963) mapped the geology of the Magadi Basin and the surrounding area. His research provided the basis for more recent geological studies. He mapped and defined the main stratigraphic units, some of which are still used today. After reconnaissance mapping, geological and geochemical investigations were undertaken by Hans Eugster. He described and analysed (Eugster, 1967, 1969) soft sodium-silicate minerals, previously reported by Baker (1958). Eugster (1967) described two new minerals -- magadiite ($NaSi_7O_{13}(OH)_3 \cdot 4(H_2O)$) and kenyaite ($Na_2Si_{22}O_{41}(OH)_8 \bullet 6(H_2O)$) -- based on their chemical composition, appearance, and properties seen in outcrop. At that time, other researchers studied the behaviour of silica in Lake Magadi and Little Magadi (Nasikie Engida) (Jones *et al.,* 1964), and making note of the abundance of siliceous sediments around the basin.

Magadiite and kenyaite both alter to a porcellaineous "Magadi-type" chert during diagenesis (Eugster, 1969). Magadi-type chert has been observed in several sedimentary basins around the world (e.g., Scotland; (Parnell, 1986), Tanzania (Hay, 1968), South Carolina (Houser, 1985)), resulting from the diagenesis of these uncommon minerals. Details of the mechanism of precipitation are unknown, though it has long been understood to be a result of changing pH in a silica-saturated, evaporative brine (Eugster, 1969; Rooney *et al.*, 1969; Eugster, 1980).

Magadiite deposited in the Magadi basin is found as laterally extensive, cm- to dm-scale layers of nearly pure magadiite, within sedimentary units composed largely of reworked volcanic tuffs, and as local patches. Magadiite is a hydrous mineral, and maintains a soft, putty-like consistency in both exposed and buried deposits. Two mechanisms have been proposed for the conversion of magadiite to chert: (1) leaching of

Na by dilute runoff (Eugster, 1969); or (2) spontaneous crystallization of quartz (Hay, 1968).

The soft, malleable nature of the magadiite deposits was considered responsible for the deformed cherts found around the basin. Chert in the Magadi basin has several morphologies, including metre-scale domal clusters, and decimetre- to metre-scale dikes, protruding from their surrounding sediments.

Magadiite precipitation had been long acknowledged as an inorganic process, so the consideration of biological influence over its precipitation was overlooked until work by Hans-Jürgen Behr (2000, 2002), who found indications of microbial activity in the cherts around Magadi. He also proposed a new sedimentary unit (the Green Beds) to which he ascribed ~ 90% of the cherts, and used sedimentological and biological evidence to argue *against* magadiite as the sole precursor to every chert type in the basin. Behr (2000, 2002) postulated, as had been considered by researchers in the past, that many cherts very likely formed from a silica gel precursor (Eugster & Jones, 1968), and as a result of silicification of carbonate biogenic structures.

A key interest of this study is to build upon the findings of Behr (2000, 2002) to better understand the origin and diagenesis of the different types of chert deposited or emplaced within the Green Beds at Lake Magadi.

1.4 Geologic Background

Lake Magadi is a hydrologically-closed, shallow, saline, alkaline, and predominantly spring-fed lake. The basin lies within an extensional continental rift, in the deepest axial depression of the southern Kenya Rift that has, over time, filled with voluminous flows of volcanics.

The East African Rift lies roughly along an old suture zone between the Archean Tanzania Craton (to the south-west), and the Proterozoic Mozambique belt (to the north-east). Rifting commenced some time during the Paleogene, defining the separation between the (now) African Plate and the Somalian Plate (Baker, 1986).

The Kenya Rift Valley represents the Kenyan portion of the East African Rift, which extends for 4000 km from Eritrea and Djibouti, to Malawi, Botswana, and Mozambique, as one branch of the two "arms" of African intercontinental rifting. The Eastern arm includes rifting expressed in Ethiopia, Kenya, and Tanzania, and the Western Branch shows rifting through Uganda, the Democratic Republic of the Congo (DRC), Rwanda, Burundi, Zambia, Tanzania, Malawi, and Mozambique (Chorowicz, 2005).

Extensional tectonics in Kenya shows E-W movement (N-S striking), often expressed as an *en echelon* pattern, as basins are often successively faulted into rhombic troughs by NW-SE-striking transverse faulting. The Magadi basin clearly expresses this tectonic regime, bounded by N-S, and NW-SE-striking fault lines and lineaments (Baker, 1986).

The central-to-southern region of the Kenyan portion of the rift experienced initial uplift and shield volcanism at *ca.* 13 Ma. Major faulting occurred from 4–3 Ma, creating an early half-graben with a prominent western scarp. The formation of the eastern fault line from 3.3–2.3 Ma produced a full graben. Faulting then migrated progressively inwards, from 3.3–2.3 Ma and again at 1.7 Ma, forming step-fault platforms, such that the graben narrowed with time. Extensive minor faulting of the rift floor occurred from 0.8–0.4 Ma, ultimately forming a narrow, block-faulted, "piano-key" horst and graben landscape (Baker, 1986).

The faulting of the landscape provided the accommodation space for the large Pleistocene lakes of the Kenyan Rift valley, during a much more humid period than that of the modern semi-arid climate of the southern Kenya Rift (Casanova, 1986). These Pleistocene water bodies have been recorded in the sediments around most Kenyan Rift lakes, including modern Lakes Turkana, Baringo, Bogoria, Nakuru, Naivasha, Elmenteita, and Magadi-Natron. Lake Magadi basin was hydrologically connected with Lake Natron of Tanzania at times when water levels were high, and the land currently separating the basins was breached. This connection is known from high-stand stromatolites, deposited along paleoshorelines (Eugster, 1980; Casanova, 1986), and from laterally extensive sedimentary deposits found in grabens that have since become isolated from the present axial graben through faulting (Baker, 1958; Eugster, 1980).

The climate and landscape around Magadi has evolved significantly since its inception. The semi-arid climate of the modern southern Kenyan rift is responsible for a highly negative hydrologic balance (430 mm of annual precipitation and 1,800 mm of annual evaporation (Behr, 2002)), which has resulted in a thick accumulation of evaporites (bedded sodium carbonate deposits, specifically), exploited by mining companies for the last 100 years. The Na-CO_3-Cl composition of the brine is mainly the result of drainage from the alkalic volcanic terrain (Eugster, 1980).

The sediments deposited over the span of the last 800,000 years include four units: the Oloronga Beds, the Green Beds, the High Magadi Beds, and the Evaporite Series. All units are composed dominantly of fine-grained volcaniclastic sediments, often altered to zeolites. The Green Beds are the main focus of this study.

1.5 Implications and context of research

Findings of this project will contribute to the Hominin Sites and Paleolakes Drilling Project (HSPDP - http://hspdp.asu.edu/), an international scientific collaboration detailing the geologic history across numerous sedimentary basins in the East African Rift, in the interest of climate reconstruction to help in understanding the migration and evolution of hominins. Drill cores have been retrieved from three sites in Kenya (Turkana, Tugen Hills, Magadi), and two sites in Ethiopia (Northern Awash, Chew Bahir) for this drilling project, specifically.

Lake Magadi was cored by the HSPDP in the summer 2014 from a drill pad constructed on the trona surface (Cohen *et al.,* 2016). The retrieved cores extend from the most recent layers of evaporite minerals, down to the volcanic basement (198 m below the pan surface), encompassing roughly 800,000 years of accumulated sediments. A related drill core was obtained roughly 25 km to the east in the Koora Graben (http://humanorigins.si.edu/ research/east-african-research/drilling). Drilling of the Koora sediments was undertaken by the Smithsonian Institution, as this region and neighbouring Olorgesailie (25 km north of Magadi) are of great interest to paleoanthropological research.

Olorgesailie is a sedimentary basin and a well-studied archaeological site, rich in fossils from large mammalian fauna, and artifacts associated with Acheulian (Lower Paleolithic) tool industries. Fragments of the cranium of a *Homo erectus* were also unearthed at Olorgesailie, on the same stratigraphic level as a number of hand-axe tools (Potts *et al.,* 2004). The stratigraphy at Olorgesailie is well understood and well calibrated (Behrensmeyer *et al.,* 2002), and the results from the Koora core will be of interest for

comparison with the Magadi core. This proximity of core sites will increase the impact of the Magadi core results, broadening the scope of the HSPDP project.

Understanding major climate transitions is of interest to the Hominin Sites and Paleolakes Drilling Project, and cored sediments are being examined for numerous climate indicators, including mineralogical and sedimentological context, diatoms, pollen, and sediment geochemistry. These findings will ultimately be compared to relevant sediments found at the surface. Chert encountered in the Magadi core will be described in detail, and compared to observations sourced from outcrop (this study).

1.6 Structure of this thesis

This thesis includes two major chapters: Chapter 2 – Sedimentology; and Chapter 3 – Geochemistry; detailing the findings pertaining to each major subject. Chapter 2 is written in manuscript style, to be submitted to an international journal upon completion of defence. Chapter 3 is a draft manuscript, and will be reformatted to the standards of a more specific journal at a later date. Chapter 4 provides the conclusion to the research project. Chapter 5 is an appendix, containing figures and tables of values.

1.7 REFERENCES

Baker, B.H. (1958) Geology of the Magadi Area: Report. 42. Kenyan Government Printer, Nairobi, pp. 88.

Baker, B.H. (1963) Geology of the Area South of Magadi: Report 61. Kenyan Government Printer, Nairobi. pp. 33.

Baker, B.H. (1986) Tectonics and volcanism of the southern Kenya Rift Valley and its influence on rift sedimentation. *Geol. Soc. London, Spec. Publ.* **25**, 45–57.

Behr, H.J. (2002) Magadiiite and Magadi Chert: A Critical Analysis of the Silica Sediments in the Lake Magadi Basin, Kenya. In: Renaut, R.W., Ashley, G. (Eds.), East African Sedimentation. SEPM Spec. Publication, vol. 73, pp. 233–246.

Behr, H.J., and **Röhricht, C.** (2000) Record of seismotectonic events in siliceous cyanobacterial sediments (Magadi cherts), Lake Magadi, Kenya. *Int. J. Earth Sci.,* **89**, 268–283.

Berelson, W.M., Corsetti, F.A., Pepe-Ranney, C., Hammond, D.E., Beaumont, W., and **Spear, J.R.** (2011) Hot spring siliceous stromatolites from Yellowstone National Park: assessing growth rate and laminae formation. *Geobiology,* **9**, 411–424.

Brasier, M., Green, O., Lindsay, J., Mcloughlin, N., Steele, and **Stoakes, C.** (2005) Critical testing of Earth's oldest putative fossil assemblage from the ~3.5Ga Apex chert, Chinaman Creek, Western Australia. *Precambrian Research,* **140**, 55–102.

Cangemi, M., Bellanca, A., Borin, S., Hopkinson, L., Mapelli, F., and **Neri, R.** (2010) The genesis of actively growing siliceous stromatolites: Evidence from Lake Specchio di Venere, Pantelleria Island, Italy. *Chem. Geol.,* **276**, 318–330.

Casanova, J. (1986) East African Rift stromatolites. *Geological Society, London, Special Publications,* **25**, 201–210.

Chorowicz, J. (2005) The East African rift system. *Journal of African Earth Sciences,* **43**, 379–410.

Cohen, A.S. , Campisano, C., Arrowsmith, R., Asrat, A., Behrensmeyer, A.K., Deino, A., Feibel, C., Hill, A., Johnson, R., Kingston, J., Lamb, H., Lowenstein, T., Noren, A., Olago, D., Owen, R.B., Potts, R., Reed, K., Renaut, R., Schäbitz, F., Tiercelin, J.-J., Trauth, M.H., Wynn, J., Ivory, S., Brady, K., O'Grady, R., Rodysill, J., Githiri, J., Russell, J., Foerster, V., Dommain, R., Rucina, S., Deocampo, D., Russell, J., Billingsley, A., Beck, C., Dorenbeck, G., Dullo, L., Feary, D., Garello, D., Gromig, R., Johnson, T., Junginger, A., Karanja, M., Kimburi, E., Mbuthia, A., McCartney, T., McNulty, E., Muiruri, V., Nambiro,E., Negash, E.W., Njagi, D., Wilson, J.N., Rabideaux, N., Raub,T., Sier,M.J., Smith, P., Urban, J., Warren, M., Yadeta, M., Yost, C., and **Zinaye, B.** (2016). The Hominin Sites and Paleolakes Drilling Project: Inferring the Environmental Context of Human Evolution from Eastern African Rift Lake Deposits. *Scientific Drilling*, **21**, 1-16.

Eugster, H.P. (1967) Hydrous Sodium Silicates from Lake Magadi, Kenya: Precursors of Bedded Chert. *Science*, **157**, 1170–1180.

Eugster, H.P. (1969) Inorganic Bedded Cherts from the Magadi Area, Kenya. *Contrib. to Mineral. Petrol.,* **22**, 1–31.

Eugster, H.P. (1980) Lake Magadi, Kenya, and its Precursors, In: Hypersaline Brines and Evaporitic Environments. (Ed Nissenbaum, A.), Elsevier Scientific Publishing Company, Amsterdam, The Netherlands, pp. 195–232.

Eugster, H.P., and **Jones, B.F. (**1968) Gels Composed of Sodium-Aluminum Silicate, Lake Magadi, Kenya. *Science,* **161**, 160–163.

Hay, R.L. (1968) Chert and its sodium-silicate precursors in sodium-carbonate lakes of East Africa. *Contrib. to Mineral. Petrol.,* **17**, 255–274.

Houser, B.B. (1985) Magadi-type chert, indicator of a lacustrine environment in the Middle Eocene McBean formation, South Carolina. *Southeastern Geology,* **25,** 185-197.

Jones, B., and **Renaut, R.W.** (2003) Hot spring and geyser sinters: the integrated product of precipitation, replacement, and deposition. *Can. J. Earth Sci.,* **40**, 1549–1569.

Jones, B.F., Rettig, S.L., and **Eugster, H.P.** (1967) Silica in Alkaline Brines. *Science* , **158**, 1310–1314.

Knauth, L.P. (1979) A model for the origin of chert in limestone, *Geology*, **7**, 274-277.

Knauth, L.P. (1992) Origin and Diagenesis of Cherts: An Isotopic Perspective. In: Clauer, N., Chaudhuri, S. (Eds), Isotopic Signatures and Sedimentary Records - Lecture Notes in Earth Sciences, vol 43, pp. 123–152.

Mel'nik, Y.P., 1982. Precambrian Banded-Iron-Formations. Elsevier Science, pp. 309.

Owen, R.B. (2002) Sedimentological characteristics and origins of diatomaceous deposits in the East African Rift System. In: Renaut, R.W., Ashley, G. (Eds.), East African Sedimentation. SEPM Spec. Publication, vol. 73, pp. 233–246.

Owen, R.B., Renaut, R.W., Behrensmeyer, A.K., and **Potts, R.** (2014) Quaternary geochemical stratigraphy of the Kedong–Olorgesailie section of the southern Kenya Rift valley. *Palaeogeography, Palaeoclimatology, Palaeoecology*, **396**, 194–212.

Parnell, J., (1986) Devonian Magadi-Type Cherts in the Orcadian Basin, Scotland. *J. Sediment. Petrol.,* **56**, 495–500.

Pepe-Ranney, C., Berelson, W.M., Corsetti, F.A. , Treants, M., and **Spear, J.R.** (2012) Cyanobacterial construction of hot spring siliceous stromatolites in Yellowstone National Park. *Environ. Microbiol.,* **14**, 1182–97.

Potts, R., Behrensmeyer, A.K., Deino, A., Ditchfield P., and **Clark, J.** (2004) Small Mid-Pleistocene hominin associated with East African Acheulean technology. *Science,* **305**, 75-78.

Renaut, R.W., and **Jones, B.** (2003) Sedimentology of hot spring systems. *Canadian Journal of Earth Sciences*, **40**, 1439–1442.

Renaut, R.W., and **Owen, R.B.** (1988) Opaline cherts associated with sublacustrine hydrothermal springs at Lake Bogoria, Kenya Rift valley. *Geology,* **16**, 699–702.

Rooney, T.P., Jones, B.F., and **Neal, J.T.** (1969) Magadiite from Alkali Lake, Oregon, *The American Mineralogist*, **54**, 1034-1043.

S**tevens, J.A.** (1932) Lake Magadi and its alkaline springs. Report prepared for the Magadi Soda Company, Kenya. (Unpublished)

Stevens, J. A., and **Spink, P. C.** (1946) Notes on the Magadi section of the Eastern Rift Valley. *Geogr. Journ.,* **107**, 236-241.

Temperley, B. N. (1951) Some geological and geophysical investigations in the vicinity of Lake Magadi." Mines and Geological Dept., Nairobi. (Unpublished)

Wopfner, H. (1983) Environment of silcrete formation: a comparison of examples from Australia and the Cologne Embayment, West Germany. *Geol. Soc. London, Special Publications,* **11**, 151–158.

CHAPTER 2

Depositional environments and origin of the chert-bearing Pleistocene Green Beds in the Magadi Basin, southern Kenya Rift

This manuscript will be submitted to an international journal.

The senior author did the fieldwork and analytical research, and wrote the manuscript.

The co-authors gave advice in the field and offered suggestions and editorial comments.

Depositional environments and origin of the chert-bearing Pleistocene Green Beds in the Magadi Basin, southern Kenya Rift

BRITNI L. BRENNA*, ROBIN W. RENAUT* and R. BERNHART OWEN†

** Department of Geological Sciences, University of Saskatchewan, Saskatoon SK, Canada S7N 5E2 (E-mail: blb823@mail.usask.ca)*

†Department of Geography, Hong Kong Baptist University, Kowloon Tong, Hong Kong

Keywords Chert, Lake Magadi, Kenya Rift, microbialite, lacustrine

ABSTRACT

Lake Magadi, geologically famous for trona and chert, lies at ca.600 m elevation above sea level in the southern Kenya Rift Valley. The lake, a hydrologically closed, hypersaline, alkaline, intermittently dry pan, is fed by ephemeral streams and hot springs that lie on N-S faults along its margins. The basin hosted several precursor lakes from *ca.* 800 ka until today, recorded by sediments that crop out around the lake. These include the zeolitic Green Beds (GB: *ca.*100-40 ka), exposed discontinuously in the axial trough, which contain abundant chert originally attributed to a magadiite precursor. Behr (2002), however, showed that some silica precipitation involved prokaryotes. This study reexamines the origins of the GB cherts. Two groups are recognized: one 'bedded', the other 'intrusive'.

Bedded cherts are cm-scale, stromatolitic cherts with structures that typify an evaporative playa-like setting including desiccation cracks, crystal pseudomorphs (trona, gaylussite), microbial laminae (couplets, triplets), and ichnofossils. These cherts cap zeolitic tuff, greenish silt and black mudstone, commonly in cycles 0.5 to 2 m thick. Younger cherts intrude the lacustrine silts and bedded cherts forming meter-scale dikes and domal mounds that are oriented along N-S faults and fractures. Quartz breccias in the mound cores are commonly mantled by microbial laminites that lie parallel to the external surface of the mounds. Thick (> 5 m) massive cherts containing oncoids are found in places. Terraced mounds present northeast of the lake (NE Lagoon) resemble subaerial sinter.

The bedded GB cherts show no unequivocal diagnostic indicators of a magadiite precursor and limited evidence for carbonate replacement. Many sedimentological features imply silica precipitation, possibly as a gel, in an ephemeral playa fed by Si-rich hot springs. Intrusive cherts show evidence of both physical emplacement (brecciation) while partly solid and cementation by a fluid or gel. Some dikes and intrusive cherts can be linked to seismic events. Other cherts, however, may be subaqueous silica bioherms linked to thermal fluid discharge along N-S faults and fractures. Some silica bioherms resemble microbialites in Archean cherts in color and morphology.

2.1 Introduction

Lake Magadi is well known as an extreme lacustrine environment with curious biology and geology. The most striking of the sediments in the basin are the bedded evaporites, the sodium silicate horizons, and the unusual and abundant outcrops of chert. The mode of occurrence of the Magadi cherts, though studied and debated for decades, remains partly unresolved.

At Lake Magadi, there is evidence to suggest both chemical precipitation of sodium silicates and siliceous gels, as well as the formation of siliceous stromatolites in sediments dating from the Mid- to Late Pleistocene. Much evidence exists to correlate their occurrence to not only lake geochemistry, but also microbial and hot spring activity.

Lake Magadi, a hydrologically closed lake, lies at *ca.* 600 m elevation above sea level at the southern end of the Kenya Rift Valley (l°50' S; 36°15' E), 120 km southwest of Nairobi (Fig. 1A, B). The lake, a hypersaline, alkaline and intermittently dry pan, is fed by ephemeral runoff and almost 200 warm springs, which discharge along the N-S oriented faults that bound the lake. Although strongly evaporative today, the basin hosted several larger, fresher lakes during the Pleistocene. Three 'precursor' lake periods have been recognized preserved in discontinuous outcrops around the lake margins and in cores from the lake floor (Baker, 1958; Behr & Röhricht, 2000; Eugster, 1986, 1980): the Oloronga Beds (*ca.* 1 to 0.3 Ma: Behr & Röhricht, 2000; Fairhead *et al.*, 1972), the Green Beds (*ca.* 100–40 ka: Goetz & Hillaire-Marcel, 1992; Williamson *et al.*, 1993), and the High Magadi Beds (*ca.* 23–9 ka: (Williamson *et al.*, 1993). Today, sodium carbonate minerals (trona, nahcolite) are precipitating from the brine, contributing to a series of bedded evaporites ('Evaporite Series' of Baker, 1958), locally up to 40 m thick. The

evaporites and brines have been exploited commercially for soda ash and common salt for the last 100 years (Baker, 1958).

The Pleistocene Green Beds are of particular interest because they contain most of the chert at Lake Magadi, the focus of this study. The cherts form discrete platy, stromatolitic beds within a sequence of zeolitic lacustrine silts, and a series of dykes, intrusive masses, and domal structures, many of which have laminated or stromatolitic textures. Eugster (1967, 1969, 1980) and Hay (1968) interpreted the cherts at Lake Magadi as 'Magadi-type cherts', originating from a soft sodium silicate precursor, either magadiite ($NaSi_7O_{13}(OH)_3 \cdot 4(H_2O)$) or kenyaite ($Na_2Si_{22}O_{45} \cdot 10H_2O$). Baker (1958), when mapping Magadi geology, noted an "extremely finely divided silica devoid of organic structure" in the High Magadi Beds. Eugster (1967, 1969) and Hay (1968) followed up on these findings, and recognized the new minerals, magadiite and kenyaite. Magadiite was believed to precipitate as beds of soft material, which would intrude overlying sediments as a result of compaction (of the magadiite), and the accompanying polygonal desiccation of overburden. This interpretation was widely accepted, and many ancient examples of 'Magadi-type chert' were recognized worldwide (e.g., Parnell, 1986; Krainer & Spötl, 1998; Kerrich *et al*., 2002; Andrews *et al.*, 2014). Hay (1968) found reticulated chert nodules (Magadi-type chert) at Olduvai in Tanzania, and magadiite soon was recognized in modern lacustrine environments (e.g., Chad (Sebag *et al.,* 2001), Oregon state (Rooney *et al.,* 1969), Lake Bogoria (Renaut *et al.,* 1986)), and in ancient lake sediments (Orkney (Parnell, 1986), Tanzania (Hay, 1968), South Carolina (Houser, 1985)).

Röhricht (1999), Behr & Röhricht (2000), and Behr (2002) re-interpreted the Green Beds cherts, and proposed microbially-controlled precipitation of chert, rather than

inorganically-precipitated magadiite, for many of the exposed cherts in the basin. They reported that the size of discrete magadiite spherules is similar to that of coccoid cyanobacteria (*ca.*10 μm diameter), and believed misidentification to be the reason microbial influence had been thus far disregarded. Some cherts, they suggested, formed by replacement of carbonate; others formed from gels created by alkaline brine interacting with volcanic detritus. According to Behr & Röhricht (2000) and Behr (2002), only the cherts of the late Pleistocene High Magadi Beds formed unequivocally from diagenesis of precipitated magadiite.

Dating of the chert horizon by Goetz & Hillaire-Marcel (1992) showed, for the first time, two distinct ages for chert layers (6300± 2800 y BP for the sodium silicates; 98,000± 20,000 y BP for an older chert layer). These ages were determined by U/Th dating, which measured co-precipitated U-$CaCO_3$. The large margin of error is due to late diagenetic calcite precipitation forming in sample pore spaces. These new age dates were the initial impetus for reinterpreting the cherts of Magadi, as the older cherts greatly exceed the age range for the High Magadi Beds. However, while the findings of Behr & Röhricht (2000) and Behr (2002) contributed greatly to the change in discussion over cherts at Magadi, they focused much of their interpretation on features found in a single outcrop (Behr, 2002; p. 262).

The depositional setting of the Green Beds and the associated cherts has not previously been studied. All outcrops are small and of limited extent, and many cherts that predate the High Magadi Beds, in which a direct link to a magadiite precursor is evident, have been disturbed by later seismotectonic events (Behr & Röhricht, 2000). The aim of this paper is to (1) describe the depositional setting of the Green Beds and their bedded

greenish cherts, and using new evidence, to interpret the paleoenvironmental setting and processes of their formation; and (2) reassess the stratigraphic and paleotectonic significance of the later reddish cherts, some of which intrude the older green cherts.

Some stromatolitic cherts exposed along the margins of Lake Magadi basin resemble Archean cherts in morphology (e.g., Noffke *et al.*, 2013). They might provide clues to interpreting the processes involved in Precambrian chert precipitation. Understanding the setting and processes of Pleistocene chert formation at Lake Magadi therefore has potentially broader geological importance.

2.2 Geological Setting

2.2.1 Tectonics and volcanism

The Magadi Basin lies at the southern end of the Kenya Rift Valley near the Tanzania border (Fig. 2.1(A)). Neogene rifting in southern Kenya began with shield volcanism along the western margin of the future rift (*ca.* 14–9 Ma). Faulting along the western margin (Nguruman Escarpment) had formed a half-graben basin by 7 Ma. Later faulting deepened the evolving half-graben. Shield volcanism, followed by faulting along the eastern margin, then led to a full N-S axial graben (*ca.* 4–3 Ma). Prolonged flood volcanism filled the new accommodation space. The flood volcanics include the Limuru Trachytes (*ca.* 1.91 Ma), Ol Keju Nero basalts (*ca.* 1.79–1.64 Ma), and Ol Tepesi basalts (*ca.* 1.65–1.4 Ma) (Crossley, 1979; Baker, 1958, 1963, 1986). The youngest volcanic rocks in the Magadi region are the Magadi (Plateau) Trachytes, which were extruded mainly from fissure eruptions from 1.4 to 0.7 Ma (Fairhead *et al.*, 1972). These trachytes are the bedrock of most of the Magadi drainage basin.

Pleistocene grid-faulting of the Magadi Trachytes produced the modern structure and topography of the basin and its environs (Baker, 1986; Plate 2.1(A)). The morphology of the modern lake basin is defined by conspicuous horst-and-graben tectonism, with three merging NNE-striking fault zones that have created a narrow basin, 40 km long by 2 km wide (Le Turdu *et al.,* 1995). The faults bounding Lake Magadi are well defined, but have lower relief than those of Nasikie Engida (Little Magadi), a small, perennial, saline and alkaline lake north of Lake Magadi (Fig. 2.1(B)). Lacustrine and fluviatile sediments were then deposited upon the faulted landscape, both during and after the final stages of trachyte volcanism.

Grid faulting followed deposition of the earliest fluvial-lacustrine sequence, termed the Oloronga Beds. These sediments are tilted westwards north of Nasikie Engida, and are broken by faults nearly parallel to the rift margins. Syndepositional tectonism occurred during deposition of the Green Beds (Behr & Röhricht, 2000). The axial graben of the Magadi Basin then underwent more downfaulting and subsidence, producing a morphology similar to that of the modern basin (Baker, 1958; 1986).

Basin morphology (tectonics) and climate both control sedimentation in closed basins such as Lake Magadi. Without surface outflow, shorelines fluctuate frequently in response to climate change: they typically recede during relatively dry periods, but rise and abut against faulted basin margins during more humid periods. From the patterns of sedimentation and associated lithofacies, the depositional history can be inferred and sometimes related to paleoclimate (Renaut & Gierlowski-Kordesch, 2010). Lakes Magadi, Nasikie Engida, and Natron (Tanzania) were united as one large lake during

several periods when water levels were high (Fig. 2.1(A); Damnati & Taieb, 1995; Eugster, 1969; Williamson *et al*., 1993; Hillaire-Marcel & Casanova, 1987).

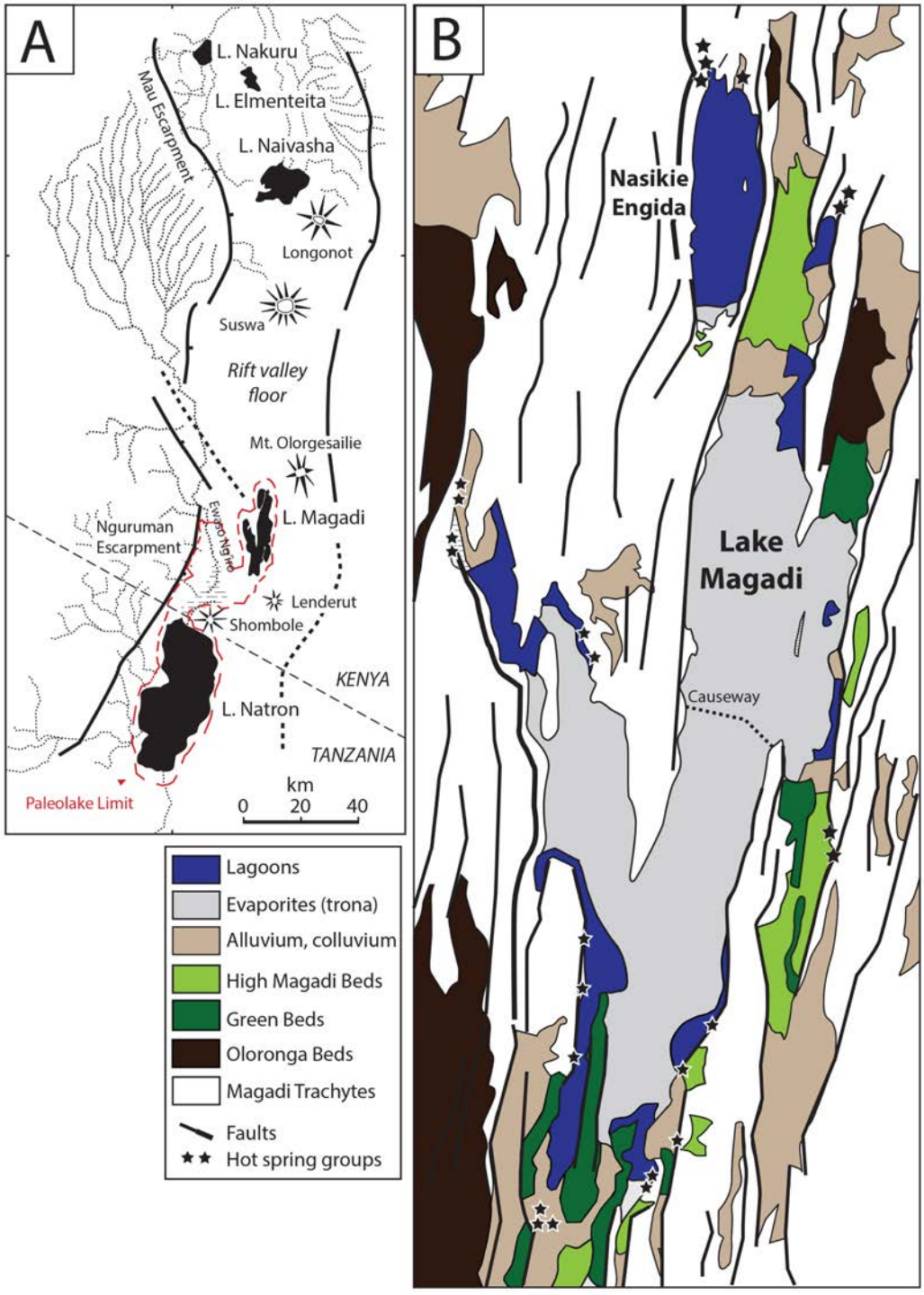

Figure 2.1 – Location and surface geology of Lake Magadi, Kenya

2.2.2 Hydrology and hydrochemistry

Lake Magadi, the lowermost basin in the southern Kenyan rift, is the sump for several sources of water inflow, though no perennial rivers flow into the lake. Most recharge in the basin comes from *ca.* 200 small warm-to-hot (23°C (S. Magadi) – 86°C (N. Nasikie Engida) (Behr, 2002; pers. comm. with R. Renaut)) springs that flow into several 'lagoons' of standing water, located mainly along the bounding faults (Plate 2.1(B)), supplemented seasonally by sheetwash. The spring waters are a mixture of three geochemically distinct sources: shallow groundwater, deep geothermal water, and recirculating lake brines (Eugster, 1970; Jones *et al*., 1977).

The Ewaso Ngiro, a major river in the southern Kenyan rift that bypasses Lake Magadi and feeds Lake Natron (Fig. 2.1(A)), infiltrates the alluvium surrounding the Magadi basin and is a major source of shallow spring recharge (Jones *et al.*, 1977; Allen *et al*., 1989). The headwaters of the Ewaso Ngiro are atop the western escarpment (Fig. 2.1(A) in Eugster, 1970), and the rains that feed the catchment also infiltrate the permeable volcanic rocks through faults and fractures to replenish the deep geothermal reservoir beneath the rift valley floor. Ephemeral runoff from local rainfall is a lesser source of inflow, and occurs mainly during the rainy season months of November to December, and April to May (Jones *et al.*, 1977). Input from slopewash is expressed as small alluvial fans around the basin margins, particularly along the eastern shoreline.

The drainage basin itself lies in a semi-arid region, receiving only *ca.* 500 mm annual rainfall. With evapotranspiration rates greater than 3500 mm y^{-1}, evaporative concentration of the spring inflow leads to very high salinity in the lake brines (> 250,000 mg kg^{-1} Total Dissolved Solids; pH: 9.0-12.5). In most years, much of the lake surface

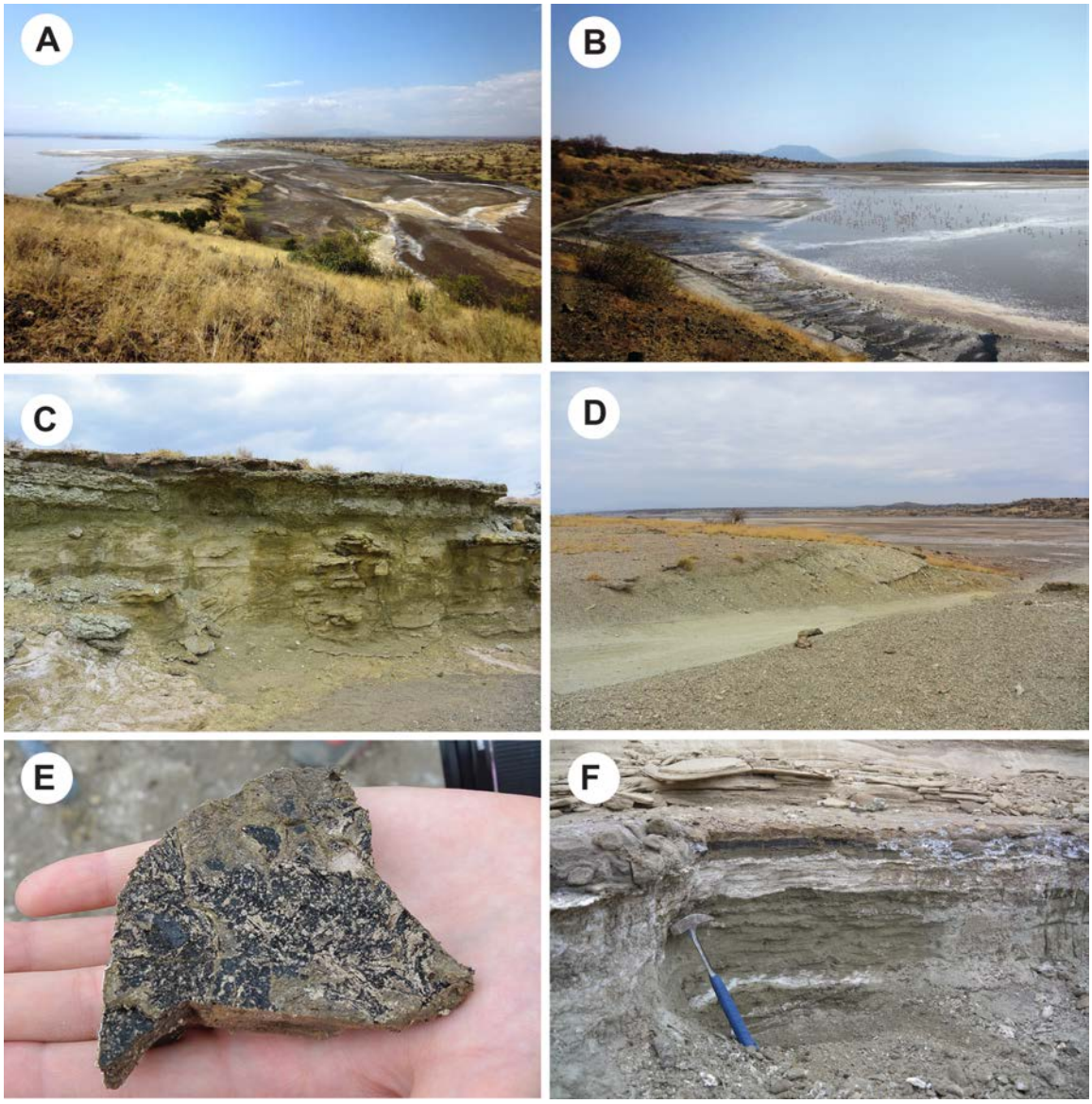

Plate 2.1 – Major topography and major sedimentary unit outcrops; (A) Faulted topography of the modern Magadi Basin; (B) Lagoons sustained by warm springs around the perimeter of Lake Magadi; (C) Oloronga Beds outcrop; found in the SW lagoon; (D) Green Beds outcrop; found on the Southern Peninsula; (E) *Tilapia* sp. fossil found in the High Magadi Beds; (F) High Magadi Beds outcrop; Eastern Lagoon

desiccates exposing subaerial trona crusts (Baker, 1958; Eugster, 1980; Damnati & Taieb, 1995; Behr & Röhricht, 2000).

The composition of the springs and lake brines is mainly the result of chemical interactions between runoff and groundwater, and the Pleistocene volcanic rocks. Chemical weathering, primarily by silicate hydrolysis, results in enrichments in Na^+, H_4SiO_4, HCO_3^-, CO_3^{2-}, Cl^- and F^-. The waters are relatively devoid of alkali earth metals such as Ca^{2+} and Mg^{2+}, which are of relatively low in abundance in the parent trachyte, and are removed by precipitation of alkali earth carbonates in soils, subsurface cements and springs, or the lake itself during wetter more dilute phases (Jones *et al.,* 1977). Through extreme evaporation and subsequent crystallization and redissolution of evaporites, the lake brines become highly saline.

There are a number of sinks for the inflowing solutes. Up to 92% of dissolved silica is lost between streamflow (e.g., Ewaso Ngiro) and dilute spring water (e.g., warm springs) (Jones *et al.*, 1977). Any calcium in the system is lost by capillary evaporation of the dilute groundwaters resulting in veinlets and aggregates of anhedral calcite in the fine-grained lakebed outcrops (Jones *et al.*, 1977). More soluble constituents (e.g., Na^+, Cl^-, CO_3^{2-}, HCO_3^-) are fractionated by wetting and drying cycles driven by seasonal evaporative concentration and the resulting capillary action acting upon the dilute groundwaters. Desiccation is expressed as efflorescent crusts of trona or thermonatrite (Na_2CO_3. H_2O) on outcrop surfaces (Jones *et al.,* 1977). Halite is one of the last minerals to precipitate at Magadi, as it is the most soluble of the evaporites, and is limited in its precipitation by the high carbonate-bicarbonate content of the basin, leading to the formation of sodium carbonates instead (Eugster, 1971).

The waters that occupy the lowest, axial parts of the basin are Na–CO_3-Cl type, and evolve along an almost "ideal" closed-basin geochemical pathway, reaching sodium carbonate saturation at maximum natural evaporative concentration in the lake (Hardie & Eugster, 1980; Jones & Deocampo, 2014). Halite precipitates in abundance in manufactured evaporative ponds created by the soda company, from brines collected after fractional crystallization of less soluble evaporites (sodium carbonates).

The paucity of alkaline earth metals (e.g., Ca^{2+}, Mg^{2+}) is responsible for the buildup of carbonate ions in solution because carbonate mineral precipitation plays a very minor role in solute removal after the initial precipitation of calcite in relatively dilute fluids (Jones *et al.*, 1977). Evaporative concentration leads to greater solubility with respect to dissolved silica as a result of high HCO_3^- and CO_3^{2-} concentrations, which create highly alkaline brines (Jones *et al.,* 1977; Eugster & Jones, 1979).

High silica solubility is essential for sodium silicate and chert formation. Silica is chiefly contributed to the basin by hydrolysis of feldspars. Silicic acid [$Si(OH)_4$] rapidly dissociates to simpler silica species [$(H_4SiO_4) \rightarrow (H_3SiO_4)^- \rightarrow (H_2SiO_4)^{2-} \rightarrow (HSiO_4)^{3-} \rightarrow (SiO_4)^{4-}$] above pH 9, as hydronium ions are consumed (Iler, 1979). The concentration of monosilicic acid (H_4SiO_4) is effectively lowered in proportion to other silica species, and overall silica concentrations can exceed 1500 ppm (Jones *et al.*, 1967; 1977). Saturation with respect to amorphous silica in an ideal solution is reached at 120 ppm $Si(OH)_4$ at 25°C (Krauskopf, 1956), but unusual conditions in Lake Magadi brines (high salinity; high pH and alkalinity; high primary productivity) allow much higher concentrations.

2.2.3 Stratigraphy of the Magadi Basin

The Pleistocene to Recent sediments of the Magadi Basin are grouped into four formations. From oldest to youngest these are the: Oloronga Beds, Green Beds, High Magadi Beds, and the Evaporite Series (Fig. 2.2). None yet are formally defined stratigraphic units because all are preserved in scattered discontinuous outcrops around the basin, or are partial units in cores. All sediments derive mainly from weathering of the Magadi Trachytes and associated volcaniclastic deposits.

2.2.3.1 Oloronga Beds

The poorly exposed Oloronga Beds include fluvial, trough cross-bedded sandstone, overlain by weakly laminated and bedded tuffaceous mudstone and siltstone that locally host contorted thinly-bedded grey cherts (Plate 2.1(C)). This unit is up to 45 m thick in places (Behr and Röhricht, 2000). South of Lake Magadi, these rocks are disconformably overlain by a grey pisolitic calcrete, up to 50 cm thick (Felske, 2016). Lacustrine carbonate rocks in the upper part of the Oloronga Beds that crop out near the southwestern margin of the modern lake contain gastropods. In some samples, the fossils, their matrix, and cements are silicified and replaced by cryptocrystalline quartz (Baker, 1958, and unpublished data).

The Oloronga Beds disconformably overlie the Pleistocene Magadi Trachyte land surface without an obvious underlying paleosol. Their outcrops extend across more of the basin than all younger units, which lie nearer to the modern lake margins. The few radiometric ages available for Oloronga sediments range from 800 ka to 300 ka (Behr, 2002; Fairhead *et al.*, 1972). Paleolake Oloronga is believed to have reached the basin's maximum upper limit (Fig. 2.1(A), 2.2).

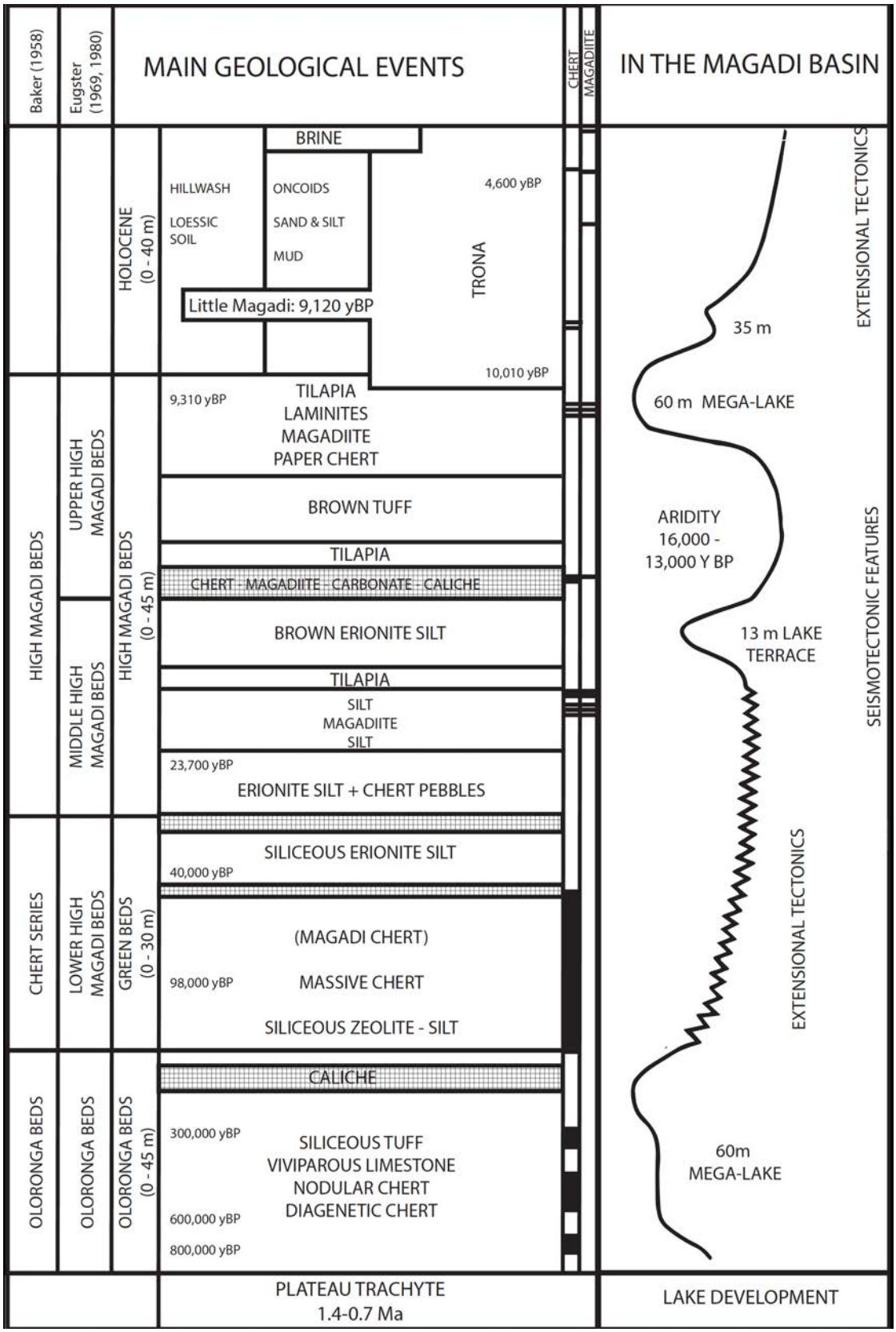

Figure 2.2 – Known Magadi stratigraphy, and inferred lake levels (modified from Behr, 2002)

Sedimentological and paleontological evidence implies that the lacustrine Oloronga sediments were deposited in mainly freshwater conditions. Authigenic zeolites in the Oloronga Beds, which formed during periods after sedimentation, have higher Si/Al ratios than those in the younger Green Beds and High Magadi Beds (Mariner & Surdam, 1970). This implies that the Oloronga paleolake and its groundwaters were generally less alkaline than those when the later sediments were deposited and undergoing diagenesis (Mariner and Surdam, 1970; Surdam and Eugster, 1976). Gastropods, ostracods, mollusc coquinas (Behr & Röhricht, 2000) and sponges in the Oloronga Beds support this interpretation. The deeper open-lake Oloronga sediments do not outcrop in the axial graben, whereas the Green Beds and High Magadi Beds do.

Hillaire-Marcel & Casanova (1987) noted and dated highstand (low and high Mg calcite) carbonate stromatolites that were deposited during exceptionally high lake levels (features found in only one locality 80 m above modern Lake Natron). The age-dates of these stromatolites exceeded the limits of U/Th method used at the time (> 200 ka), but the features were nonetheless attributed to the Oloronga Beds. This may imply that the Oloronga paleolakes were the deepest, most extensive, and most dilute of the Pleistocene precursor lakes at Magadi.

2.2.3.2 Green Beds

The Green Beds, lying between the Oloronga and High Magadi Beds, are the focus of this paper. Deposited in the Mid-Pleistocene, these sediments crop out discontinuously within the axial trough of the modern basin, showing a more restricted depositional extent than the overlying and underlying sedimentary units. The Green Beds, in outcrop, are composed of greenish tuffs; dark brown organic mudstone; yellowish brown

volcaniclastic silts; fine sands and siltstones; and thinly bedded cherts, locally capped by calcrete (Plate 2.1(D)). They also host voluminous intrusions of chert, described in detail later.

Baker (1958) originally mapped this unit as the 'Chert Series' and placed it above the Oloronga Beds, only to reconsider their stratigraphy five years later (Baker, 1963), placing the 'Chert Series' right above the Magadi Trachytes (Table 2.1). Eugster (1969, 1980) reinterpreted the cherts as being stratigraphically equivalent to the late Pleistocene High Magadi Beds. After reviewing the field evidence, Behr & Röhricht (2000) remapped and renamed this chert-rich unit separately as the 'Green Beds', which unlike the High Magadi Beds, is restricted to the modern axial graben.

Author	Baker (1958)		Baker (1963)		Eugster (1969)		Eugster (1980)		Behr (2002)	
Sedimentary unit and associated ages	*Evaporite Series*	Recent	*Evaporite Series*	Recent	*Evaporite Series*	0-10 ka	*Evaporite Series*	0-9ka	*Evaporite Series*	0-10.1ka
	High Magadi Beds	Upper Pleistocene	*High Magadi Beds*	Upper Pleistocene	*High Magadi Beds*	20 ka	*High Magadi Beds*	9.1ka	*High Magadi Beds*	9.3-23.7ka
	Chert Series	Middle Pleistocene	*Oloronga Beds*	Middle Pleistocene	*(faulting)*	--	*Trachyte flows*	--	*Green Beds*	40-98ka
	Oloronga Beds	Middle Pleistocene	*Chert Series*	Middle Pleistocene	*Oloronga Beds*	--	*Oloronga Beds*	400 – 780ka	*Oloronga Beds*	300-800ka

Table 2.1 - Temporal interpretations of Magadi Basin stratigraphy

Eugster (1969, 1980) stated that the Oloronga Beds are capped by a laterally extensive Pleistocene calcrete, which in places is overlain by the lacustrine High Magadi Beds (Eugster, 1969). The calcrete, therefore, would be the only preserved sedimentary unit between the youngest preserved sediments of the Oloronga Beds, and the much younger High Magadi Beds. Behr & Röhricht (2000), however, noted an intervening greenish silty unit with a distinct geochemical signature. Eugster (1980, 1986) had not recognized

the stratigraphic unit between the Oloronga calcrete and the High Magadi Beds that Behr & Röhricht (2000) termed the Green Beds.

2.2.3.3 High Magadi Beds

In outcrop, the High Magadi Beds unit is up to 12 m thick. A lower member and an upper member can be distinguished. The thinner (0–100 cm) laminated lower member (Eugster, 1969) consists of black, dark brown and greenish volcanic silts, pale grey sodium silicates (magadiite, kenyaite), and, in the upper portion of the lower member, fine laminae containing black well-preserved fossil fish bones (*Tilapia* sp.) (Plate 2.1 (E & F)). After deposition of the fossiliferous laminites, an upper member up to 7 m thick of light brown volcaniclastic silts and tuffs was deposited on the lacustrine silts, including isolated *Tilapia* fossils (Baker, 1958). The High Magadi Beds were deposited when the lake level was higher than today, as shown by gravel strandlines on fault ramps around the lake margins, which are *ca.* 13 m above the modern depositional surface (Behr & Röhricht, 2000). Thin (1–3 cm) stromatolitic limestone crusts, composed of calcite that encrusts hard substrates including gravel clasts around the paleoshoreline, and the diatom flora from cores (Barker *et al.*, 1990; Damnati & Taieb, 1995) confirm that the late Pleistocene High Magadi paleolake(s) was frequently dilute.

The High Magadi Beds were deposited during a period of high lake levels from *ca.* 23,700 to 9,310 y BP (Williamson *et al*., 1993). This implies that a period of relatively dry conditions might have existed after deposition of the lacustrine Green Beds, and the earliest lacustrine sediments of the High Magadi lake period (Behr and Röhricht, 2000).

2.2.3.4 Evaporite Series

After deposition of the High Magadi Beds, the basin underwent aridification, resulting in evapoconcentration of the lake waters and solutes in the lake brines, and ultimately, supersaturation of the brines with respect to nahcolite ($NaHCO_3$) and trona ($Na_3(CO_3)(HCO_3)•2H_2O$). The most recent evaporite unit consists of bedded sodium carbonate salts that are cumulatively up to *ca.* 40 m thick, but which contain intercalated layers of very dark brown to black organic silts and muds (Baker, 1958), some rich in silica (Cohen *et al*., 2016).

2.3 Methods

Fieldwork at Lake Magadi and Nasikie Engida included study and sampling of the exposed Green Beds sediments and cherts. Laboratory studies included thin section petrographic, and scanning electron microscope (SEM) examinations of more than 30 chert samples, X-ray diffraction (XRD) analyses of the cherts, and geochemical analyses (majors; traces) of the siliceous sediments (chert, magadiite, gels, silts and tuffs).

A PANalytical Empyrean X-Ray diffractometer (XRD) was used for mineral identification of powdered samples. Samples were powdered using a tungsten carbide swing mill. Select samples were rinsed with DI and dried before pulverizing. Finely ground powdered-samples were analyzed using a Co X-ray source, with a scanning rate of 1.2° a minute from 4 to 80 2 theta. A JEOL JSM 840A Scanning Microscope (SEM) was used to examine surface textures of the samples, and the details of the open pores. Samples for SEM analysis were rinsed with DI water to remove efflorescent crusts of

evaporites, broken to reveal fresh surfaces, desiccated, glued to sample stages, carbon-coated and then sputter-coated with a thin veneer of gold.

Major and trace element compositions were determined by Activation Laboratories Ltd., Ancaster, Ontario (Code 4E: exploration) using FUS-ICP, INAA, and TD-ICP techniques (http://www.actlabs.com/page.aspx?page=522&app=226&cat1=549&tp=12&lk=no&menu=64). The geochemical results will be discussed in Chapter 3.

2.4 The Green Beds

2.4.1 Stratigraphy and sedimentary facies

The Green Beds crop out peripheral to the bounds of the modern margins of the basin. Discontinuous outcrops can be found in the Northeast Lagoon, on the flanks of the Magadi (town) horst block, in the Eastern Lagoon, and in several locations south of the lake (Fig. 2.1). The Green Beds are composed of reworked volcanic detritus from the Oloronga Beds, and silts and tuffs rich in authigenic erionite, which give the outcrops a green colour after which this informal stratigraphic unit was named (Behr and Röhricht, 2000). This unit is up to 30 m thick in places, though observed frequently between 1 and 5 metres (Behr, 2002).

The Green Beds are easily identifiable by the resistant nature of the cherts within the formation. The Green Beds host ~ 90% of the chert in the Magadi Basin (Behr, 2002). This unusual chert crops out in both bedded and intrusive contexts. Outcrops of the Green Beds are both thin and rare. Study focused on the southern peninsula of the lake, where lacustrine sediments and cherts attributed to the Green Beds are common. Evidence and samples were obtained from an excavated road-cut and a pit dug in the adjacent plain (Plate 2.2).

Overall, a large proportion of the Green Beds is comprised of volcaniclastic silts and tuffs, as well as authigenic zeolites that replace some of the finer grained material. The silts of the Green Beds are distinguishable as a slightly coarser clastic portion within the overall lacustrine unit, though muds dominate. Röhricht (1999) found the silts to be composed of K-feldspar, plagioclase, pyroxene, ilmenite, magnetite, and calcite, sourced from the Oloronga Beds, the surrounding volcanic catchment, and as far away as the Nguruman Escarpment. The chert fragments and K-feldspar clasts are slightly rounded, whereas the plagioclase is idiomorphic (Behr and Röhricht, 2000).

Volcaniclastic tuffs are common in the Magadi Basin. The Green Beds contain many fines as a result of ash falls or volcanic rocks physically and chemically weathering to fine-to-coarse ash-size (1 μm – 2 mm) particles. The matrix of the Green Beds tuffs is predominantly composed of the zeolite erionite.

Erionite forms columnar aggregates some of which have been replaced by amorphous silica (Röhricht, 1999). The larger grains in the tuffs are composed of green chert fragments (1–3 mm), dark trachyte fragments (1–2 mm; <5% by volume), and granular brown calcite. The trachyte fragments include crystalline Na-sanidine, aegirine-augite, plagioclase, ilmenite and magnetite (Behr and Röhricht, 2000). The non-silt clastic component in the Green Beds is minor, however, making up only 5% of the tuffaceous sediments (Röhricht, 1999).

The following observations were made by digging a small trench, and clearing an exposed face of Green Beds outcrop. The top of the trenched sediments (lower Green Beds; Plate 2.2 (A)) is stratigraphically equivalent to the bottom of the cleared outcrop section (upper Green Beds; Plate 2.2(B)).

The lowermost sediments (Plate 2.2(A)) exposed in the dug-trench are a poorly bedded, 10 cm thick blue-grey silt layer grading upwards into 40 cm thick laminated black silt with a rubbery texture. This black silt unit contains a thin (1–2 cm) nodular chert horizon with a reticulate patterning on the chert surface. The black sediments directly overlying this horizon contain both fossil fish and carbonized (?) plant fragments, lying within a vertical cm of each other. The host sediments of the fish fossils, which are found below the plant fragments, show evidence of synsedimentary tectonism, with structures that resemble "molar-tooth structure" (Pollock *et al.*, 2006) Above these black sediments are grey-green silts exhibiting a weathered orange mottling. These mottled grey-green silts extend to the top of the dug pit (23 cm thick), and are capped by a 2–3 cm thick-bedded chert preserving shrinkage cracks and reticulate patterning. The top 14 cm of the bed of grey-green silts show a faint laminated fabric, which grades into a more burrowed and massive fabric from 14 to 23 cm from the top of the section. This grey-green silt unit is intersected by a very thin (< 1 cm), uniform ash layer.

Another section (Plate 2.2(B)) was cleared to expose sediments stratigraphically higher than the previously described sediment. The bottom 75 cm of sediment, resting upon a wavy chert bed, consists of a massive green mudstone that exhibits visible jointing and pervasive oxidation of iron-bearing minerals. This layer is burrowed near the base, with a granular infill occupying the burrows. Capping this green mudstone is a heavily iron-stained, orange-coloured layer, 7 cm thick. This layer is laminated toward the top and massive toward the base. Above this layer is a 25 cm thick unit of green muds, which exhibit fine laminations and burrows near the top. Above this is 15 cm thick unit, exhibiting the same sedimentation style as the previous layer (green mudstone;

Plate 2.2 - Green Beds sediment profile; (A) – Lower Green Beds section; Southern Peninsula; (B) Upper Green Beds section; Southern Peninsula

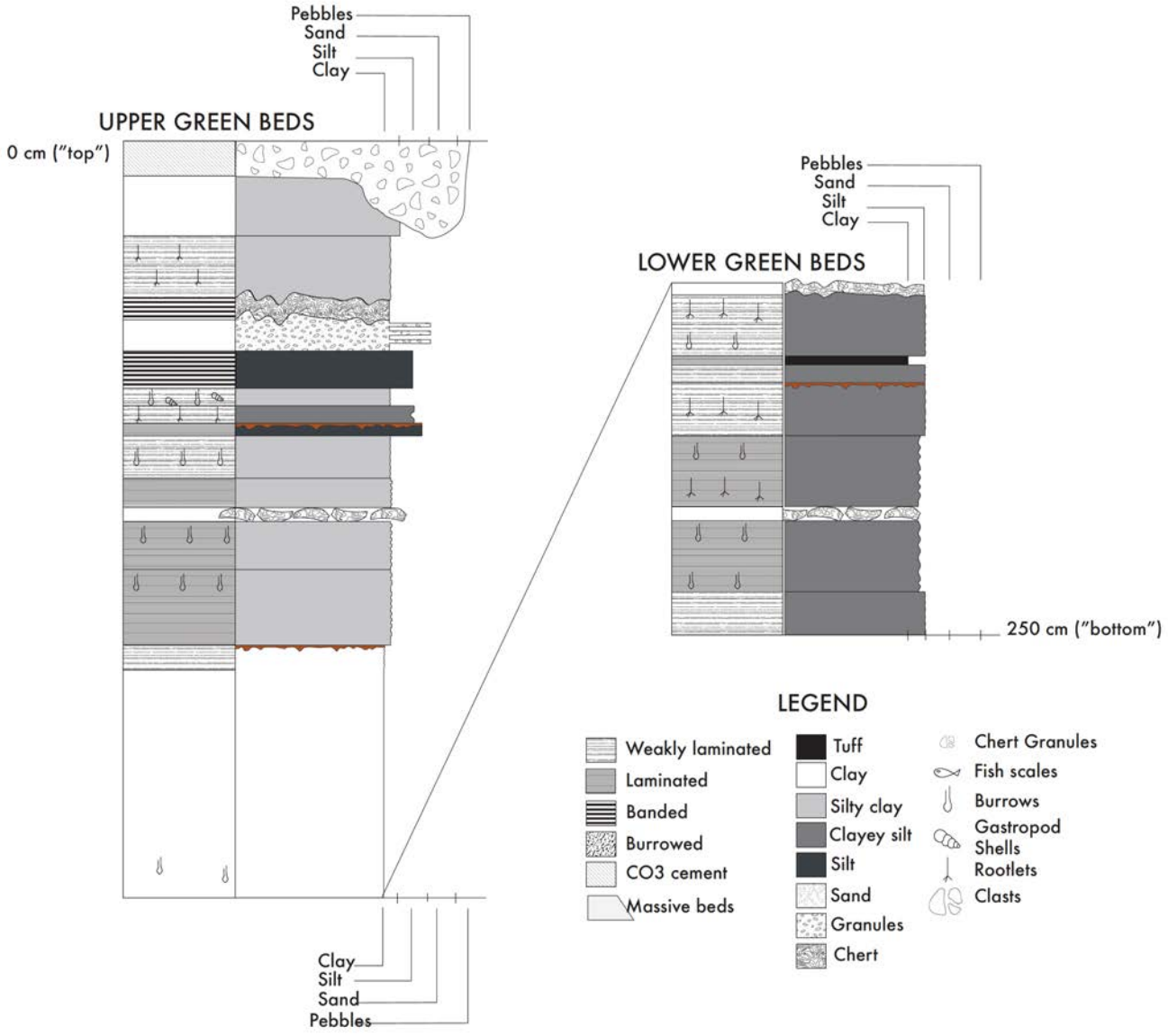

Figure 2.3 – Detailed lithostratigraphy of the Green Beds section(s)

massive at the base, finely laminated and burrowed near the top). A thin horizon of nodular chert intersects this laminated green mud, which continues for another 10 cm above the chert. Laminations above this horizon exhibit alternating green/white layers for 15 cm. This unit is burrowed with a pellet infill (Fig 2.3).

The largely green mud sediments seen thus far in this section quickly grade into a depositional variety. A thin iron-stained (orange) crust on top of the green muds is overlain by a green muddy siltstone, 5 cm thick, containing rootlets and plant fragments. This muddy siltstone is capped with weakly laminated gastropod shells, the first occurrence seen in this study of the Green Beds. The sediments grade into a 25 cm thick dark grey-green mud, "waxy" with white streaks in the bottom half and containing chert granules near the top. A banded, undulating, laterally extensive chert layer, nearly 6 cm thick, caps the dark muds.

Above this chert layer is a distinct 25 cm thick deposit of a white-to-buff mud and clay unit with abundant plant debris. A layer of yellow-green silty-clay rests above the buff sediments, pinching out laterally. The entire sequence is capped by a 15 cm thick calcrete, containing chert clasts as well as clasts of silty-clay. This calcrete layer was observed to transition laterally to a bedded chert layer.

2.4.1.1 Occurrences of chert in the Green Beds

Near the top of the second section is the first observed occurrence of *in situ* bedded cherts as defined by Behr & Röhricht (2000). The surface of the southern peninsula is blanketed with cm-dm scale fragments (plates) of bedded chert debris, much of it resting loosely on an eroded silty surface. In section, the bedded cherts appear to form two

cycles, capping units of silt 0.5–2 m thick. In places, the silts have been washed away to leave only piles of chert plates. These cherts will be discussed in the next section.

The exposed Green Beds sediments have been intruded by various forms of voluminous dyke-like or pillow-like chert breccias. However, the intrusive cherts are not seen well in vertical profile with the sediments they crosscut.

Other occurrences of Green Beds cherts were observed in the Northeast Lagoon, the East Lagoon, and along the Magadi horst fault lines (Fig. 2.1(B)). Each location hosts its own unique chert features.

The subaerially exposed surface of the Northeast Lagoon and the southern peninsula (Fig. 2.4) hosts many morphological subsets of cherts. A weathered light-orange to light-grey, 3-5 cm thick, discontinuous bedded chert with mm-wide and cm-to-dm long evaporite moulds, exhibiting striations and penetrative twinning (Plate 2.3(A)), covers patches up to tens of metres in diameter. These moulds occur on the surface of the samples, penetrate inwards at random, and show mould intersections at 120-140 degree angles. Intrusive chert ridges, 2-to-30 m in length, 10 cm – 2m in height, and up to 30 cm wide (Plate 2.3(B)), intrude the sediments of the valley floor (Behr, 2002) . These intrusions lie parallel to regional N-S strike, and commonly taper in one direction. The internal chert structure shows brecciation.

A possible fossil spring vent was also observed in the NE lagoon (Plate 2.3(C, D)) approximately 200 m north of the shoreline in July 2013. The deposit, composed of chert, consist of low (< 40 cm high) central mound about 8 m in diameter surrounded by a series of low terraces, most of which lie to the south and west. The mound consists of a discontinuous subcircular dam enclosing a rubbly central depression. The dam, up to 4 m

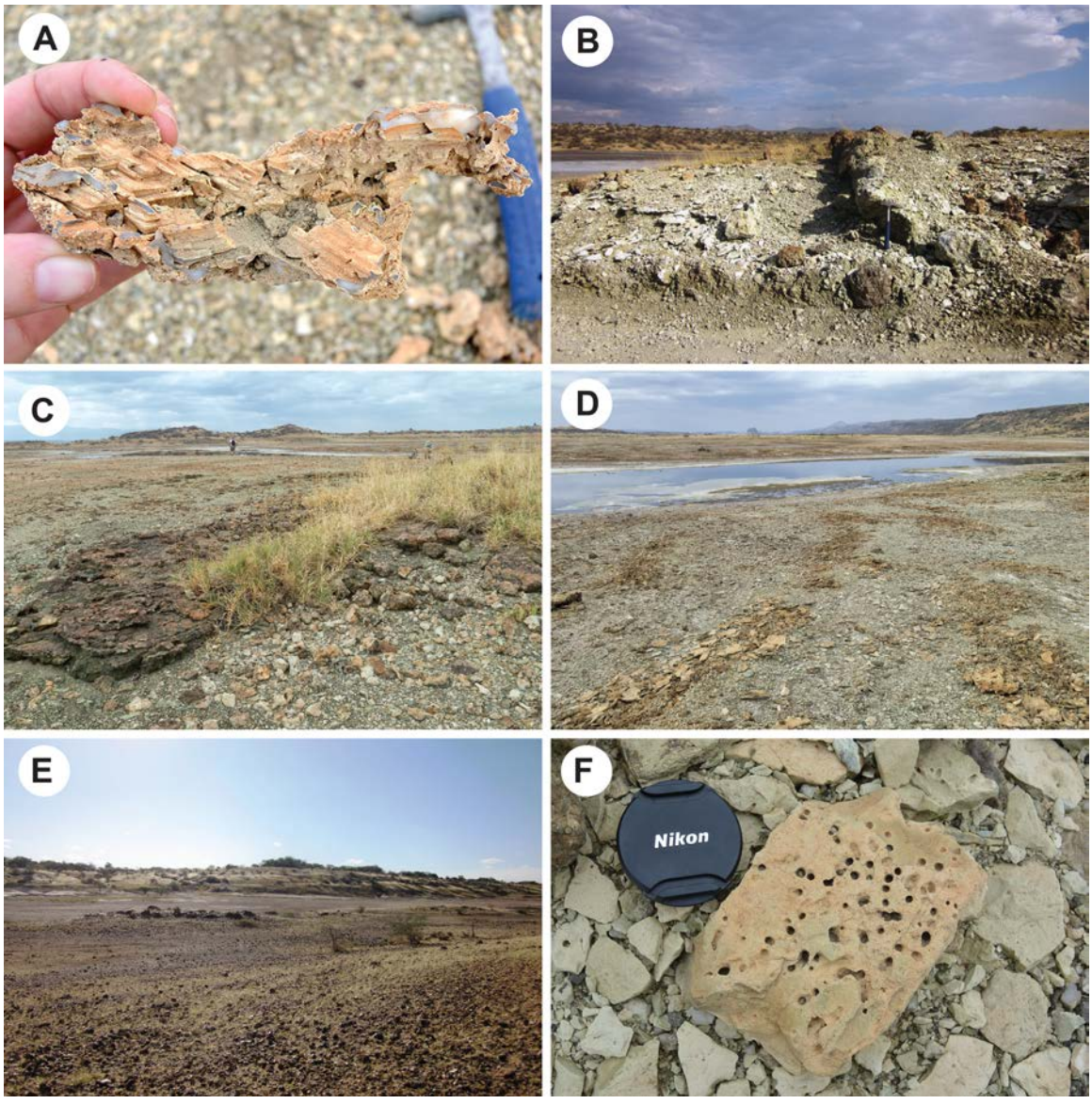

Plate 2.3 – Green Beds – Notable Outcrop Features; (A) Bedded chert with pervasive evaporite moulds; Green Beds outcrop; Northeast Lagoon; (B) Intrusive chert ridges; Green Beds outcrop; Southern Peninsula; (C) Possible fossil spring vent mound; Northeast Lagoon; (D) Silica terraces associated with possible fossil spring vent mound; Northeast Lagoon; (E) Clusters of diapiric pillow chert mounds; Eastern Lagoon; (F) *Skolithos* traces found in Green Beds silts

wide along the southern margin, consists of thin (< 5 cm) beds of red and green chert dipping at a few degrees towards the south and west. Crude terraces with rims about 50 cm apart are visible on the dam surface. Below the dam are a series of well-preserved linear and arcuate terraces. Each terrace consists of platy broken and recemented chert fragments, most of which are reddish. The terraces enclose former shallow (< 5 cm) pools composed of mainly broken fragments of pale green to grey chert. Individual terrace rims are up to a metre across; the inferred pools are up to 4 m from rim to rim and 2 to ~10 m wide. The terraces extend from the mound for at least 30 m before losing definition.

The central mound with peripheral terraces indicates that this feature was a subaerial spring. It is present in an area of Green Beds outcrop. Although it is younger than the Green Beds, from its chert composition and state of preservation it is reasonable to assume it is of the same general age and records a former spring with substantial discharge, given the size of the outflow terraces. No clear indicator of water temperature was recognised, but the cherts do not have typical features of high-temperature sinters. The fluids were silica rich but not necessarily very hot. The deposit nonetheless is good evidence for spring inflow into the Green Beds paleolake.

The East Lagoon hosts the diapiric pillow-cherts (Behr & Röhricht, 2000), which form as clusters aligned to the general regional strike (N-S) (Plate 2.3(E)). The East Lagoon is terminated at the west by the horst upon which the town sits (Magadi horst), which is flanked by cherts that are intrusive and voluminous, in places showing uniformly deposited concentric layering on outer surfaces covering brecciated chert cores. These cherts are found along the surface expression of the presumed N-S striking fault planes between the Magadi horst and the adjacent lake basin grabens (Fig. 2.1).

2.4.1.2 Lower and upper Green Beds contacts

A lower Green Beds contact with the underlying Oloronga Beds has not been recognized in outcrops. However, the base of the Green Beds has been observed in places to be in disconformable contact with the trachyte, witnessed south and southwest of Lake Magadi (Baker, 1958). Contacts between the Green Beds and High Magadi Beds are seen on the southern peninsula (Fig. 2.4(C)), with the fine grained brown silts of the High Magadi Beds resting disconformably on calcrete of the Green Beds, west of the Southwest Lagoon, and also in the "Dry Lagoon" (Eugster, 1980) along the track from Magadi town to the south end of the lake (Baker, 1958). Pale brown tuffaceous silts of the upper unit of the High Magadi Beds overlie intrusive and domal Green Beds cherts at several sites in the East Lagoon (Fig. 2.4).

2.4.1.3 Ichnofossils in the tuffs and silts

Röhricht (1999) noted ichnofossils in the Green Beds, describing mm-scale *Skolithos* in the tuffs and silts (Plate 2.3(F)), and mm-to-cm scale *Skolithos* and *Arenicolites* in the bedded cherts. Scott (2010) noted small, open vertical burrows (*Skolithos*), and small-to-medium sized 3D burrow systems in the silts of the Green Beds, believed to have been created by various insects (tiger beetles, spiders, and/or earwigs). Not to be confused with the marine *Skolithos* facies, traces in the Magadi basin are classified morphologically. The observed ichnofossils give evidence for periodic subaerial exposure because the organisms that produced the traces require atmospheric oxygen to survive.

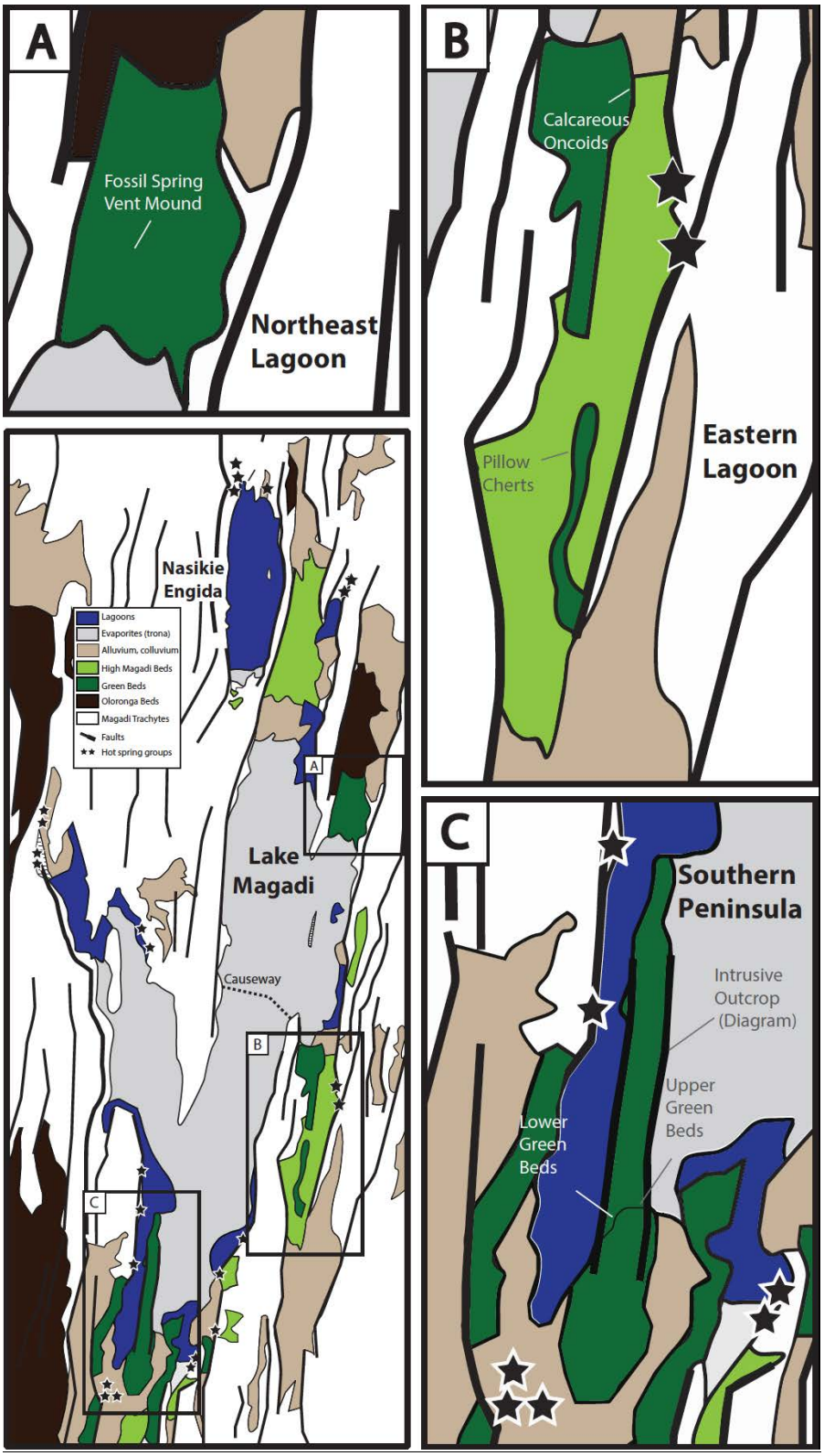

Figure 2.4 - Green Beds Outcrops

*** HMB sediments in the Eastern Lagoon have weathered around GB intrusive cherts ***

2.4.1.4 Calcrete

A calcrete horizon at the top of the Green Beds unit consists of coarse Green Beds sediments with a mm-scale calcite coating and, in places, incorporations of angular chips of chert, producing a calcite-cemented chert gravel. The calcrete unit in outcrop is traceable as a continuous layer, up to 10 cm thick, occurring only on the uppermost exposures of the Green Beds outcrop (higher elevations of the southern peninsula). This capping calcrete horizon was noted by Behr & Röhricht (2000), and in the past may have been mistaken for the 'caliche' horizon thought to lie between the Oloronga Beds and the High Magadi Beds (Eugster, 1980; Plate 2.1(D)). The calcretes of the Magadi basin have been studied in detail in Felske (2016).

2.5 The Cherts of the Green Beds

Behr & Röhricht (2000) reinterpreted the origin of many of the cherts after discovering trace fossils and evidence of microbial activity within the cherts themselves. They used these observed features along with U/Th dating of the cherts (Goetz & Hillaire-Marcel, 1992) to separate the Magadi-type cherts of the High Magadi Beds (6.3 ± 1.8 ka), from the cherts of the Green Beds (98.5 ± 20 ka). Williamson *et al.* (1993) reported a U/Th age of 40 (+6/-7) ka for the upper Green Beds sediments.

Behr & Röhricht (2000) defined distinct groups of chert in the Green Beds, based on their field appearance and relationship to the overlying and adjacent strata. Two main types of Green Beds chert are recognized in this study: bedded and intrusive. Within these chert groups are related morphological subsets. The bedded cherts are a laterally extensive, platy chert unit occurring near the top of the exposed Green Beds and are

interspersed with layers of detrital sediment of variable thickness (cm–dm). The intrusive cherts cross cut the Green Beds unit and are formed by the amalgamation of two siliceous precursors (one viscous and one, more fluid). Together, they form a cemented chert breccia that occurs in various intrusive forms (dykes, diapirs, domes). These intrusions are restricted to the Green Beds and are not seen cross-cutting the Oloronga Beds or High Magadi Beds in outcrop.

2.5.1 Field Observations

2.5.1.1 Bedded cherts

The bedded cherts are abundant and laterally extensive on the southern peninsula, and in the northeastern embayment (Fig. 2.1 & 2.4). Behr & Röhricht (2000) described the bedded cherts as a 1–2 m-thick unit of platy chert intercalated with layers of green tuffs and silts. The chert beds themselves are weathered to a light-grey to buff to reddish-orange colour on the surfaces, display a light-to-dark grey fresh broken surface, occur as 1–3 cm thick undulating layers with low amplitude, and on the uppermost surface, in places, occurs as piles of 20–50 cm diameter "plates". Locally extensive chert surfaces are preserved intact, and show exposures up to 5 m across (Plate 2.4(A)). The chert beds are observed as the resistant upper surface of the outcrop in many locations.

The main morphological features observed in the bedded cherts are either preserved on the upper surface of the cherts, or are characteristic of the entire bed itself. Features observed on the surface of the cherts include evaporite pseudomorphs, raindrop impact structures, shrinkage cracks, lobate protrusions (Eugster, 1969), water escape structures, and current ripple bedforms (Behr, 2002).

Evaporite pseudomorphs have been documented several times in Magadi literature (Baker, 1958; Eugster, 1969; Behr and Röhricht, 2000). The moulds are commonly preserved with sharp, undeformed crystal mould margins. Many are 1–3 mm deep, and mm- to cm in length, depending on morphology. Morphologies include fan-like sheaves (up to 15 cm in length) (Plate 2.4(B)), crystal 'trains' (5–30 cm in length, which consist of several crystal moulds aligned in a row), or scattered individual moulds without orientation (3–10 mm in length). One exceptional specimen shows large (2 mm deep, 8–10 mm across) cubic and rhombic crystal moulds. The most common mould morphologies are locally filled with crystalline calcite to form casts.

Circular pits that resemble raindrop impact structures are rare, but were observed on a broken and loose plate of chert on the southern peninsula. The depressions were observed as round, shallow (*ca.* 1 mm) circular marks (2–5 mm in diameter) very densely spaced on the chert surface.

Polygonal cracks, though also rare, are present only on chert bed surfaces that lack evaporite pseudomorphs, and (or) possible sliding, petee, or tepee structures (Plate 2.4(C)). The polygonal cracks are v-shaped, 1–2 mm deep, 1–3 mm wide, are connected in a network to create by 1–2 cm wide, irregularly-sided polygons, and display a fine-grained infill of calcite-cemented silts. A platy chert sample was found in a pile of loose chert plates, and 'way up' could not be determined definitively, but the polygon edges are rounded, making an argument for a cast of a lower bed (positive hyporelief).

Lobate protrusions were found on a few of the bedded chert surfaces, with 1–2 cm lobes occurring in dense clusters. The platy samples containing these features were not found *in situ,* so 'way-up' could not be determined.

Scott *et al.* (2012) noted 1-mm wide, 1-cm deep excavation pits, as well as associated traces that indicated 'creeping' on a bedded chert surface. Those traces might have been created by beetle larvae (Behr and Röhricht, 2000). Scott (2010) also noted small, shallow 'pock marks' on the surface of the bedded cherts, which she interpreted as feeding pits of insects (*Diptera*, *Ephydridae*) (Plate 2.4(D)). Possible vertebrate footprints (hyena and rhinoceros) were observed on the surface of the bedded cherts near the Southwest Lagoon (Scott, 2012).

Water escape structures and current ripples were noted by Behr (2002), but not recognized in this study.

The features that are characteristic of the chert beds themselves include many microbial mat-like structures. These features include laminae or 'growth bedding', petee structures, and 'fairy rings'. 'Growth bedding' (Gerdes *et al*., 1993) is observable as cyclic beds of slightly wavy surfaced chert, mm-to-cm thick (Plate 2.4(E)). These beds are observed as small two- or three-layer "stacks" or repetitions of chert beds.

Petee structures (Gerdes *et al.*, 1993) are common in the bedded cherts, with folds up to 5 cm in amplitude and 10s of cm in length. The folds are complex, with multiple generations of folding oriented in several directions. In some samples, the folds appear to have rolled over on themselves (Plate 2.4(F)).

'Fairy rings' (Gerdes *et al.*, 1993) were observed in the Northeast Lagoon near a possible former spring-vent (described below). These features are nearly cylindrical, up to 20 cm tall, and 7–10 cm in diameter. The outer surface of the ring is laminated, having the appearance of incremental growth. However, the internal structure of these features is

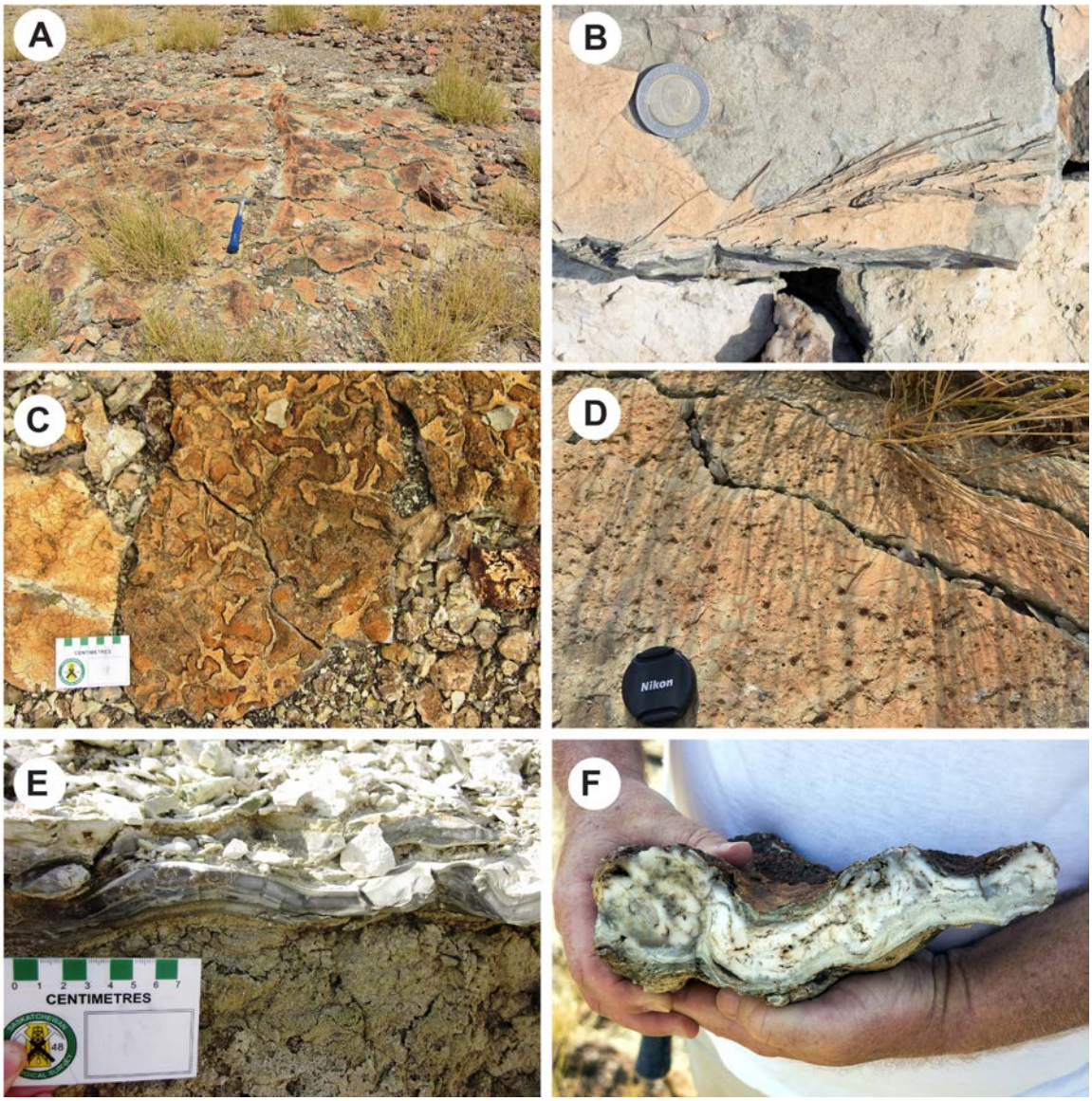

Plate 2.4 – Bedded cherts of the Green Beds unit; (A) Intact bedded chert surface exposure; Green Beds; Southern Peninsula; (B) Evaporite moulds in fan-like sheaves preserved in bedded chert surface; Green Beds; Southern Peninsula; (C) Tepee and petee structures in the bedded chert; Green Beds; Southern Peninsula; (D) Small, shallow 'pock marks' on the surface of the bedded cherts; Green Beds; Southern Peninsula; (E) Cyclic beds of wavy chert layers; Green Beds; Southern Peninsula; (F) Complex "rollover" folding in the bedded chert; Green Beds; Southern Peninsula

brecciated, with two generations of chert (white brecciated chert fragments and grey chert cement). These features are associated with bedded cherts in outcrop, but are anomalous in their compositional characteristics in comparison to the platy bedded cherts. Their internal structure is more similar to that of the intrusive cherts (see next section).

2.5.1.2 Intrusive Cherts

Intrusive cherts are found in several locations, including lagoonal embayments (m-scale domal cherts that superficially resemble pillow lavas; Plate 2.5(A)), and along surface expressions of presumed fault lines flanking N-S horsts (pillow cherts and dykes) (Fig. 3 (A&C - dykes), 3 (B - pillow cherts) in Behr & Röhricht, 2000). Where present, these light-to-dark red weathered cherts intrude exposed Green Beds sediments. Most of these internally chaotic, voluminous intrusive cherts crop out parallel to N-S faults and along inferred regional N-S striking fractures (Fig. 2.1). Behr & Röhricht (2000) classified them according to their deformational structures:

1. *Pillow chert* – round to ovoid diapiric mounds consisting of brecciated masses of white chert sealed by greyish silica that might have been emplaced in a fluid state. Some of these cherts superficially resemble pillow lavas in morphology (hence their name), but many mounds are internally laminated on a cm-scale or show successive brecciated laminae.
2. *Chert dykes* – linear or curvilinear intrusions of silica that form dyke-like bodies many metres long and up to a metre wide, composed of subangular chert fragments cemented by cryptocrystalline silica.

'Pillow cherts' (Plate 2.5(A)) are common in the middle of the Eastern Lagoon, where most chert masses are aligned in N-S striking clusters, following the regional tectonic trends. These mounds are 0.5–1 m high and *ca.* 1 m to 3 m in diameter.

The east and west fault lines defining the edges of the Magadi horst show voluminous, internally brecciated cherts mantled by a few centimetres of thin concentric chert laminae, exposed from the graben floor up to half-way up the horst flanks. The mounds are up to ~5 m high, 1–3 m wide, and tens of metres long along the fault lines. These fault-flanking, internally-brecciated cherts do not form discrete pillows, but instead appear to be large chaotic masses.

The Northeastern Lagoon also hosts many intrusive cherts, though their morphology is intermediate between pillows and dykes. The intrusive cherts of the NE lagoon show large intrusive masses, 1–2 m wide, that taper into more dyke-like intrusions (30–50 cm wide), with the tapered end trending down, disappearing beneath the sediments in 10–20 m of length.

Most chert dykes are located on the southern peninsula and in the Northeastern Lagoon. Eugster (1969) described them as the borders of desiccation polygons, extruded upon compaction. They typically rise 0.5–1 m above the adjacent land surface, and are 30–50 cm wide, and up to tens of metres long (Plate 2.5(C)). Many are oriented N-S, cross-cut by secondary intrusions that have an E-W orientation. In outcrop, the dykes show brecciation, with 1–10 mm irregular white chert fragments cemented in a denser microcrystalline grey chert. The chert dykes are white to grey on fresh surfaces. On exposed weathered surfaces they vary from greyish-green to greyish-red, and from

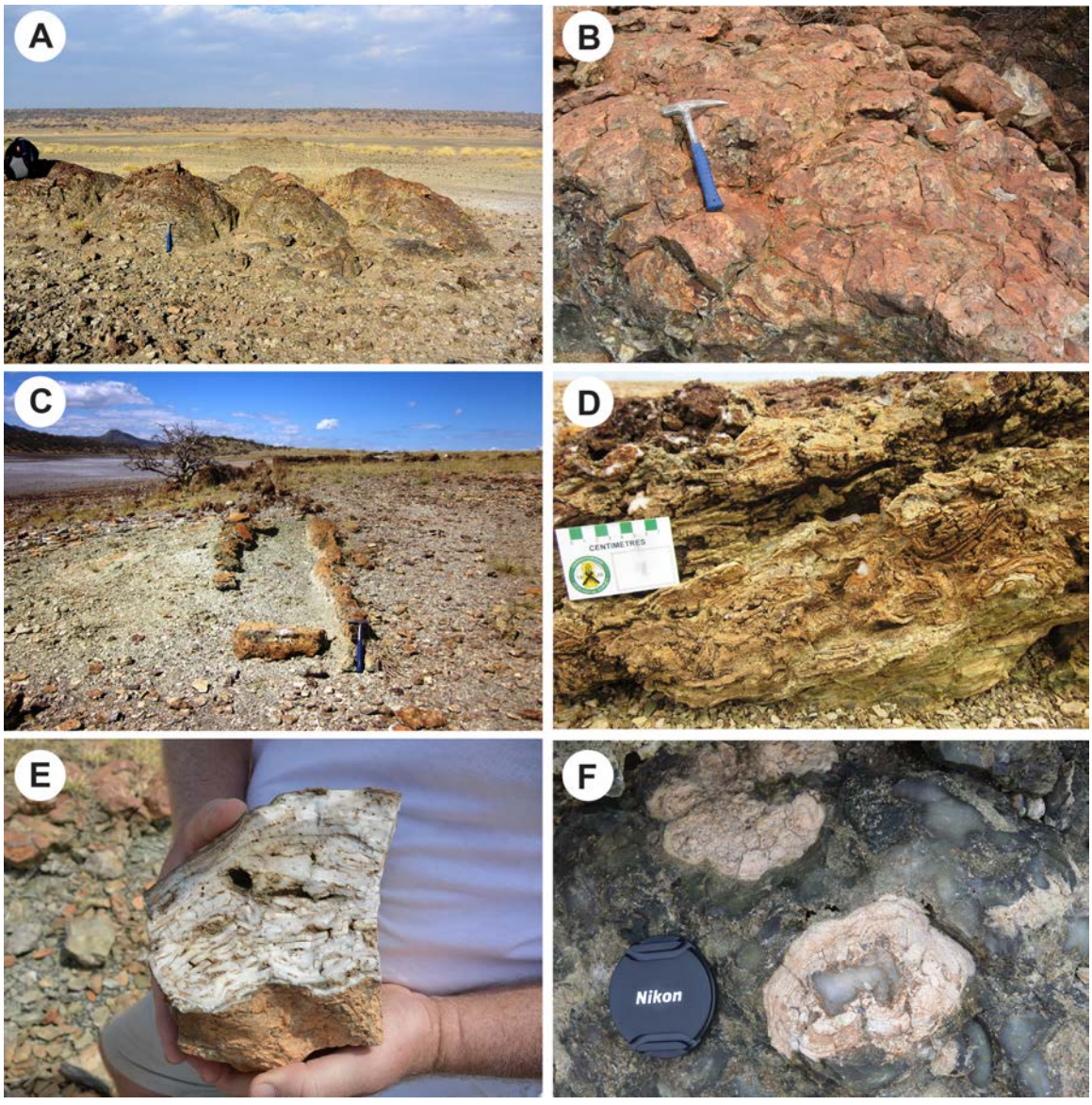

Plate 2.5 – Intrusive cherts of the Green Beds unit; (A) Cluster of diapiric pillow-like cherts; Green Beds; Eastern Lagoon; (B) Pillow chert with cumulative mound structure; Green Beds; Southern Peninsula; (C) Chert dykes; Green Beds; Southern Peninsula; (D) Deformed and weathered banding in chert dyke exposure; Green Beds; Southern Peninsula; (E) Autobrecciation of chert layers within an intrusive mound sample; Green Beds; Southern Peninsula; (F) Small calcareous oncoids in intrusive chert surface; Green Beds; east side of Town Horst Block

orange to deep red. Surfaces often show preservation of deformed and weathered banding (Plate 2.5(D)). These dyke cherts have locally pushed up the adjacent silty green sediments along their margins by a few cm.

In several locations (Fig. 2.3; Eastern Lagoon and South Peninsula), pillow cherts show a central brecciated chert body mantled by smaller "parasitic" mounds. These cherts are white-grey on fresh surfaces, and weathered to orange-red-grey on the surface. The central brecciated chert bodies are 0.5–1 m in diameter. The attached parasitic mounds are 0.2–0.5 m in size, seen on the top and sides of the central chert bodies. The cumulative mounded structure is draped with cm-scale bands of chert, which join over the numerous clustered chert bodies to fuse the central body and parasitic mounds into one large united mass of chert (Fig. 2.5; Plate 2.5(B)). These drape structures are stromatolitic in appearance, showing 0.5–1 cm thick layering, with local crystal pseudomorphs preserved between laminae.

Some mounds exhibit autobrecciation of the outer mm-scale layers of chert. These broken laminations exist as subparallel intraclasts commonly with sharp edges and slight displacements, so that one can observe complementary margins (Plate 2.5(E)).

Small nodular calcareous oncoids (Plate 2.5(F)) in the intrusive cherts of the Green Beds were sampled from the surface of an intrusive chert outcrop on the eastern shore of the SE Lagoon, and from an chert outcrop along the eastern fault line of the Magadi horst (Fig. 2.4(B)). Behr (2002) described in detail these "bacterial stromatolites". These pinkish concentric structures, considered oncoids in this study, are embedded in the chert outcrop, are individually up to 20 cm in diameter, and are composed of thin, concentric laminae of calcite, which thickens slightly on the pinnacle crests.

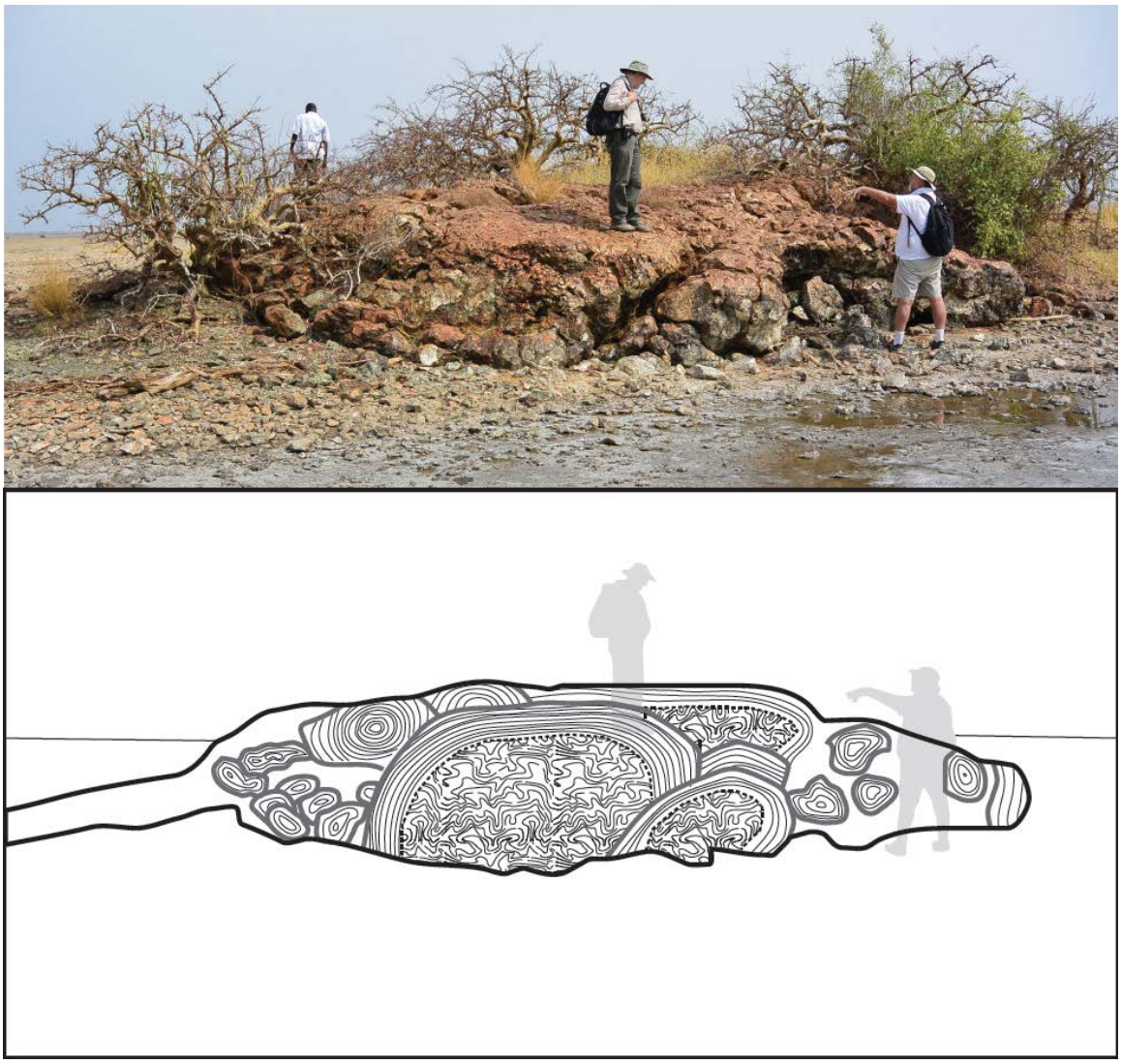

Figure 2.5 – Intrusive chert – cumulative mound structure

They form small colonies, occurring in groups of three to eight (as seen in outcrop). Aside from these structures, no other original carbonate structures or replacement textures were observed in the intrusive cherts.

2.5.2 Laboratory analyses

2.5.2.1 Bedded cherts

All varieties of bedded chert are composed of micro- and cryptocrystalline quartz and chalcedony. Most bedded cherts show fracturing along their outer edges, commonly perpendicular to bedding, and exhibit sharp boundaries, many vacant of infill but locally filled by silt sized detrital particles derived from trachyte and authigenic minerals. Less commonly, silts partly fill the primary porosity of the bedded cherts. Detrital minerals include anorthoclase and sanidine, aegerine, and iron-bearing minerals (Baker, 1958). Authigenic phases include erionite, analcime, and illite (Behr, 2002; Schubel & Simonson, 1990).

Pore spaces and deeply rooted (>1 cm) fractures are locally lined by fibrous radiating chalcedony cement (Plate 2.6(A)), but pore space is rarely fully occupied. Unlike the intrusive cherts, pores in the bedded cherts rarely contain calcite cement.

Bedded cherts exhibiting rolls and folds (Plate 2.4(F)) also display internal brecciation and chalcedonic cement. The brecciated fragments are from two to eight microns long, and composed mainly of cryptocrystalline quartz (Plate 2.6(B)).

In places, a few mm (1–3) of the upper and lower margins of the bedded chert layers have a ‘rind’ of fine impurities. The groundmass of the rind is composed of fine-grained detrital minerals cemented by calcite. When viewed by SEM, the bedded cherts show

smooth massive fresh surfaces with little topographic relief, and open fractures partly lined by euhedral quartz crystals, 5–10 microns long (Plate 2.6(C)).

2.5.2.2 Intrusive Cherts

Behr & Röhricht (2000) described the intrusive facies as a brecciated chert cemented by spherulitic quartzine. This is seen in most intrusive Green Beds cherts. XRD analyses confirmed that most samples are indeed composed of crystalline quartz (Fig. 3.2; Fig. 3.3).

In thin section, the intrusive cherts show a brecciated texture with angular clasts, 0.5 to 3 mm in size, composed of micro- to cryptocrystalline quartz. Clasts are supported by a matrix of radiating length-fast and –slow chalcedony (Plate 2.6(D)). The brecciated samples show subsequent fracturing (post-cementation) resulting in an extensive pore and fracture system within each sample.

The most notable difference from sample to sample is the style and degree of fracturing and infill following lithification. The fracturing is not that of the initial brecciation, but of the whole sample (post-cementation – Plate 2.6(E)). Pore spaces and fractures, examined in thin section, display textures from crescentic to bubble-like to a ripped or torn appearance, indicating a range of pre-lithification processes.

Pore and fracture cement infills consist of fibrous radiating chalcedony and crystalline calcite. Only peripheral fracture systems host detrital sediments, which in places have altered to authigenic minerals (with the same composition as the infill in bedded chert fractures).

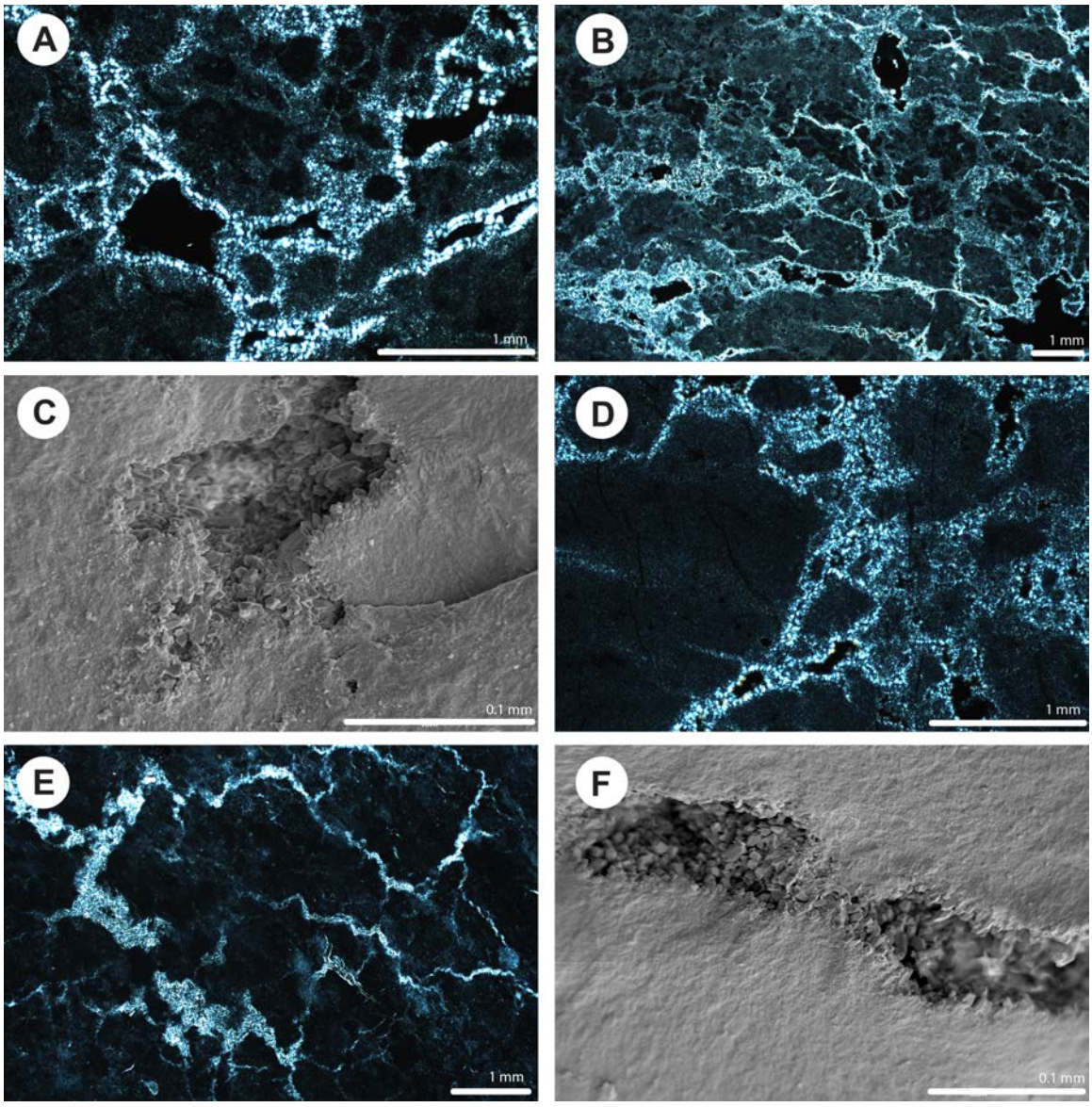

Plate 2.6 – Thin section and SEM micrographs – Green Beds cherts; (A) – Chalcedony cement filling fractures and lining pore spaces in a bedded chert samples; 40X magnified; XPL; (B) – Internal brecciation of bedded chert sampling; cementation by chalcedony; 12.5X magnified; XPL; (C) – SEM image of bedded chert pore space lined with quartz crystals; (D) – Microcrystalline quartz fragments supported by a chalcedonic cement in an intrusive chert samples; 40X magnified; XPL; (E) – Pervasive fracturing of the intrusive chert sample; post-lithification; 40X magnification; XPL; (F) – SEM image of intrusive chert pore space lined with quartz and calcite crystals

Many chert samples examined by SEM display a massive chert surface, with details preserved only in open pore spaces. As observed petrographically, many pores are lined with euhedral crystals of quartz and calcite, commonly 5–10 microns long (Plate 2.6(F)).

Microbial remains were not recognized in any of the bedded or intrusive chert samples. Most cherts appear to be mosaics of massive microcrystalline and cryptocrystalline quartz when viewed by SEM.

2.6 High Magadi Beds

2.6.1 Field Observations

The lower portion of the High Magadi Beds, which directly overlies the Green Beds, contains the bedded magadiite horizon that Eugster (1969) initially assigned as the precursor for all of the Magadi cherts. Eugster (1969) described the High Magadi Beds as being stratigraphically equivalent to the 'Chert Series' unit assigned by Baker (1958). The High Magadi Beds contain true Magadi-type chert, typified often by association with soft magadiite, chert surface reticulation, and in places, low-angle slickensides. Surface reticulations are small networks of shallow (1–3 mm deep), interconnected cracks (Plate 2.7(A)).

In places, outcrops of the High Magadi Beds display a lateral transition from magadiite to Magadi-type chert (Fig. 5 in Eugster, 1969). A fully exposed putty-like outcrop of pure magadiite is exposed in the Eastern Lagoon (Plate 2.7(B)).

2.6.2 Laboratory Analyses

The magadiite horizon of the lower High Magadi Beds was confirmed as magadiite by means of XRD (Chapter 5 (Appendix): Figure 5.9) and major element geochemical

analyses. In thin section, the magadiite samples from the southeast lagoon are shown to contain a large (30–50%) fraction of inclusions, including calcite, analcime, albite, siderite, illite, and/or potassium feldspar (Schubel & Simonson, 1990), but the optical properties of soft magadiite have not proven to be ideal for detailed petrography (primarily opaque). Magadi-type chert, on the other hand, shows a few unique characteristics.

In samples that have been converted to chert, the "grid-work" texture of the chalcedony (Plate 2.7(C)), described by Sheppard & Gude (1986), and Schubel & Simonson (1990), is easily observed by petrography. Also observed petrographically in Magadi-type chert samples is a mesh of irregularly-shaped, fine-grained chalcedony, interlocking to form a uniform cherty groundmass (Plate 2.7(D)). Unlike the grid-work texture, the interlocking habit is less indicative of a magadiite precursor. Edges of pore spaces in Magadi-type chert samples display radiating chalcedony with a connective mammillary surface, growing upon and even replacing the original magadiite.

Late-stage calcite cement is present in many pore spaces, with sub- to anhedral crystals 100 μm to 3 mm in length.

Schubel & Simonson (1990) noted that the surface of Magadi-type chert samples under a scanning electron microscope is "massive to lumpy with sparse small ridges" (Plate 2.7(D)), which was also recognized in this study. Pore spaces in Magadi-type chert samples locally preserve unaltered magadiite and kenyaite spherules, *ca.* 10 μm in diameter, which both display a fine-lepispheric to a book-like texture (Sheppard and Gude, 1986) (Plate 2.7(E & F)).

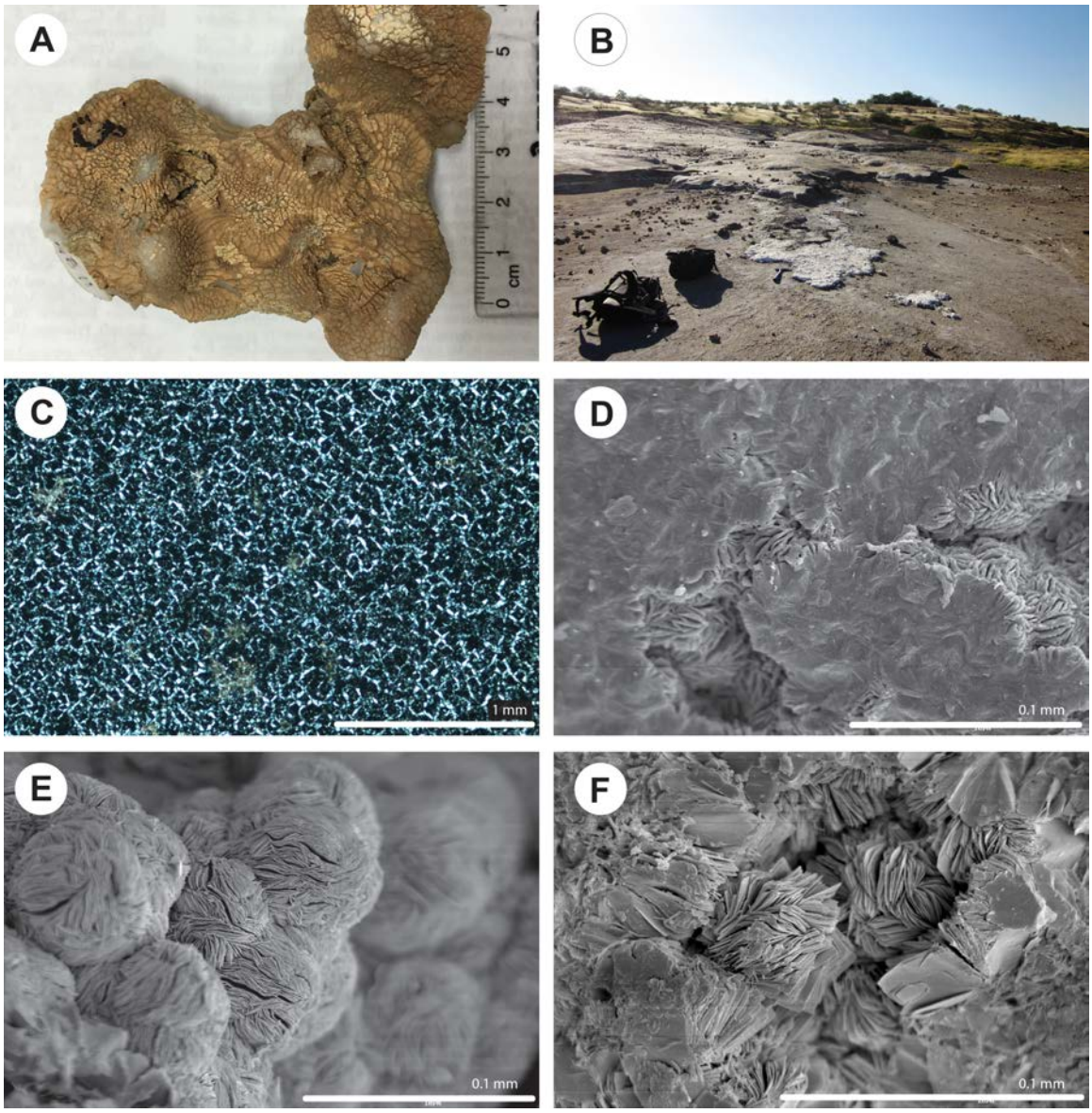

Plate 2.7 – Magadiite and Magadi-type chert; (A) Magadi-type chert sample displaying surface reticulation; (B) Outcrop of soft magadiite; High Magadi Beds; Eastern Lagoon; (C) "Gridwork" texture observed in Magadi-type chert sample; 100X magnification; XPL; (D) SEM image of Magadi-type chert; spherulitic structure of precursor magadite preserved along edges of the pore space; (E) SEM image of soft magadiite sample; interlocking sheets of the sodium silicate mineral forming a lepispheric texture; (F) SEM image of hardened magadiite sample; magadiite/kenyaite shown forming a flattened "book-like" texture

In Magadi-type chert samples, the pore space between the bladed spheres of magadiite became occluded with deposits of massive silica until a non-porous, interlocking chert surface formed, maintaining the original radiating textures of the lepispheres (Plate 2.7(D)). In some examples, the platy blades of the lepispheres appear to have disarticulated into flat, parallel layers.

2.6.3 Cherts from the High Magadi Beds

A few features observed in the cherts of the High Magadi Beds are unique to Magadi-type cherts, and have been consistently referenced in literature. The first, and most obvious, would be the lateral transition from magadiite to Magadi-type chert, with intermediate samples displaying a soft magadiite/kenyaite rind. These samples show an indisputable magadiite-chert relationship. The most well-known and most striking physical characteristic is reticulate patterning, which is observable at outcrop scale of Magadi-type chert (Plate 2.7(A)). This trait has been observed in many studies (e.g., Sheppard & Gude, 1986; Parnell, 1986; Krainer & Spotl, 1998; Sebag *et al.*, 2007), and has been taken as a primary means of identification. At Magadi, the presence of soft sediment deformation and low-angle slickensides are also characteristic of the deposit, though this might be a result of occurring in a tectonically active sedimentary basin (Behr & Röhricht, 2000).

SEM analysis is also very useful in Magadi-type chert identification. The edges of pore spaces are decorated with the radiating sheet-like growths of magadiite and kenyaite (Plate 2.7(E)). These mineral structures are observable in soft magadiite samples, which can be additionally identified by means of XRD. Magadi-type chert, on the other hand,

shows a strong crystalline quartz peak pattern in XRD analyses, which has overprinted the magadiite signal seemingly entirely (Fig. 3.2).

While fully chertified magadiite (Magadi-type chert) has a number of macro characteristics that aid in its identification, microscopic characteristics are at times subtle. "Grid-work" chalcedony has been observed in a number of instances (Sheppard & Gude, 1986; Schubel & Simonson, 1990; Bustillo, 2001), as well as this study. Schubel & Simonson (1990) interpret the grid-work texture to "be the result of a volume-for-volume replacement of magadiite by quartz with retention of the crystallographic orientation of the former by the latter", the latter being the lepispheric texture of individual magadiite spherules.

2.7 **Discussion and Implications**

2.7.1 Magadi-type Chert

The stratigraphic position of the chert-bearing unit has been contentious throughout the history of geologic exploration in the Magadi Basin. In the course of survey mapping the basin, Baker (1958, 1963) recognized two chert-bearing units: his 'Chert Series' and the High Magadi Beds. Baker described the Chert Series as lacustrine sediments containing both massive and platy cherts, but also included a "thin horizon of white slightly plastic powder" (later identified as magadiite) in the High Magadi Beds. Eugster (1969), however, believed magadiite to be the precursor to all chert in the Magadi basin, and assigned all chert to a singular unit, the High Magadi Beds. These conflicting conclusions reflect both the discontinuous exposure of the chert-bearing units, and the lack of age dating of the sediments during early investigations.

A significant theoretical conflict regarding the origin of the various chert types in Magadi was how the inferred precursor, magadiite, was thought to form in the lake (Eugster, 1969, 1967; Hay, 1968; Jones *et al.*, 1977). As this mineral had not been encountered previously, early theories described precipitation in relatively deep water conditions (compared to today). The 'High Magadi' lake was believed to be up to 13 m deep, based on strandlines observed around the basin margins, and exist seasonally as a stratified water mass (Eugster, 1969). The seasonal hypolimnion was theorized to be dense, saline, and alkaline (and therefore Si-rich), evolving geochemically through evaporative concentration during the dry season (Fig. 2.6). A seasonal hyperlimnion was thought to be sourced from rainfall and runoff, placing a layer of fresher water over the denser saline perennial waters. Magadiite was believed to form at the chemocline between the two distinct water masses, with a drop in pH allowing for the saturation and precipitation of the hydrous sodium silicate. Magadiite would have accumulated on the lake bottom in a continuous layer. Magadiite was thought to convert to (Magadi-type) chert upon evaporation, exposure, and subsequent surface leaching by dilute water. Although there is evidence of a deep lake during High Magadi Beds deposition (strandlines (Hillaire-Marcel and Casanova, 1987), preservation of fish fossils), the evidence for magadiite and Magadi-type chert forming in deep water is not clear.

The magadiite in the lower unit of the High Magadi Beds was deposited largely as a continuous layer. In the regions where the magadiite has lithified to chert, this chert is found to crudely and superficially resemble (in terms of thickness and lateral continuity) that of the bedded cherts of the Green Beds. The soft, putty-like consistency of the magadiite was also believed to have the necessary thixotropic properties to create the

dyke and pillow cherts seen around the basin. This phenomenon was thought to have occurred during sediment compaction (Eugster, 1969). With these macro-observations, magadiite was long considered to be the precursor to the basin's cherts.

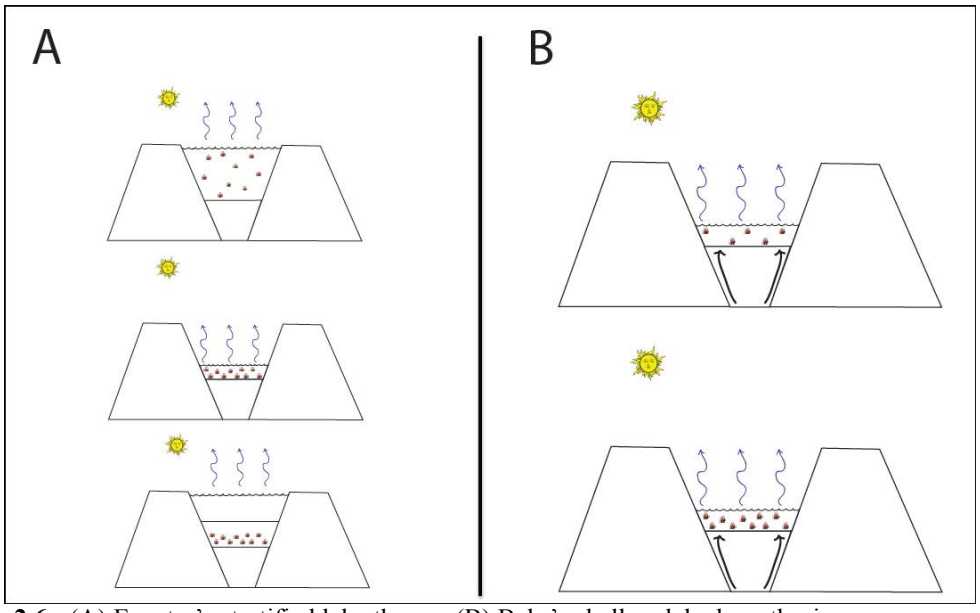

Figure 2.6 - (A) Eugster's stratified lake theory; (B) Behr's shallow lake hypothesis

"Magadi-type chert" has become entrenched in literature as the type of chert that forms readily in saline, alkaline basins (e.g., Sheppard & Gude, 1974 (United States); Parnell, 1986 (Scotland); Krainer & Spötl, 1998 (Italy); Sebag *et al.,* 2001 (Chad)). Certain indicators of saline, alkaline environments (e.g., evaporite pseudomorphs, zeolites) have led researchers to characterize cherts as "Magadi-type", when it is possible that chert formed from other precursors. "Magadi-type chert" is, by definition, chert that forms from magadiite, but only certain methods allow for proper identification. References to Magadi-type chert in literature all share one defining characteristic: fine reticulate patterning; believed to occur as the result of volume loss from magadiite during diagenesis. While this pattern is observable on a number of chert specimens around the

basin, the vast majority of chert in the Magadi basin does not exhibit this fine dewatering pattern.

2.7.2 Recent reconsideration of lake history

The deep, stratified lake hypothesis was challenged by Behr (Behr & Röhricht, 2000; Behr, 2002) upon the discovery of ichnofossils in the chert precursor, which implied shallow conditions during magadiite formation. Behr believed that most (90%) of the chert in the basin was in fact not "Magadi-type", and that chert precipitation was often influenced by evaporative (to achieve supersaturation with respect to dissolved silica) and microbial processes (influencing pH with photosynthesis and respiration). Behr & Röhricht (2000) and Behr (2002) discussed the plausibility of much of the chert forming from silica sols and gels. Polymerization of silica into gels and sols occurs as a result of supersaturation, which can be induced by a drop in temperature, a drop in pH, or a catalyst such as dissolved alumina (Iler, 1979; Mariner & Surdam, 1970).

This microbial hypothesis was developed from observations of silicified spheres *ca.* 10 to 20 microns in diameter in intrusive chert samples that they analyzed in thin section and under scanning electron microscope. These silicified spheres resemble silicified magadiite lepispheres, but were interpreted by Behr & Röhricht (2000) and Behr (2002) as silicified coccoid microbes. The microbes were reported as preserved cyanobacterial cells, including the genera *Gloecapsa*, *Pleurocapsa* and/or *Entophysalis,* as well as other unidentified genera. These preserved features were viewed in samples sourced from a specific feature in one outcrop (Behr, 2002: p. 262).

2.7.3 Primary calcite vs. primary silica

The source material for the intrusive chert has not been found in outcrop exposure, but Behr & Röhricht (2000) suggested that, rather than a magadiite source, a 1-to-2 m thick massive siliceous layer "developed from calcareous stromatolitic microbial mats and thrombolitic bioherms of coccoid cyanobacteria". The bedded cherts that they described show preservation of filamentous cyanobacteria, attributed to calcification of their sheathes. These supposed calcareous structures were reported to have been silicified "concurrently with precipitation of the silica phases". Silica phase precipitation within the calcified mats (silica-sol → opal-A → opal-C → quartzine) was attributed to microbially controlled pH values within the mat.

Much of the chert, however, would have formed from the silica gels (Behr & Röhricht, 2000; Behr, 2002). Mechanisms for siliceous sodic gel formation at Nasikie Engida had been described previously by Eugster & Jones (1968).

Behr (2002) believed that gel formation was triggered by bacterial CO_2. Bacterial CO_2 effectively lowers the pH of its immediate surroundings, by forming carbonic acid ($CO_2 + H_2O \rightarrow H_2CO_3$) . High pH fluids with high silica content, though undersaturated with respect to amorphous silica, could reach saturation in proximity to the bacterial community and polymerize on or near the bacteria.

One of the most important "branching points" in the evolution of evaporating brines involves the precipitation of calcite, often the earliest mineral phase to precipitate (Eugster and Jones, 1979). Calcite precipitation removes Ca^{2+} and CO_3^{2-} in equal molar proportions. If either of these constituents exceeds the other, precipitation of calcite exhausts the deficient constituent from fluid. Due to the geochemical composition of the

underlying trachyte, weathering of rocks in the Magadi catchment provides little dissolved Ca^{2+} to the basin. Dominant anions contributing to the high alkalinity of the modern lake are bicarbonate and carbonate (Jones *et al*., 1977). This high alkalinity allows for rapid precipitation of calcite at the surface or in the shallow subsurface upon inflow of dilute Ca-bearing surface water to the basin, and therefore, removal of Ca^{2+}. Evidence for high alkalinity during the deposition of the Green Beds is inferred by the presence of zeolites in the sedimentary unit. Zeolites in saline, alkaline lake basins are formed as a result of fine-grained glassy volcanic detritus interacting with alkaline waters (Hay, 1986). Instead of calcite precipitation requiring pH buffering by means of microbial respiration, it is likely that the lake waters during Green Beds deposition were often void of Ca^{2+} (Jones *et al*., 1977; Riding, 2006). Late pore-filling calcite is attributed to periodic incursions of dilute inflow (e.g., sheetwash from rainfall).

According Jones *et al.* (1977), Ca^{2+} and Mg^{2+} are undetectable in waters with Total Dissolved Solid (TDS) concentrations greater than 2.5 g/l. They measured (around Magadi) TDS values for dilute waters in the 100s of mg/L, warm springs from 10-45 g/L, hot springs from 20-30 g/L, and the lake brines from ~60-300 g/L. Many of the bedded and intrusive chert samples display evaporite pseudomorphs (Plate 2.3(A); Plate 2.4(B)), indicating high salinity during the deposition of the soft silica species. This evidence can be used to surmise a paucity of Ca^{2+} in the basin during precipitation of silica species.

Furthermore, microbial preservation by calcite is often achieved by the "CO_2 concentrating mechanisms" of those microbes, which creates a microenvironment favourable for calcite precipitation (Riding, 2006). However, this process may be insufficient to override the low pCO_2 fluids in highly alkaline lakes, not to mention the

paucity of Ca^{2+}. Even in calcium-rich lakes, such as the Pyramid Lake in Nevada, calcification of cyanobacterial sheaths does not occur because of Ca^{2+}-binding by extracellular polymeric substances (Arp *et al.*, 1999a; 1999b). The presence of calcified microbes in Green Beds oncoids at Magadi could be due to periods of freshwater incursions during and after the emplacement of the intrusive chert. The modern mudflats at Magadi are littered with cm-scale oncoids that accumulate a thin layer of calcite with each sheetwash (Casanova & Tiercelin, 1982).

The idea brought forth by Behr & Röhricht (2000) that the Green Beds cherts originated from "calcareous stromatolitic microbial mats and thrombolytic bioherms of coccoid cyanobacteria", poses a problem as many chert surfaces, as mentioned, preserve evidence of evaporite formation in the soft surface (crystal moulds). If the mats were initially mineralized by crystalline calcite, possible though unlikely, their surface would have had to remain soft through the crystallization of the sodium carbonates. This is possible in a micritic mud (Fig. 9(A) in Eugster & Hardie, 1975), although the supposed silicification event should have filled open crystal moulds with silica, which is rarely observed. As well, the uniform draping of the layers over the stromatolitic mounds, an effect of microbial growth, may not be preserved by a soft mud, unless the mat maintains its own cohesion.

Behr (2002) reported "discovery of a horizon with bacterial stromatolites" which have been interpreted in this study as oncoids. Many analyses were performed by Behr (2002) on these features, and their interpretation was a major focal point in his reinterpretation. These oncoids are, in fact, quite rare in the basin. They are composed of laminated calcite, and appear to have grown on the surface of the intrusive chert bodies, rather than

an integral part of the chert body. Though microbial growth is implied by the presence of the laminae, microbial remains were not observed in these or any other sample in this study, most likely due to pervasive silicification and recrystallization of the primary calcite structures.

2.7.4 Silicification of microbes

Silicification of microbial material at Lake Magadi during Green Beds deposition is suspected. Repeated growth of microbial layering is observable in both bedded and domal morphologies, and may have been passively silicified to become part of the rock record.

Both microbe surfaces and extracellular polymeric substances provide substrates for silica deposition (Konhauser *et al*., 2004). Microbes, often present in geothermal settings (Berelson *et al.*, 2011; Inagaki *et al*., 2003; Jones *et al*., 2004; Konhauser *et al*., 2004; Pepe-Ranney *et al.*, 2012; Schultze-Lam *et al.*, 1995; Walter *et al*., 1972), have been shown to play a passive role in silica mineralization (Konhauser *et al.*, 2004), providing a charged surface for nucleation of dissolved species. Konhauser *et al.,* (2004) showed that microbes do not increase silicification kinetics, and but rather provide nucleation sites.

Silicification of microbes has been demonstrated at Lake Bogoria in active geothermal spring waters. Renaut *et al*. (1998) found that amorphous silica nucleates and precipitates in the microbial substrates in hot spring outflow. This and other studies (Walter *et al*., 1972; Konhauser *et al*., 2004; Jones *et al*., 2004; Schultze-Lam *et al*., 1995; Berelson *et al*., 2011; Pepe-Ranney *et al*., 2012; etc.) confirm that primary silicification of microbes is common, and that replacement of microbes preserved in carbonate is not a necessary

intermediate step. Active silicification of microbial mats can be observed at Lake Specchio di Venere, Pantelleria Island, Italy, where silica was seen to aggregate on microbial surfaces, likely via hydrogen bonds, and within biofilm exopolysaccharides (EPS) (Cangemi *et al.,* 2010). Cangemi *et al.* (2010) believed that hydrogen bonding and particle entrapment in EPS represents the initial immobilization of silica, which is followed by inorganic silica precipitation aiding in 'fossilization'. Lack of microbe preservation in the Green Beds cherts may be due to subsequent silicification event or silica recrystallization.

2.7.5 Spring activity, microbial growth, and gel formation

Observations of features in the Green Beds support a shallow, mudflat-like environment during deposition (e.g., salt casts, ichnofossils), and it may be reasonable to suspect a penecontemporaneous increase in alkaline spring activity as well, arguably rich in dissolved silica. Increased spring activity can be inferred by evidence of faulting in the Green Beds.

Modern springs at Magadi and Nasikie Engida have pH values over 9 (Jones *et al.,* 1977), which increases silica solubility (Iler, 1979). Springs are also often rich in silica due to their elevated temperature (Iler, 1979). High pH spring activity not only introduces silica to the basin, but allows silica to dissolve upon interaction with fine-grained silicate detritus.

Eugster & Jones (1968) and others (Jones *et al.*, 1977; Surdam & Eugster, 1976) suggested briefly that much of the chert in the Magadi Basin could have formed from siliceous gel, either precipitated directly from spring water, with saturation achieved by

means of cooling, or where alkaline spring waters interacted with trachytic detritus to form gels:

(1) (trachyte debris + Na_2CO_3 (in water) → gel + SiO_2 (in lake)).

Lake- and hot-spring waters, linked to the creation of modern Na-Al-Si gels at Nasikie Engida (Little Magadi), have a pH exceeding *ca.* 9 and Na concentrations > 11,500 ppm (Eugster & Jones, 1968). Modern spring hydrochemistry points towards a greater probability of interaction of lake- and springwater with debris, as opposed to direct precipitation for the formation of gels, as the springs are not sufficiently concentrated with respect to Si and Al for direct precipitation (Eugster & Jones, 1968). As noted in Eugster & Jones (1968), gels observed in the Magadi basin are associated with some of the hottest springs.

Eugster (1970) showed both the temperature and relative dissolved constituent concentrations in the springs surrounding Lake Magadi and Nasikie Engida (Fig. 3 in Eugster, 1970). Springs surround the lake basin on all sides, but the warmest and most concentrated springs are situated on the far north and south ends. Without direct evidence of springs creating gels in modern Lake Magadi, large accumulations of chert occur in regions with the warmest and most concentrated springs. The warmest springs also have the highest HCO_3^- and CO_3^{2-} concentrations, and therefore a higher chemical potential in terms of reactivity with the detritus, compared to the cooler springs.

Eugster & Jones (1968) suggested that trachyte rich in alkali feldspars yielded sodium aluminum silicate gels, and that quartz-rich trachytes yielded sodium silicate gels, upon

interaction with alkaline waters. Baker (1958) reported quartz-rich trachytes south of the southwest lagoon, and this could possibly explain the remarkable abundance of chert found in the southern Magadi region.

Modern sodium aluminosilicate gels are often present at the northern end of Nasikie Engida (Fig. 2.1(B)) in association with microbial mats. Gels at Nasikie Engida incorporate significant organic matter in their matrix, and are often observed to have a protective microbial mat layer. These gels often form in calm, shallow, littoral settings associated with hot-spring outflow, but are also present at sites without direct hot-spring influence. It is possible that the alkaline lake brines have altered detritus into gels along some shorelines in the basin, with longer exposure times possibly substituting for the higher temperatures of the springs. Microbial mats are noted in all occurrences.

The theory of chert formation from siliceous gels, however, was largely ignored in many publications, including Eugster (1980), while the theory of magadiite precipitation and chertification persisted.

Green Beds outcrop observations strongly support microbial mat activity during deposition, based on morphology (growth bedding, petees, etc.) and the superficial similarity to modern analogs (gels and mats at Nasikie Engida). Microbial mats present during Green Beds deposition at Magadi are regarded in this study as likely templates for silicification. Preserved microbial evidence, including filaments, however, was absent in the petrographic and scanning electron microscope analyses of all samples collected for this study (bedded and intrusive). Samples were found to have been subject to pervasive silicification, and microbial features were presumably lost during alteration of the soft siliceous precursor to quartz. Furthermore, evidence from more modern silicified

filamentous microbes in hot spring pools in New Zealand (Jones *et al.*, 2001) suggests that preservation of even recent microbial activity by silica is inconstant. Silicification is known to mask or obliterate attributes used for microbial identification, adding volume to the microbes or covering fine detailed features within their structure, even in recent samples (Renaut *et al.,* 1998).

High-temperature spring waters often precipitate silica sinter (e.g., Jones & Renaut, 2003; Berelson *et al.*, 2011)). This is often due to cooling of geothermal waters upon exposure to the atmosphere, reaching silica saturation through a decrease in temperature. At temperatures below *ca.* 73°C, cyanobacterial mats promote evaporation of spring waters through capillary action (wicking). An example of microbial mat preservation by silicification has been observed at Yellowstone, USA, with precipitation of amorphous silica within a microbial mat, generating an ultimate product of a solid material permeated by filamentous microbes (Berelson *et al*., 2011).

The uniform thickness of the thinly laminated layers of the pillow cherts at Magadi might indicate subaqueous discharge of clusters of silica-rich springs. Repeated colonization of the microbial surface results in stromatolitic layering, with layering cemented by passive silicification through seepage of spring water. In contrast, subaerial seepage would result in non-uniform macro-layering, exhibited in features such as terraces and discharge aprons (Jones & Renaut, 2003).

Scott (2010) noted the superficial resemblance between the “pillow cherts” and fissure-ridge travertine spring-mounds from the Lake Turkana region, though the Turkana mounds are fully subaerial (Renaut *et al.*, 2002), potentially implying spring activity.

Though many lines of evidence exist to suggest active tectonism during Green Beds deposition (e.g., tilted beds, intrusions along fault lines), new evidence supporting an increase in geothermal activity includes a possible subaerial spring vent discharge mounds with rim pools (Plate 2.3(C & D), stromatolitic chert built upon cores of brecciated chert at point-source discharge points (Fig. 2.4(A)), and occurrences of increased geothermal activity at Magadi along fault lines even in the last 100 years.

Crane (1981) noted two boiling springs in the south end of Lake Magadi in 1958. These springs were accompanied by geysers and mud volcanoes, and their activity ceased after a seismic disturbance in 1960. The observance of active springs in this area is direct evidence of geothermal activity along the fault lines, and supports theorizing long-lived "plumbing" along fault boundaries (up to 10^4 years) (pers. comm. with Robin Renaut, 2016).

The relationship of many chert features with fault lines is unequivocal, and evidence exists to suggest there was, even in the recent past, increased hydrothermal output in areas that are currently inactive. The relationship of chert to spring activity is unobservable, as there is no actively-forming chert, but it is possible that the processes of geothermal activity and silica deposition were linked.

2.7.6 Seismicity

Increased hot spring activity has been considered, and increased seismicity must also be considered. Active tectonism during deposition has been recorded by gently folded "Chert Series" lake beds (Baker, 1958), extrusion of pillow cherts and chert dykes, and

slumping chert (Behr & Röhricht, 2000), not to mention the evidence of increased geothermal activity.

The central bodies of the pillow cherts are, as mentioned, a cemented brecciated chert. The siliceous precursor material for this chert likely formed in the subsurface, with alkaline spring brines interacting with the shallow unconsolidated layers of deposited trachytic debris. The intrusion of the material through younger overlying layers was likely triggered by seismic activity, and aided by either overburden pressure or the relative buoyancy of the semi-soft siliceous mash. A subaqueous environment is inferred from the isopachous nature of the stromatolitic chert layering, unaffected by soft sediment deformation that might occur as a result of gravity in a subaerial setting (e.g., slumping, sliding, etc.). This fluid not only mineralized the microbial communities, but also cemented ('fossilized' with chalcedony) the chert breccia (a micro- to cryptocrystalline chert). These chert mounds experienced growth and deposition through intrusion and seepage of viscous and fluid silica, respectively, subsequent desiccation through evaporation, and repeated injections of brecciated semi-soft silica to result in a multi-stage system. The stages of formation are observable in outcrop, and are interpreted as: 1) initial intrusion/brecciation; 2) colonization of the mound surface by microbial mats; 3) silicification of the microbial layers and cementation of the breccia; 4) new injected pulses of semi-soft and fluid silica; 5) breaking and re-cementing the initial mineralized layers; 6) recolonization of the new surface by microbial communities; and 7) mineralization of the new surfaces (Fig. 2.7).

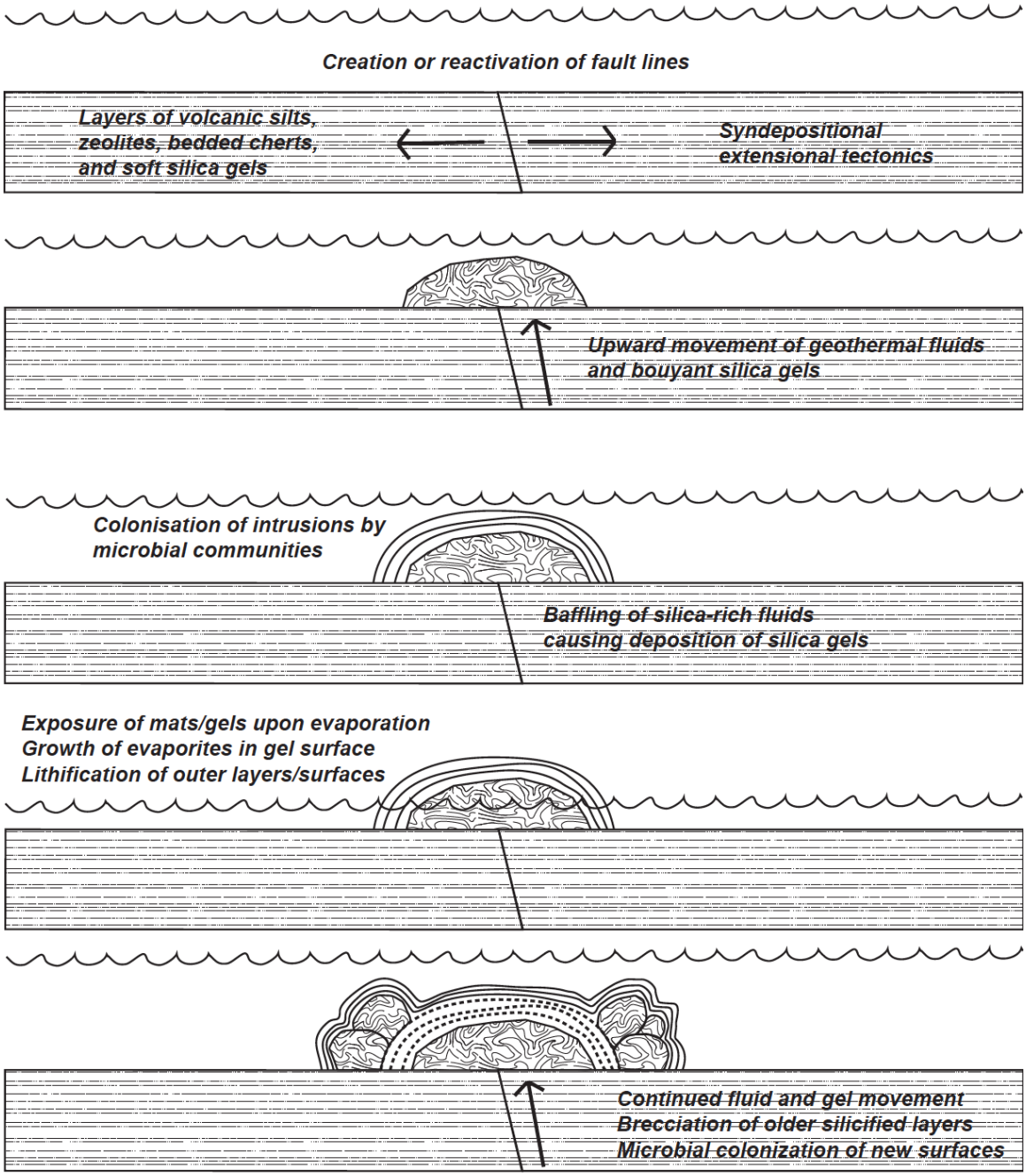

Figure 2.7 – Intrusive Chert Formation Hypothesis

Bedded and intrusive chert facies each show indications of unique conditions affecting the transition between precursor material and lithified rock. Determined from outcrop and laboratory studies, bedded cherts likely lithified through auxiliary silicification. Silicification is possible through supersaturation with respect to amorphous silica, which is reached by means of evaporative concentration. With evaporative concentration, the Magadi brines become saturated to the point of trona precipitation, with waters highly concentrated in Na and HCO_3. Once trona precipitates [$Na_3(CO_3)(HCO_3)\cdot 2H_2O$], these constituents ($Na^+$, CO_3^{2-}, & HCO_3^-) become depleted in the brine, with HCO_3^- as the limiting factor. Before reaching saturation with respect to trona, HCO_3^- concentrations in the system are controlled by calcite precipitation/dissolution, silicate hydrolysis, and geothermal input of CO_2 (Earman *et al*., 2005; Lee *et al*., 2016). As HCO_3^- is consumed/depleted, the pH of the brine is effectively lowered, lowering the effective solubility of silica and allowing the dissolved silica to reach supersaturation. Chertification occurred at Magadi prior to the dissolution of evaporite crystals in soft surfaces, therefore preserving moulds from crystals that formed in the soft gel surface.

2.7.8 Green Beds tuffs and silts

Behr & Röhricht (2000: p. 273) suggested that the depositional environment for the bedded chert might have been an expansive mudflat cross cut with ephemeral channels with occasional small shallow ponds, similar to what is seen at the north end of modern Nasikie Engida and the south end of modern Lake Magadi. While much of Magadi chert preserves features indicative of deposition on a shallow, expansive mudflat (e.g., crystal pseudomorphs), additional evidence of periodic subaerial exposure preserved in the

surrounding sediments help support the hypothesis of an evaporative setting during Green Beds deposition. Cyclical occurrences of Fe-oxidation surfaces indicate repeated subaerial exposure. Incorporation of rootlets between sediment layers, and ichnofossils in the sediment fabric also indicates very-shallow-to-subaerial conditions. Evaporative conditions are assumed, based on the presence of evaporite moulds, but these supplementary features help to substantiate the hypothesis.

The Green Beds contain abundant fine-grained sediments. Much of the sediment constituting the Green Beds is clay- and silt-sized particles, believed to be a product of reworking of Oloronga Beds (Behr, 2000). These clay- to silt-sized sediments were initially sourced from the surrounding trachyte, released by chemical weathering. Fine ash layers, observed in this study as thin, pure layers of ash, are a direct result of volcanic activity.

These fine sediments can be deposited by eolian processes alone. Modern Magadi receives noticeable incursions of wind-blown sediment into the basin on a daily basis. Warm air rising from the basin floor in the midday heat is vigorous enough to disturb, entrap, and transport fine-grained sediment in the form of a dust devil. During semi-arid to arid climate periods (including modern Magadi), the area surrounding the basin is thinly vegetated and fine-grained sediments are unencumbered to transportation. With this, loess has even accumulated along the NE margin of the Magadi Town horst. Lack of thorough cementation of older sediments also allows for sediment reworking, and incorporation of these sediments into younger sedimentary units.

Additionally, there are features in the Green Beds also supporting periodic flooding of the mudflat. The incorporation of various particle sizes of detrital minerals in the thick

layers above and below the cherts beds suggests the depositional surface received incursions of not only fine-grained eolian deposits, but also sheetwash-, and flood-related deposits. This is observed by the size, and mineralogy of the granular clastics incorporated in the unit. Grains larger than fine-sand require water transport, and the observance of minerals sourced, although rarely, from the exposed metamorphic basement near the Nguruman escarpment indicate significant distance travelled (Röhricht, 1999). Late crystalline calcite, common in chert fractures and both lining- and filling pore spaces, is also indicative of periodic incursions of fresh water. Carbonate oncoids, found on the intrusive chert outcrops, also indicate periods of fresher water. It is believed that this occurred well after the emplacement of the intrusion, but during the prolonged soft silica state.

2.7.9 Depositional environment of the Green Beds

The lowermost sediments of the Magadi Basin (Oloronga Beds) were largely composed of "airfall tuffs, lacustrine carbonates, and diatomaceous cherts" (Behr, 2002). Zeolites in the Oloronga Beds imply periods of high alkalinity (Surdam and Eugster, 1976), but much evidence exists to suggest a largely fresh depositional environment (e.g., limestone, freshwater gastropod shells, stromatolites up to 80 m above present lake) (Baker, 1958; Behr, 2002; Eugster, 1980).

A calcrete layer capping the Oloronga beds implies a prolonged drop in lake level after the period of Oloronga sedimentation. The sedimentological features observed in the overlying Green Beds imply the influence of microbes, hot springs, and periodic

subaerial exposure during sedimentation. These features support a significant drop in lake level, and an increase in hydrothermal input into the basin.

The Green Beds tuffs are largely composed of pyroclastic silts, often reworked Oloronga sediments, and the zeolites erionite and analcime, which form under saline, alkaline conditions (Hay, 1966; Surdam & Eugster, 1976).

The Green Beds exposures are found within or immediately peripheral to the faulted margins of the modern basin, implying that the Green Lake was similarly constrained. The Oloronga and High Magadi Beds exposures, however, extend beyond the modern bounds, implying that those paleolakes were larger, or alternately, that there existed several paleolakes across the landscape (Baker, 1958; Shipman *et al*., 1983).

The Green Beds also experienced syndepositional tectonics, known from structurally aligned intrusive features and slightly tilting of the beds. The unit is capped by a calcrete horizon, representing a pronounced period of aridity following the deposition of the Green Beds (Behr & Röhricht, 2000).

Chert formation and Green Beds sediment silicification are the result of increased dissolved silica in the Magadi waters during deposition. Reasons for increased dissolved silica in the basin include (1) increased hot spring inflow, with high temperatures facilitating higher dissolved silica content; (2) increased geothermal CO_2 input, helping to increase the rate of silicate hydrolysis; (3) increased evaporative concentration, resulting in higher pH waters, allowing silica species to dissociate and become highly concentrated in the brines.

2.8 Conclusions

The change in sedimentation style from the Oloronga Beds to Green Beds reflects a change in lake hydrochemistry. High silica content likely reflects high silica input, which can represent hydrothermal recharge in the southern Kenya Rift Valley, as warm, alkaline waters are known to have a higher capacity for dissolved silica (Iler, 1979). Ultimately, the lower lake levels, inferred for the depositional environment of the Green Beds, are a product of less available surface water, likely linked to a change in climate (aridification). Hydrothermal inputs during low lake levels would have become proportionally more significant. Evidence of tectonism during Green Beds deposition provides the mechanism in which the basin could experience a higher geothermal-to-surficial-water ratio, with faulting allowing for fluid flow.

Tectonics might not only have changed the physical conduits for hydrothermal transport and input, but might also have, on a broader geographical and temporal scale, altered the landscape such that rain shadow effects became a factor in aridification of the Magadi Basin. The elevated rift shoulders, as seen today, experience pronounced wet seasons, while the rift valley floor remains arid, under the influence of a prominent rain shadow (Olaka *et al*., 2010).

Subsequent aridification allows for great evaporation and a more negative hydrologic balance, which is believed to have occurred during the deposition of the Green Beds.

These factors (increased seismicity, spring input, and evaporative concentration) provided a suitable environment for extensive silica accumulation and precipitation. The low lake levels would have accommodated considerable mudflats, believed to have been colonized by microbial mats, which through silica mineralization became the bedded

cherts we see today. Seismic activity promoted the intrusion of brecciated chert material through the Green Beds sediments, which experienced microbial colonization, silica mineralization, and subsequent evaporation and desiccation, inferring a shallow depositional environment, influenced by periodic fluctuations in lake level.

Acknowledgments

Permission to conduct research in Kenya was granted by the Government of Kenya, and the chiefs of local Maasai villages. Thanks are due to the Tata Chemicals Magadi, who provided facilities during field work. B.L.B. and R.W.R. acknowledge an NSERC research grant and post-graduate scholarship, respectively, and R.B.O. acknowledges the Research Grant Council of Hong Kong for research support. Thanks are also due to Blaine Novakovski and Tom Bonli of the University of Saskatchewan for helping with sample preparation and analysis.

2.9 References

Allen, D.J., Darling, W.G., and **Burgess, W.G.** (1989) Geothermics and hydrogeology of the southern part of the Kenya Rift Valley with emphasis on the Magadi Nakuru area. UK: British Geological Survey. pp. 197.

Andrews, S.D., Kelly, S.R.A., Braham, W. and **Kaye, M.** (2014) Climatic and eustatic controls on the development of a Late Triassic source rock in the Jameson Land Basin, East Greenland. *J. Geol. Soc., Lond.,* **171**, 609–619.

Arp, G., Reimer, A., and **Reitner, J.** (1999a) Calcification in cyanobacterial biofilms of alkaline salt lakes. *Eur. J. Phycol.,* **34**, 393–403.

Arp, G., Thiel, V., Reimer, A., Michaelis, W., and **Reitner, J.** (1999b) Biofilm exopolymers control microbialite formation at thermal springs discharging into the alkaline Pyramid Lake , Nevada , USA. *Sediment. Geol.* **126**, 159–176.

Baker, B.H. (1958) Geology of the Magadi Area: Report. 42. Kenyan Government Printer, Nairobi, pp. 88.

Baker, B.H. (1986) Tectonics and volcanism of the southern Kenya Rift Valley and its influence on rift sedimentation. *Geol. Soc. London, Spec. Publ.* **25**, 45–57.

Barker, P., Gasse, F., Roberts, N., and **Taieb, M.** (1990) Taphonomy and diagenesis in diatom assemblages; a Late Pleistocene palaeoecological study from Lake Magadi, Kenya. *Hydrobiologia,* **214**, 267–272.

Behr, H.J. (2002) Magadiiite and Magadi Chert: A Critical Analysis of the Silica Sediments in the Lake Magadi Basin, Kenya. In: *Sedimentation in Continental Rifts* (Eds R.W. Renaut and G.M. Ashley)*, SEPM Special Publication,* **73***,* 257–273.

Behr, H.J., and **Röhricht, C.** (2000) Record of seismotectonic events in siliceous cyanobacterial sediments (Magadi cherts), Lake Magadi, Kenya. *Int. J. Earth Sci.,* **89**, 268–283.

Berelson, W.M., Corsetti, F.A., Pepe-Ranney, C., Hammond, D.E., Beaumont, W., and **Spear, J.R.** (2011) Hot spring siliceous stromatolites from Yellowstone National Park: assessing growth rate and laminae formation. *Geobiology,* **9**, 411–424.

Bustillo, M.A. (2001) Cherts with Moganite in Continental Mg-Clay Deposits: An Example of "False" Magadi-Type Cherts, Madrid Basin, Spain. *Journal of Sedimentary Research,* **71**, 436–443.

Cohen, A.S. , Campisano, C., Arrowsmith, R., Asrat, A., Behrensmeyer, A.K., Deino, A., Feibel, C., Hill, A., Johnson, R., Kingston, J., Lamb, H., Lowenstein, T., Noren, A., Olago, D., Owen, R.B., Potts, R., Reed, K., Renaut, R., Schäbitz, F., Tiercelin, J.-J., Trauth, M.H., Wynn, J., Ivory, S., Brady, K., O'Grady, R., Rodysill, J., Githiri, J., Russell, J., Foerster, V., Dommain, R., Rucina, S., Deocampo, D., Russell, J., Billingsley, A., Beck, C., Dorenbeck, G., Dullo, L., Feary, D., Garello, D., Gromig, R., Johnson, T., Junginger, A., Karanja, M., Kimburi, E., Mbuthia, A., McCartney, T., McNulty, E., Muiruri, V.,

Nambiro,E., Negash, E.W., Njagi, D., Wilson, J.N., Rabideaux, N., Raub,T., Sier,M.J., Smith, P., Urban, J., Warren, M., Yadeta, M., Yost, C., and **Zinaye, B.** (2016). The Hominin Sites and Paleolakes Drilling Project: Inferring the Environmental Context of Human Evolution from Eastern African Rift Lake Deposits. *Scientific Drilling*, **21**, 1-16.

Cangemi, M., Bellanca, A., Borin, S., Hopkinson, L., Mapelli, F., and **Neri, R.** (2010) The genesis of actively growing siliceous stromatolites: Evidence from Lake Specchio di Venere, Pantelleria Island, Italy. *Chem. Geol.,* **276**, 318–330.

Casanova, J., and **Tiercelin, J.-J. (**1982) Algal-Built Stromatolites from Sodic Carbonate Environment: Flood Plains Oncolites of Lake Magadi. *Sédimentologie*, **295**, 1139-1144.

Crane, K. (1981) Thermal Variations in the Gregory Rift of Southern Kenya. *Tectonophysics*, **74**, 239–262.

Crossley, R. (1979) The Cenozoic stratigraphy and structure of the western part of the Rift Valley in southern Kenya. *Journal of the Geological Society of London*, **136**, 393–405.

Damnati, B., and **Taieb, M.** (1995) Solar and ENSO signatures in laminated deposits from Lake Magadi (Kenya) during the Pleistocene/Holocene transition. *J. African Earth Sci.,* **21**, 373–382.

Earman, S., Phillips, F.M., and **McPherson, B.J.O.L.** (2005) The role of "excess" CO2 in the formation of trona deposits. *Appl. Geochemistry*, **20**, 2217–2232.

Eugster, H.P. (1967) Hydrous Sodium Silicates from Lake Magadi, Kenya: Precursors of Bedded Chert. *Science*, **157**, 1170–1180.

Eugster, H.P. (1969) Inorganic Bedded Cherts from the Magadi Area, Kenya. *Contrib. to Mineral. Petrol.,* **22**, 1–31.

Eugster, H.P. (1970) Chemistry and Origin of the Brines of Lake Magadi, Kenya. *Mineral. Soc. Am. Spec. Pap.,* **3**, 213–235.

Eugster, H.P. (1971) Origin and Deposition of Trona. *Rocky Mt. Geol.,* **10**, 49–55.

Eugster, H.P. (1980) Lake Magadi, Kenya, and its Precursors, In: Hypersaline Brines and Evaporitic Environments. (Ed Nissenbaum, A.), Elsevier Scientific Publishing Company, Amsterdam, The Netherlands, 195–232.

Eugster, H.P. (1986) Lake Magadi, Kenya: a model for rift valley hydrochemistry and sedimentation. *Geol. Soc. London, Spec. Publ.,* **25**, 177–189.

Eugster, H.P., and **Jones, B.F. (**1968) Gels Composed of Sodium-Aluminum Silicate, Lake Magadi, Kenya. *Science,* **161**, 160–163.

Eugster, H.P., and **Jones, B.F.** (1979) Behaviour of major solutes during closed-basin brine evolution. *Am. J. Sci.*, **279**, 609–631.

Fairhead, J.D., Mitchell, J.G., and **Williams, L.A.J.** (1972) New K/Ar Determinations on Rift Volcanics of S. Kenya and their Bearing on Age of Rift Faulting. *Nat. Phys. Sci.,* **238**, 66-69.

Felske, G.N. (2016) Genesis of calcrete and related carbonate rocks in the southern Kenyan Rift. University of Saskatchewan, M.Sc. thesis, pp. 168.

Gerdes, G., Claes, M., Dunajtschik-piewak, K., Riege, H., Krumbein, W.E., and **Reineck, H.** (1993) Contribution of Microbial Mats to Sedimentary Surface Structures. *Facies*, **29**, 61–74.

Goetz, C., and **Hillaire-Marcel, C.** (1992) U-series disequilibria in early diagenetic minerals from Lake Magadi sediments, Kenya: Dating potential. *Geochim. Cosmochim. Acta*, **56**, 1331–1341.

Hardie, L.A., and **Eugster, H.P. (**1975) Sedimentation in an Ancient Playa-Lake Complex: The Wilkins Peak Member of the Green River Formation of Wyoming. *Geological Society of America Bulletin*, **86**, 319–334.

Hardie, L.A., and **Eugster, H.P.** (1980) Evaporation of seawater: calculated mineral sequences. *Science*, **208**, 498–500.

Hay, R.L. (1966) Zeolites and Zeolitic Reactions in Sedimentary Rocks. *Geological Society of America Special Papers*, **85**, 1-122.

Hay, R.L. (1968) Chert and its sodium-silicate precursors in sodium-carbonate lakes of East Africa. *Contrib. to Mineral. Petrol.,* **17**, 255–274.

Hay, R.L. (1986) Geologic occurrence of zeolites and some associated minerals. *Pure Appl. Chem.,* **58**, 1339–1342.

Hillaire-Marcel, C., and **Casanova, J. (**1987) Isotopic Hydrology and Paleohydrology of the Magadi (Kenya)- Natron (Tanzania) Basin During the Late Quaternary. *Palaeogeography, Palaeoclimatology, Palaeoecology,* **58**, 155–181.

Houser, B.B. (1985) Magadi-type chert, indicator of a lacustrine environment in the Middle Eocene McBean formation, South Carolina. *Southeastern Geology,* **25,** 185-197.

Iler, R.K. (1979) The Chemistry of Silica: Solubility, Polymerization, Colloid and Surface Properties and Biochemistry of Silica. John Wiley & Sons, Chichester, pp. 896.

Inagaki, F., Motomura, Y., and **Ogata, S.** (2003) Microbial silica deposition in geothermal hot waters. *Appl. Microbiol. Biotechnol.,* **60**, 605–611.

Jones, B., Konhauser, K.O., Renaut, R.W., and **Wheeler, R.S.** (2004) Microbial silicification in Iodine Pool, Waimangu geothermal area, North Island, New Zealand: implications for recognition and identification of ancient silicified microbes. *J. Geol. Soc. London,* **161**, 983–993.

Jones, B., and **Renaut, R.W.** (2003) Hot spring and geyser sinters: the integrated product of precipitation, replacement, and deposition. *Can. J. Earth Sci.,* **40**, 1549–1569.

Jones, B., Renaut, R.W., and **Rosen, M.R.** (2001) Taphonomy of silicified filamentous microbes in modern geothermal sinters — implications for identification. *Palaios,* **16**, 580–592.

Jones, B.F., and **Deocampo, D.M.** (2003) Geochemistry of Saline Lakes, in: *Treatise on Geochemistry.* pp. 393–424.

Jones, B.F., Eugster, H.P., and **Rettig, S.L.** (1977) Hydrochemistry of the Lake Magadi basin , Kenya. *Geochim. Cosmochim. Acta,* **41**, 53–72.

Kerrich, R., Renaut, R.W., and **Bonli, T.** (2002) Trace Element Composition of Cherts from Alkaline Lakes in the East African Rift: A Probe for Ancient Counterparts, In: *Sedimentation in Continental Rifts* (Eds R.W. Renaut and G.M. Ashley)*, SEPM Special Publication,* **73***,* 275–294.

Konhauser, K.O., Jones, B., Phoenix, V.R., Ferris, G., and **Renaut, R.W.** (2004) The microbial role in hot spring silicification. *Ambio,* **33**, 552–8.

Krainer, K., and **Spotl, C.** (1998) Abiogenic silica layers within a fluvio-lacustrine succession, Bolzano Volcanic Complex , northern Italy: a Permian analogue for Magadi-type cherts?. *Sedimentology,* **45**, 489–505.

Krauskopf, K.B. (1956) Dissolution and precipitation of silica at low temperatures. *Geochim. Cosmochim. Acta,* **10**, 1–26.

Le Turdu, C., Tiercelin, J., Renaut, R., Rolet, J., Richert, J., Xavier, J. and **Coquelet, D.** (1995). Rift basin structure and depositional patterns interpreted using a 3-D

remote sensing approach: The Baringo-Bogoria Basins, central Kenya Rift, East Africa. *Bulletin des Centres de Recherches Exploration - Production Elf Aquitaine*, **19**, 1-37.

Lee, H., Muirhead, J.D., Fischer, T.P., Ebinger, C.J., Kattenhorn, S.A., Sharp, Z.D., and **Kianji, G.** (2016) Massive and prolonged deep carbon emissions associated with continental rifting, *Nature Geoscience* **9**, 145–149.

Mariner, R.H., and **Surdam, R.C.** (1970) Alkalinity and formation of zeolites in saline alkaline lakes. *Science,* **170**, 977–980.

Noffke, N., Christian, D., Wacey, D., and **Hazen, R.M.** (2013) Microbially Induced Sedimentary Structures Recording an Ancient Ecosystem in the ca. 3.48 Billion-Year-Old Dresser Formation, Pilbara, Western Australia. *Astrobiology,* **13**, 1103–24.

Olaka, L. a., Odada, E.O., Trauth, M.H., and **Olago, D.O.** (2010) The sensitivity of East African rift lakes to climate fluctuations. *J. Paleolimnol.,* **44**, 629–644.

Parnell, J., (1986) Devonian Magadi-Type Cherts in the Orcadian Basin, Scotland. *J. Sediment. Petrol.,* **56**, 495–500.

Pepe-Ranney, C., Berelson, W.M., Corsetti, F.A. , Treants, M., and **Spear, J.R.** (2012) Cyanobacterial construction of hot spring siliceous stromatolites in Yellowstone National Park. *Environ. Microbiol.,* **14**, 1182–97.

Perry, E.C.J., and **Lefticariu, L.** (2005) Formation and Geochemistry of Precambrian Cherts. In: Mackenzie, F.T. (Ed.), Sediments, Diagenesis, and Sedimentary Rocks: *Treatise on Geochemistry.* Elsevier Ltd, Oxford, UK, pp. 446.

Pollock, M.D., Kah, L.C., and **Bartley, J.K.** (2006) Morphology of Molar-Tooth Structures in Precambrian Carbonates: Influence of Substrate Rheology and Implications for Genesis. *J. Sediment. Res.,* **76**, 310–323.

Renaut, R.W. and **Gierlowski-Kordesch, E.H. (**2010) Lakes. In: *Facies Models, 4th Edition*, (Eds Dalrymple, R. and James, N.), Geological Association of Canada, Toronto, 541-575.

Renaut, R.W., Morley, C.K., and **Jones, B.** (2002) Fossil Hot-Spring Travertine in the Turkana Basin, Northern Kenya: Structure, Facies, and Genesis, In: *Sedimentation in Continental Rifts* (Eds R.W. Renaut and G.M. Ashley)*, SEPM Special Publication,* **73***,* 123–141.

Renaut, R.W., and **Owen, R.B. (**1988) Opaline cherts associated with sublacustrine hydrothermal springs at Lake Bogoria, Kenya Rift valley. *Geology,* **16**, 699–702.

Riding, R. (2006) Cyanobacterial calcification, carbon dioxide concentrating mechanisms, and Proterozoic-Cambrian changes in atmospheric composition. *Geobiology,* **4**, 299–316.

Röhricht, C. (1999) Lithologie und Genese der Chertserien des Magadi Beckens, Lake Magadi, Kenia. Georg-August-Universitat zu Gottigen, Ph. D. Thesis, pp. 106.

Rooney, T.P., Jones, B.F., and **Neal, J.T.** (1969) Magadiite from Alkali Lake, Oregon, *The American Mineralogist*, **54**, 1034-1043.

Schubel, K.A., and **Simonson, B.M.** (1990) Petrography and Diagenesis of Cherts From Lake Magadi, Kenya. *J. Sediment. Petrol.,* **60**, 761–776.

Schultze-Lam, S., Ferris, F.G., Konhauser, K.O., and **Wiese, R.G.** (1995) In situ silicification of an Icelandic hot spring microbial mat: implications for microfossil formation. *Can. J. Earth Sci.*, **32**, 2021–2026.

Scott, J.J. (2010) Saline Lake Ichnology: Composition and distribution of Cenozoic traces in the saline, alkaline lakes of the Kenya Rift Valley and Eocene Green River Formations, U.S.A. University of Saskatchewan, Ph. D. thesis, pp. 546.

Scott, J.J., Renaut, R.W., and **Owen, R.B. (**2012) Impacts of flamingos on saline lake margin and shallow lacustrine sediments in the Kenya Rift Valley. Sedimentary *Geology*, **277-278**, 32–51.

Sebag, D., Verrecchia, E.P., Lee, S., and **Durand, A.** (2001) The natural hydrous sodium silicates from the northern bank of Lake Chad : occurrence , petrology and genesis. *Sediment. Geol.,* **139**, 15–31.

Sheppard, R.A., and **Gude, A.J.** (1986) Magadi-Type Chert - A Distinctive Diagenetic Variety From Lacustrine Deposits, Studies in Diagenesis - U.S. Geological Survey Bulletin. Washington. 301-333.

Shipman, P., Potts, R., and **Pickford, M.** (1983) Lainyamok, a new middle Pleistocene hominid site. *Nature,* **306**, 365–368.

Surdam, R.C., and **Eugster, H.P.** (1976) Mineral reactions in the sedimentary deposits of the Lake Magadi region, *Kenya. Geol. Soc. Am. Bull*., **87**, 1739–1752.

Walter, M.R., Bauld, J., and **Brock, T.D.** (1972) Siliceous algal and bacterial stromatolites in hot spring and geyser effluents of Yellowstone National Park. *Science,* **178**, 402–405.

Williamson, D., Taieb, M., Damnati, B., Icole, M., and **Thouveny, N.** (1993) Equatorial extension of the younger Dryas event: rock magnetic evidence from Lake Magadi (Kenya). *Glob. Planet. Change,* **7**, 235–242.

CHAPTER 3:

Geochemistry of the Green Beds sediments

This chapter is written as a draft manuscript.

The senior author did the fieldwork and analytical research, and wrote the manuscript.

The co-authors gave advice in the field and offered suggestions and editorial comments.

ABSTRACT

The Green Beds unit (98-40 ka) consists of volcanoclastic silts and tuffs, intercollated with bedded chert layers and intruded by both domal and dyke-like instrusions of chert. The Green Beds unit lies above the Oloronga Beds (800-300 ka) and below the High Magadi Beds (23.7-9.3 ka), is separated into upper and lower sedimentary sections.

Several geochemical characteristics in the Green Beds cherts and tuffs/silts were noted: (1) relatively flat, but negatively fractionated, REE patterns; (2) positive Ce but negative Eu anomalies; (3) high absolute concentrations of U and Zr (as well as normalized enrichments of U and Zr in relation to REE); (4) profound fractionations of U/Th and Zr/Hf. These characteristics may be indicative of deposition in a saline, alkaline setting (Kerrich *et al.,* 2002).

Major element geochemistry and a Chemical Index of Alteration suggests that the High Magadi Beds sediments show the closest relationship to the parent material, the Magadi Trachyte, experiencing the least amount of weathering. The High Magadi Beds, including magadiite, is enriched in Na_2O with respect to the Magadi Trachyte, and other sediments. The lower Green Beds and part of the upper Green Beds are relatively enriched in CaO, indicating periodic incursions of fresh water.

3.1 Introduction

The abundant quartzose cherts and silicified sediments at Lake Magadi were first mentioned by Parkinson (1914) and were described much later by Baker (1958, 1963). Eugster (1967, 1969, 1980) studied the Magadi sediments in detail and discovered two new sodium-silicate minerals – magadiite ($NaSi_7O_{13}(OH)_3 \cdot 4(H_2O)$) and kenyaite ($Na_2Si_{22}O_{45} \cdot 10(H_2O)$) – in the Late Pleistocene High Magadi Beds radiometrically dated from 23 ka to 9.3 ka (Williamson *et al.,* (1993); Tichy & Seegers (1999)).

Chert is abundant in the exposed sediments of the Magadi basin, displaying various morphologies reflecting soft-state deformation. Amongst these cherts is a unique type of chert that forms from sodium silicate minerals, with a visible lateral transition in outcrop from soft hydrous mineral layers into a porcellainous quartzose chert, termed "Magadi-type chert". For decades, the origin of all chert in the Magadi basin, and many other lacustrine cherts around the world, was attributed to diagenesis of a magadiite precursor .

Behr & Röhricht (2000) and Behr (2002) reinterpreted the origin of the chert at Magadi, attributing the formation of ~90% of the exposed chert to the precipitation of siliceous gels as a result of microbially-induced falls in pH in the lake water, or from silicification of carbonate material. True "Magadi-type cherts" are still recognized at Magadi, but according to Behr (2002) are exclusive to the High Magadi Beds, one of three chert-bearing sedimentary units in the basin. Most chert at Magadi is thought to have formed from amorphous gel, and belongs to the Green Beds (98–40 ka) (Röhricht, 1999; Behr, 2000)).

Magadiite and siliceous gels form under relatively similar conditions (Behr, 2002), but are nonetheless geochemically distinct from each other, and this should be reflected in the composition of the cherts that formed from then during diagenesis. The diagenetic pathways from the precursor material to the resulting chert are still poorly understood, for both magadiite- and gel-derived cherts, though several mechanisms have been suggested (Hay, 1968; Eugster, 1969; O'Neil & Hay, 1973).

The aim of this paper is to define geochemically the different morphological types of chert (Röhricht, 1999; Behr & Röhricht, 2000; Behr, 2002) at Lake Magadi. The geochemical difference between unequivocal Magadi-type chert, and other chert morphologies is of particular interest. To achieve this, major and trace element distributions of chert and associated sediment samples will be considered. One reason for this study is to try to provide geochemical clues for distinguishing the different types of chert found in sediment cores obtained from the floor of Lake Magadi in 2014 as part of the Hominin Sites and Paleolakes Drilling Project (HSPDP) (Cohen *et al.*, 2016). Surdam & Eugster (1976) had previously reported abundant quartz from earlier drilling, but overall recovery was very poor, and the chert-bearing sedimentary units have since been redefined (Behr & Röhricht, 2000; Behr, 2002).

3.1.1 Previous Work

Chemical analyses have been performed on both waters and sediments throughout the history of geological and limnological research at Magadi.

3.1.1.1 Hydrochemistry

Baker (1958) presented chemical analyses of the springs, lagoons and brine produced by the (at the time) Magadi Soda Company to help trona production. Early hydrochemical and geochemical investigations in the Magadi basin were conducted by Jones *et al.* (1964), and Eugster & Jones (1968) to understand the silica composition of both the brine and modern gels found at the northern end of Nasikie Engida (Little Magadi), respectively. Eugster (1970) made great advances in understanding the hydrochemistry of Lake Magadi and Lake Natron, comparing temperature and composition of the springs and evaporating brines to interpret how fluids cycle through the basin subsurface. Jones *et al.* (1977) refined the hydrochemical model for Lake Magadi and showed how the lake water evolves from dilute inflow to concentrated brines, losing and gaining dissolved constituents at various points along its physical flow path. Eugster & Hardie (1978) and Eugster & Jones (1979) used lessons learned at Magadi and other saline lakes to develop general models for the chemical evolution of saline lakes. Eugster (1980, 1986) later gave a comprehensive overview of the lake chemistry, focusing on the interplay between tectonics, climate, and sedimentation in brine evolution.

3.1.1.2 Geochemistry

Eugster (1967) first noted the occurrence of new sodium silicate minerals, magadiite ($NaSi_7O_{13}(OH)_3 \bullet 4(H_2O)$) and kenyaite ($Na_2Si_{22}O_{41}(OH)_8 \bullet 6(H_2O)$), including their x-ray diffraction patterns and geochemical compositions in their findings. Eugster & Jones (1968) sampled and studied sodium-aluminum silicate gels from the north end of Nasikie

Engida and Lake Magadi. They analyzed the major element distribution within the gels and focused on the difference between their chemistry and that of the parent trachyte. Sheppard *et al.* (1970) reported another new sodium silicate, makatite ($Na_2Si_4O_8(OH)_2$•$4(H_2O)$), believed to have precipitated from the lake water. O'Neil & Hay (1973) investigated the $\partial^{18}O$ values of the cherts in Magadi basin to try to understand the conditions in which they were deposited, notably the degree of evaporation. Surdam & Eugster (1976) studied the conversion of volcanic material to various zeolites and other minerals, which building the work by Hay (1966). Eugster (1986), using decades of experience studying Magadi hydrochemistry, published a study to help determine if Lake Magadi itself can serve as a modern analog to ancient evaporitic deposits. Hillaire-Marcel & Casanova (1987) reconstructed Magadi paleohydrology by sampling and analyzing high-stand carbonate stromatolites. Röhricht (1999) reported geochemical values for each Magadi sedimentary unit. Kerrich *et al.* (2002) analyzed the trace element geochemistry of the cherts and sediments of interest, and compared them to marine cherts, to determine if certain elemental distributions are characteristic of alkaline lakes.

Since Behr & Röhricht (2000) redefined the stratigraphy of the Magadi basin to include the Green Beds, analyses have not yet been performed using their chert classification. Earlier petrographical and geochemical analyses are difficult to compare (e.g., Schubel & Simonson, 1990) with the "new" chert types, but will be considered by general comparison.

3.2 Geological Setting

Lake Magadi occupies a narrow, block-faulted basin at the southern end of the Kenya Rift Valley. The exposed rock of the catchment is trachytic in composition (Plateau- or Magadi Trachyte – 0.8 to 1.25 Ma), and caps a series of thick flood basalts and trachytes that occupy the entire valley floor. The uniform composition of the catchment is very useful for understanding water-rock interactions.

The faulted basin has accommodated lakes since the Mid-Pleistocene (*ca.* 0.8 Ma), with four main paleolakes corresponding to the following sediment units (from oldest to youngest): Oloronga Beds (800 ka to 300 ka; Fairhead *et al.,* 1972; Behr, 2002); Green Beds (98.5 ka to 40 ka; Goetz & Hillaire-Marcel, 1992; Williamson *et al.,* 1993); High Magadi Beds (*ca.* 23,700 to 9,310 y BP; Williamson *et al.,* 1993; Tichy & Seegers, 1999); and the Evaporite Series (10,010 ka to 4,600 ka; Butzer *et al.,* 1972). The water bodies of the Magadi Basin have experienced large fluctuations in aerial extent (and therefore depth), and in hydrochemical composition, known from the location and the geochemical composition of the sediments. The presence of zeolites, formed from the alteration of fine-grained volcanic sediments, in all sedimentary units has been valuable in terms of understanding basin hydrochemistry through time.

3.2.1 Hydrology and Hydrochemistry

Perennial surface flow does not reach the modern lake, but small peripheral lagoons are sustained by *ca.* 200 small warm springs that issue along the faulted lake margins (Chapter 2; Fig. 2.1(B)). These waters are sourced from both shallow groundwater and deep geothermal reservoirs, and replenished by rain that falls on the rift shoulders and percolates through faulted volcanic rocks and Quaternary alluvium to reach the rift floor.

Seasonal runoff generated by local rainfall is a subordinate source of inflow (Jones *et al.*, 1977).

The Magadi region is semi-arid, receiving only ~500 mm/yr annual rainfall. With evapotranspiration rates exceeding 3500 mm/yr, the negative hydrological balance causes the evaporative concentration of the spring outflow, very high TDS values in the lake brines (> 250,000 mg kg^{-1}), and the frequent desiccation of the lake surface (Jones *et al.,* 1977).

Chemical weathering, primarily by silicate hydrolysis of the Magadi Trachytes, results in enrichments in Na^+, HCO_3^-, CO_3^{2-}, Cl^-, and deficiencies of alkali earth metals such as Ca^{2+} and Mg^{2+}, in the waters flowing into the basin (Eugster, 1980; Jones *et al.*, 1977).

Equation (1), from Jones *et al.* (1977), shows the release of many of the dominant ions through one weathering reaction:

$$NaAlSi_3O_8 + 6½\ H_2O + CO_2 = Na^+ + HCO_3 + 3Si(OH)_4 + ½\ A1_2O_3 \quad (1)$$

Jones *et al.* (1977), recognized five distinct types of fluid in the Magadi Basin: 1) dilute streamflow; 2) dilute ground water; 3) saline ground water (or hot spring reservoir); 4) saturated lake brines and; 5) residual brines. They documented the evolution of the chemical composition from streams descending from the rift shoulders to the most concentrated basinal brines, relating the dissolved major elemental abundances to the conservative chloride ion (up to halite saturation).

Understanding the geochemical evolution of the modern lake brine provides insight into the geochemistry of the lacustrine history. The lake basin experienced a pronounced aridification during the late Pleistocene and Holocene, with temporary fluctuations in lake level recorded by strandlines and stromatolites.

3.3 Methods

Cherts were sampled from many outcrops around the Magadi basin. Samples of magadiite and associated Magadi-type chert were sampled from the lower High Magadi Beds, in both the Southwest Lagoon and the Eastern Lagoon (Chapter 2; Fig. 2.1(B)). Associated High Magadi Beds sediments, from above and below the magadiite layers were also sampled and analyzed.

Representative chert types from the Green Beds were sampled from the Eastern Lagoon, the Southern Peninsula, the Southwest Lagoon and the Northeast Lagoon (Chapter 2; Fig. 2.1), as well as associated sediments. The chert types in this study include: (1) *Bedded Cherts*: extensive thinly bedded, platy cherts, deposited in cyclic layering near the top of the Green Beds outcrops; (2) *Dyke cherts*: intrusions of a once-viscous silica mash that pushed up through the Green Beds sediments to produce dykes decimeters wide and metres long; (3) *Pillow cherts*: metre-scale domal intrusions that form clusters along fault lines and major fractures, especially in the Eastern Lagoon.

Exposures of Green Beds (GB) sediments in section are rare. Three informal units were recognized in a small outcrop 250 cm thick south of the lake (Chapter 2; Fig. 2.4 – South Peninsula): lower GB, upper GB, and GB calcrete (Chapter 2; Plate 2.2; Fig. 2.3) The calcrete caps the unit, and is observable across portions of the south peninsula (Chapter 2; Fig. 2.4(C)). The upper GB (187 cm thick) are exposed along a road cut; the lower GB (63 cm thick) was dug below the land surface until the pit became waterlogged (Chapter 2; Plate 2.2). The sediment units were defined by grain size, sediment colour, and evidence of lamination, burrowing, and/or exposure.

In most cases, only the surface of the outcrop was sampled. Most exposures are discontinuous, and stratigraphic equivalency has been a problem throughout the decades (Chapter 2; Table 2.1).

Each sample was processed for geochemical analysis. Every lithified sample was brushed, and rinsed with deionized water, dried, and split to obtain uncontaminated representative samples. Uncemented sediment samples were broken down to cobble-size. Magadiite samples and the softer sediments were powdered by hand using an agate pestle and mortar. The cherts and silica-cemented sediments samples were pulverized to a fine powder using a tungsten-carbide swing mill, as an agate mill has similar rock strength to these samples. Powdered samples were sent to ActLabs in Ancaster, Ontario, where they were geochemically analyzed for major and trace element (Package 4E - Research – INAA; TD-ICP; FUS-ICP (see below for method description)).

Major elements were analyzed by FUS-ICP: samples were mixed with a flux of lithium metaborate and lithium tetraborate and fused in an induction furnace, and then analyzed on a Thermo Jarrell-Ash Enviro II ICP/MS. Trace elements of rock and sediment samples were studied by means of INAA (Instrumental Neutron Activation Analysis), TD-ICP (Total Digestion - Induced Coupled Plasma Mass Spectrometry), and FUS-ICP.

Detection limits for samples varied with each element analyzed. See Tables 5.1 to 5.12 in Appendix (Chapter 5) for analytical precision.

Behr & Röhricht (2000) did not analyze all the chert types that they defined. This study is partly a reconnaissance to see if the different types of chert have distinctive chemistry and element distributions. This work may also help to determine the origins of the

precursor material, as unaltered magadiite and silica gel are geochemically distinct from one another, confirming the theories of either Eugster or of Behr, or perhaps both.

3.4 Results

As the siliceous sediments are of greatest interest, these sediments are referred to by their mineral name (e.g., magadiite) or their informal rock name (e.g., bedded chert – adopted from Behr & Röhricht (2000) and Behr (2002)). "Other" sediments refer to the volcaniclastic silts and tuffs, which "host" the siliceous sediments, and have been distinguished as host sediments in this chapter.

3.4.1 Major Elements

The major element distributions in the soft sediments of the Green and the High Magadi Beds, collected above and below the various chert types, correlate well with their inferred parent material, the Magadi Trachytes. Variations in major-element composition of volcanically derived sediments can be attributed to weathering, recent efflorescent-salt encrustation, cementation and other diagenetic processes. From 10- to 15% of most sediment samples analyzed were lost on ignition due to their late pore-filling carbonate content. Cherts are dominantly composed of SiO_2 (90–95%), with each chert type displaying minor variations in other constituents, commonly reflecting pore-filling and pore-lining cements such as calcite.

3.4.1.1 Major element composition by rock type

Geochemical results for analyses of each siliceous rock type are found in the appendix (Tables 5.1 to 5.3). For comparison, the relevant average geochemistry of the Magadi Trachyte is plotted in each graph.

Magadiite, confirmed by XRD analyses (Fig. 3.1), shows a characteristic geochemical signature, high in Na_2O. Major element geochemistry (Appendix; Table 5.1) shows a wide range of SiO_2 content. It also shows the highest Na_2O values (Na_2O vs. TiO_2) for all of the siliceous rocks examined. The CaO values of magadiite samples, in comparison to other sediment types, show mid-range to low values for % content. K_2O content for magadiite is the mid- to upper-range in comparison to other sediments analyzed (Fig. 3.4; Fig. 3.5).

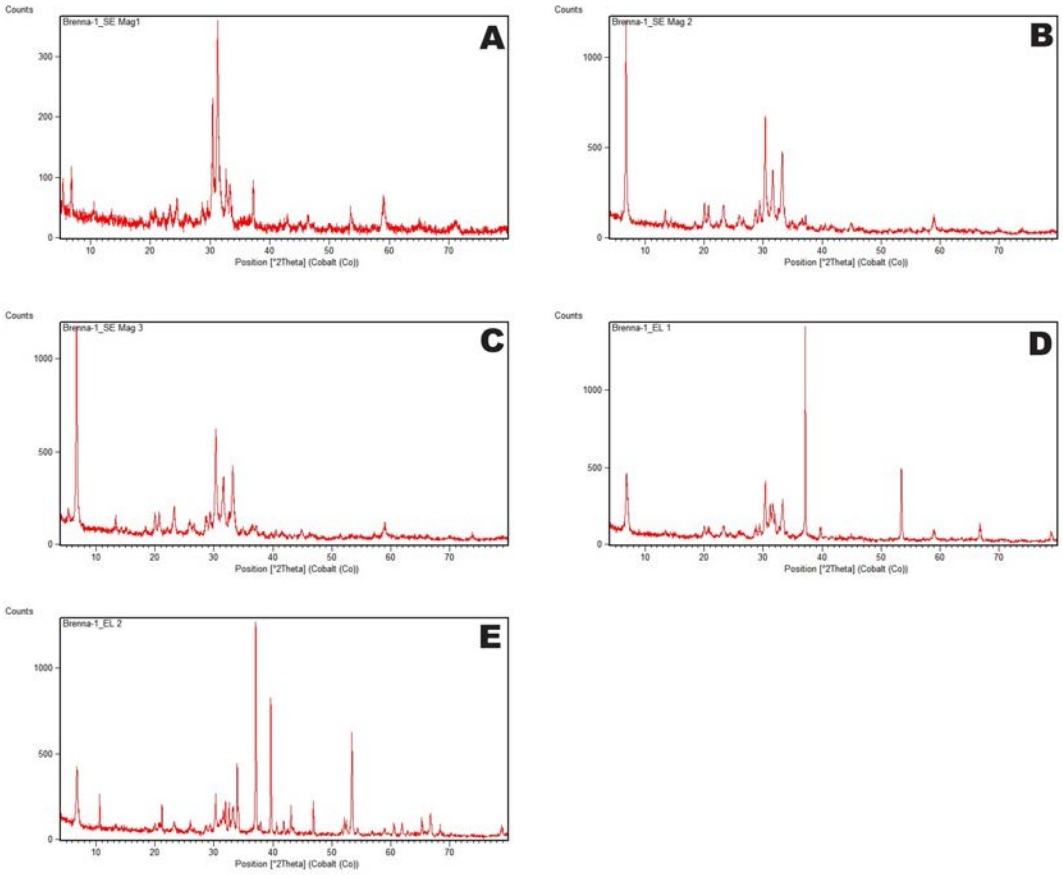

Figure 3.1 - XRD – magadiite

All cherts (Magadi-type, bedded, and intrusive) have been silicified to a high degree, and their XRD patterns are reflective of their uniformity (Fig. 3.2 (Magadi-type chert; Fig. 3.3 (Green Beds Cherts)).

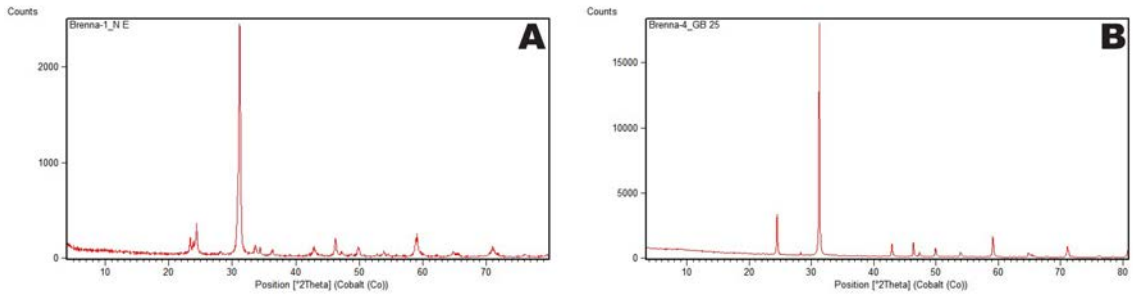

Figure 3.2 – XRD – Magadi-type chert

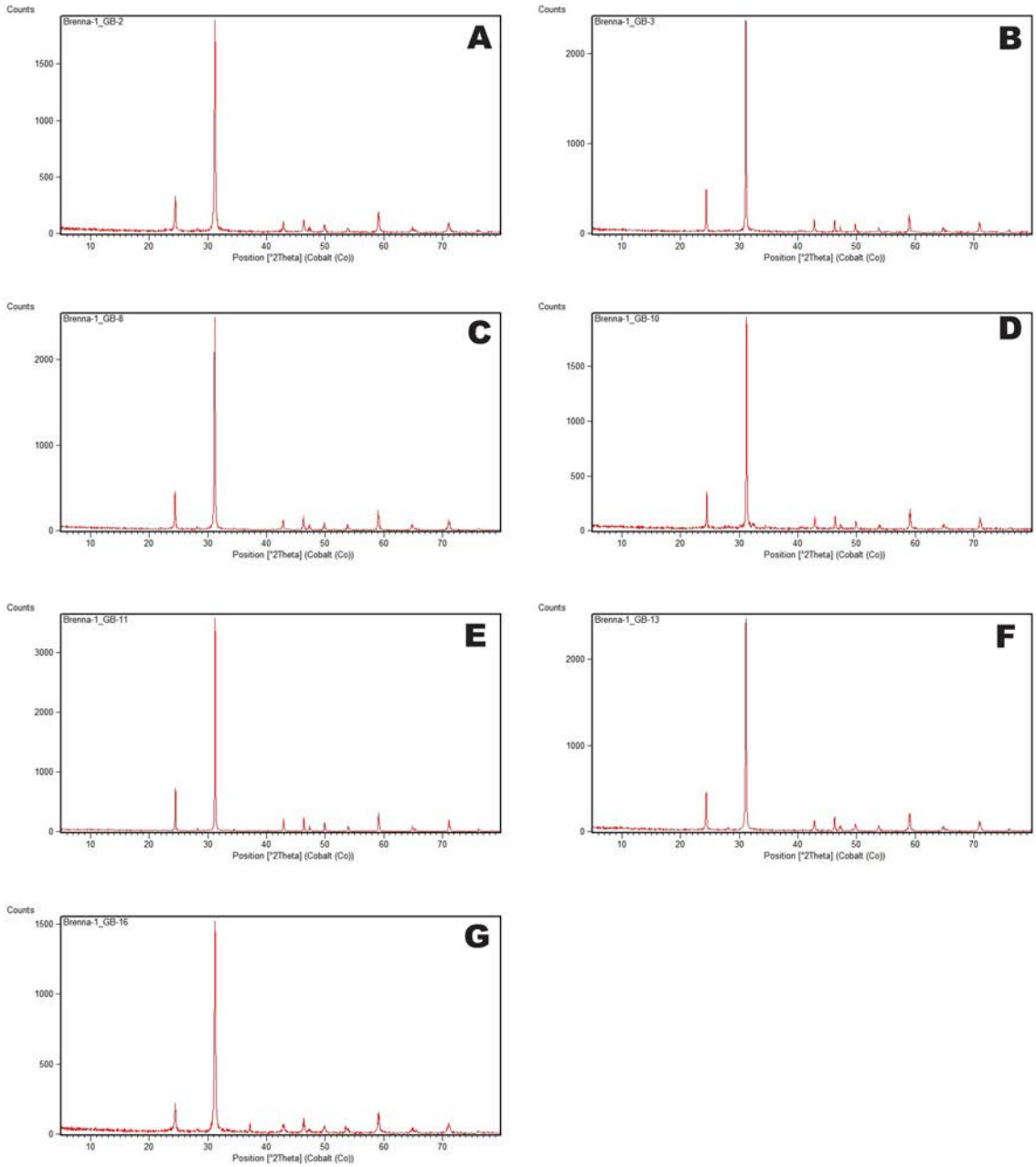

Figure 3.3 – XRD – Green Beds cherts

Unequivocal Magadi-type chert (Fig. 3.4) contains from 80 to 95% SiO_2, and shows the largest range in Na_2O content (plotted against TiO_2), when compared to other varieties of chert. Magadi-type chert shows the greatest range in CaO content, and very low values for K_2O content.

All bedded cherts have a very high SiO_2 content, low Na_2O content, mid-range CaO, and mid- to high range K_2O content (Fig. 3.4).

The intrusive cherts are enriched in SiO_2 content, have low Na_2O content, mid- to high range CaO content, and mid- to high range K_2O content (Fig. 3.4).

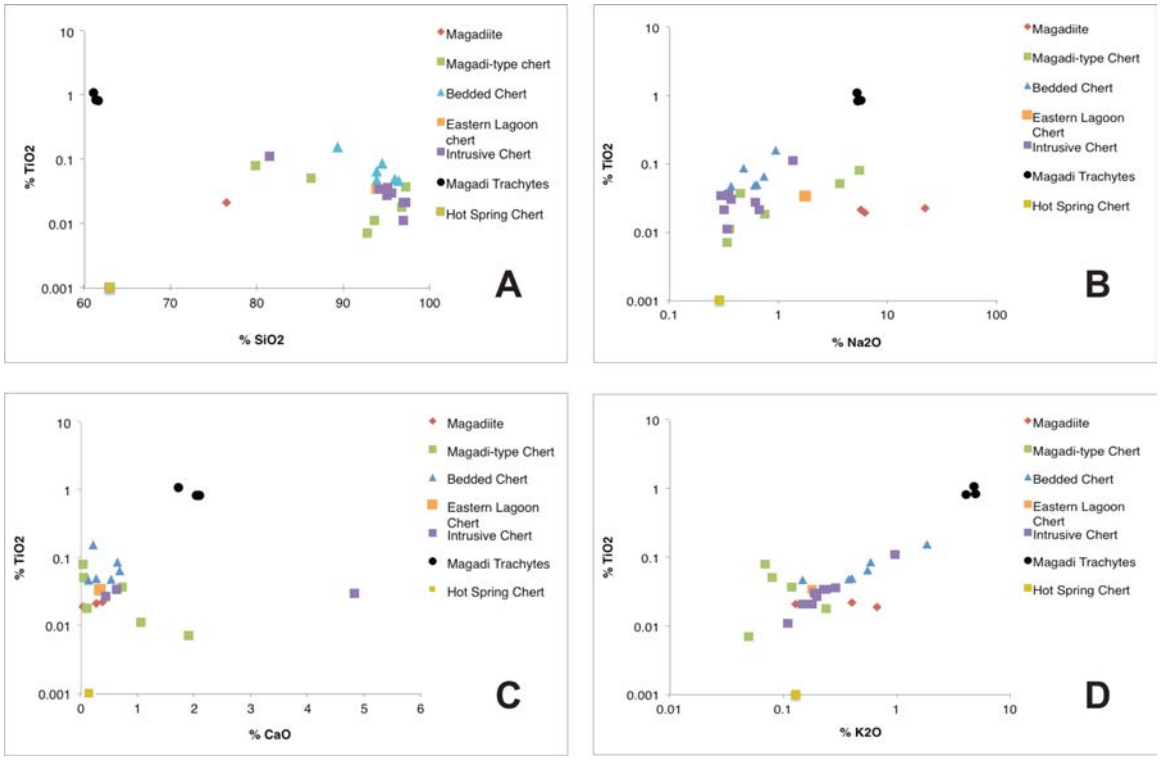

Figure 3.4 - Major elements - siliceous sediments

3.4.1.2 Major element composition by host sediment type

The Lower GB (Fig. 3.5; Appendix; Table 5.3) show a narrow range of values for all major elements analyzed with an outlier in each graph (described in the field as an undisturbed ash

layer). The outlying data point from this sediment group in each graph is a thin ash layer "depleted" in TiO_2 relative to the other sediments.

The Upper GB (Fig. 3.5) shows a near-linear trend of relative depletion of TiO_2 with increasing SiO_2 and Na_2O. No obvious trend is noted for the CaO content of the Upper GB, with concentrations ranging from 0.19 to 9.76%. This unit is markedly depleted in K_2O relative to the Magadi Trachyte, with the lowest values of K_2O recorded near the top of the unit.

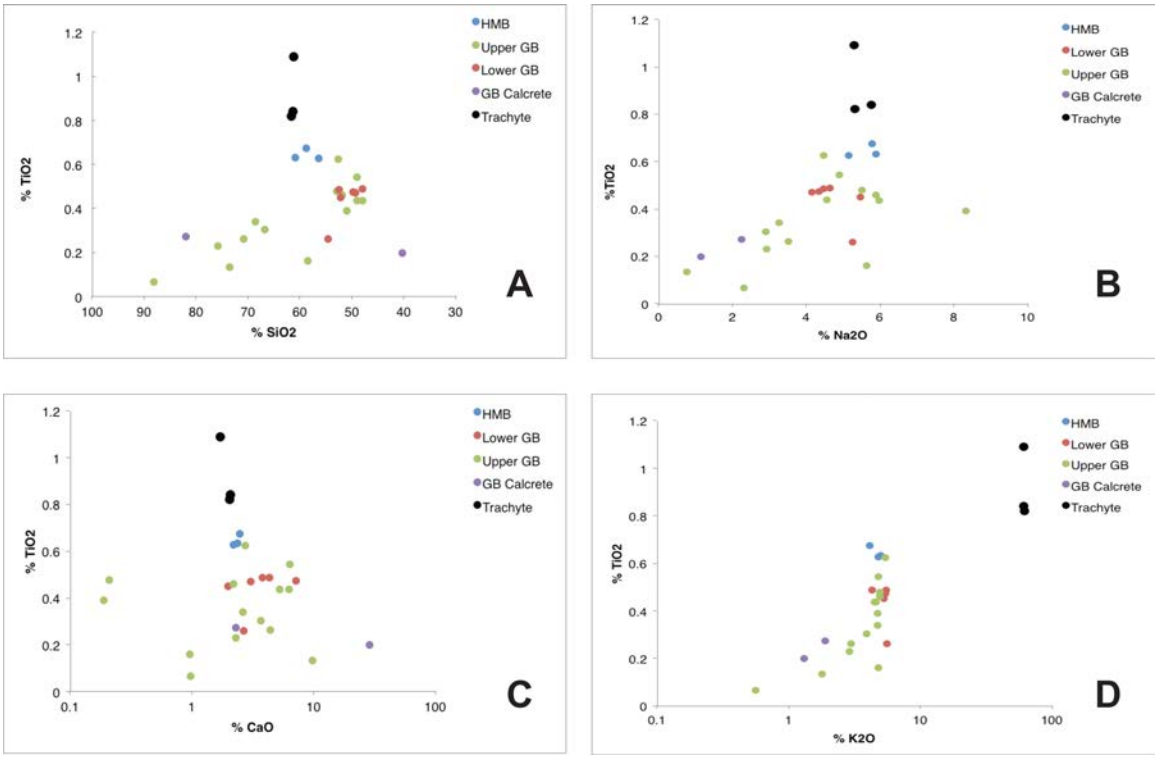

Figure 3.5 – Major elements – host sediments

The GB Calcrete (Fig. 3.5) which caps the Green Beds sequence, is represented by two samples (one rich in chert clasts, the other primarily carbonate cement). The chert-rich calcrete is high in SiO_2; the other has less SiO_2 but more CaO, as expected. Both samples are low in Na_2O and K_2O.

The High Magadi Beds (HMB) (Fig. 3.5) has the highest TiO_2 values of all the sediments analysed. The SiO_2 and Na_2O values are similar to those of the Magadi Trachyte. The CaO

values are clustered, and only slightly enriched relative to the volcanic rocks. The K_2O contents are average compared to most sediments analyzed.

3.4.2 Tri-Plots (A-CN-K Diagrams)

Tri-plots are commonly used to show the chemical alteration of sediments. At Magadi, clastic sediments are altered mainly through reactions between alkaline brine and trachytic debris to form zeolites (Surdam & Eugster, 1976), which are rich in cations, though zeolites are known for their ion exchange capacities (Hay, 1966). The sediments analyzed in this study trend mainly towards the $CaO + Na_2O$ (CN) apex on tri-plots, with Na_2O accounting for most of this trend.

This geochemical interpretation of the chert sediments is considered with a high degree of caution, as the Chemical Index of Alteration (CIA) is commonly used for siliciclastic sediments (Owen *et al.,* 2014), not chemically precipitated rocks. This interpretation considered here in the context of cherts forming from siliceous gels, created by the reaction of trachytic debris and alkaline spring waters. The following observations are considered in relation to the alteration of the parent material, the volcanic tuffs and silts.

Magadiite, which contains substantial sodium (5.55-5.9% by wt. (Eugster, 1969); 3.67 – 6.19 % by wt. (this volume)) trends strongly towards the CN apex and away from the Magadi Trachyte field, the presumed sodium source (Fig. 3.6(A)). The Magadi-type cherts also trend towards the CN apex (Fig. 3.6(B)), whereas the more-variable Green

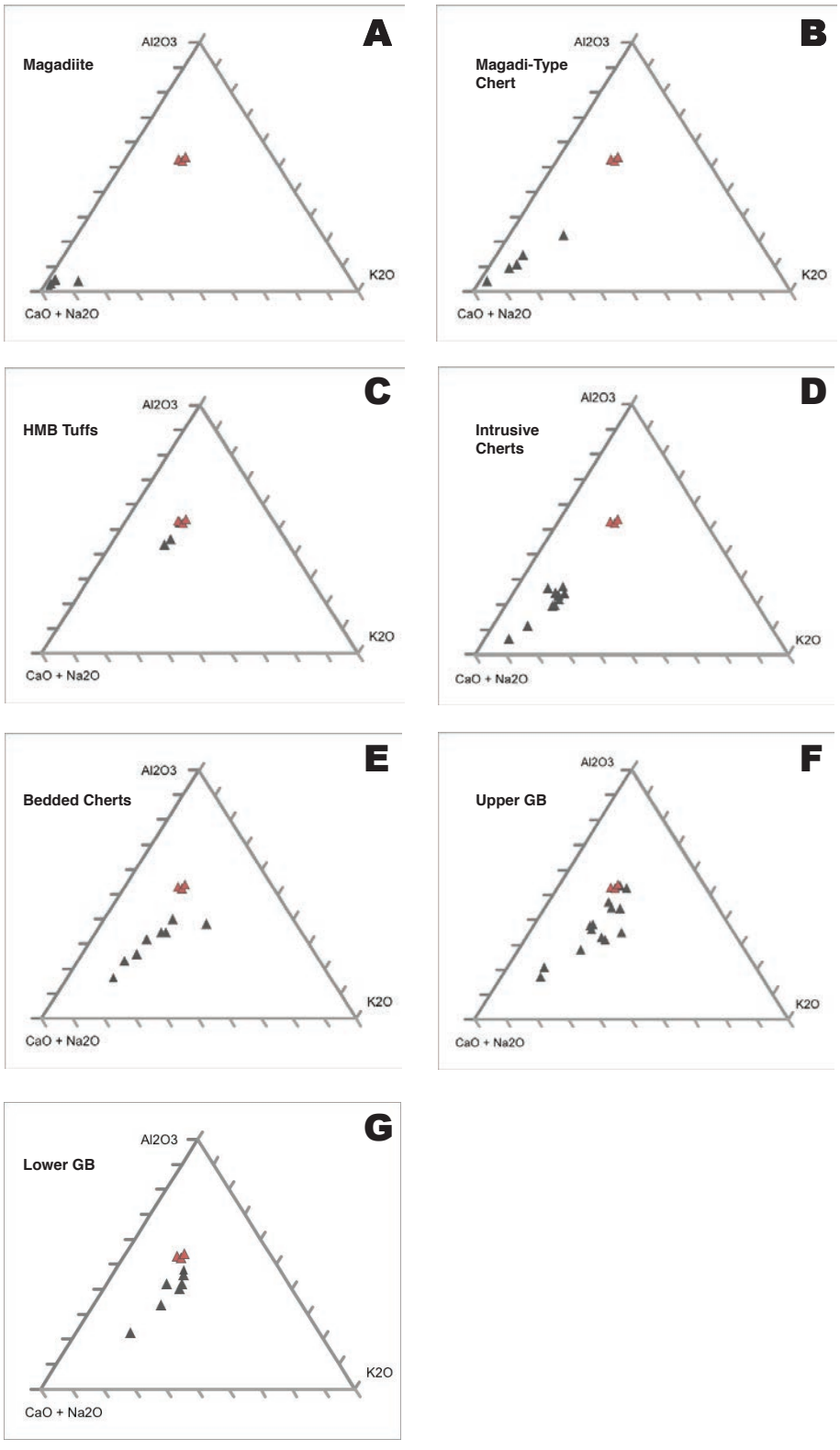

Figure 3.6 – A-CN-K Diagrams (Magadi Trachyte values in red)

Beds cherts trend towards the CN apex , but have a broader spread in values (Fig. 3.6(D & E)). The intrusive cherts cluster more closely, but still towards CN (Fig. 3.6(D)), while the bedded cherts maintain a more variable chemical index of alteration (CIA - see Equation 2; Fig. 3.6(E)).

(2) $\text{CIA} = \left(\frac{Al2O3}{Al2O3+Na2O+K2O+CaO}\right) \times 100$

Host sediments plot much more closely to their parent material, and trend dominantly toward the CN axis. The High Magadi Beds sediments are the most closely related to the Magadi Trachyte in these plots (Fig. 3.6(C)), while the lower Green Beds show a stronger trend towards CN, away from the Magadi Trachyte "origin" (Fig. 3.6(G)), and the upper Green Beds show a characteristically strong trend away from the Magadi Trachyte as well, in the CN apex direction (Fig. 3.6(F)).

3.4.3 Principal Components Analysis (PCA) Plot

Figure 3.7 shows relationships between the chemical constituents (composition) based on their covariance. Samples were grouped under general headings ('zones') to show relationships based on the rock or sediment type. Table 3.1 outlines the groups used (chert types) for statistical analysis.

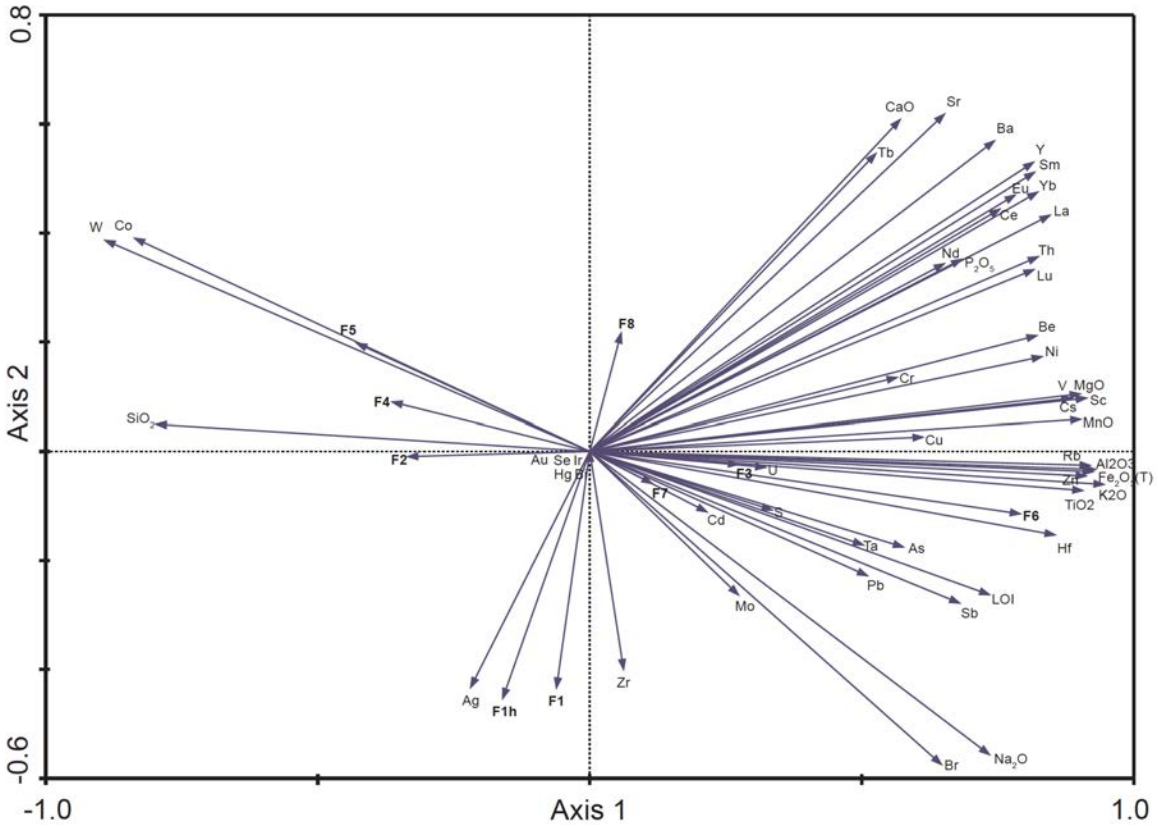

Figure 3.7 – Principle Component Analysis (PCA) plot

The PCA plot (Fig. 3.7) shows a strong separation of SiO_2, W, and Co from most other chemical constituents. Zones F2, F4, and F5 show the strongest correlation with SiO_2, with F5 plotting close to W and Co.

Zone	Description	Sedimentary Unit
F1	Magadiite (soft)	HMB
F1h	Magadiite (firm)	HMB
F2	Magadi-type Chert	HMB
F3	High Magadi Beds sediments	HMB
F4	Bedded Chert	GB
F5	Intrusive Chert	GB
F6	Green Beds sediments	GB
F7	GB oncoids	GB
F8	GB calcrete	GB

Table 3.1. Principal Component Analysis – bulk sample groupings

F1 (magadiite) plots between SiO_2 and Na_2O, as expected from its chemical formula. F1 also correlates with Zr, as also seen in Multi-element plots (discussed later). F1h (firm magadiite) plots slightly closer to SiO_2 than F1, which supports its close chemical relationship.

F3 (HMB sediments) and F6 (Green Beds sediments) plot contrary to SiO_2, amid many of the more stable oxides (TiO_2, Al_2O_3, Fe_2O_3). They also show a close relationship to U and Hf (Appendix; Table 5.9).

Rare earth elements and transition metals are plotted in close proximity in the PCA plots, respectively, with no strong relationship to any of the sediments analyzed. F8 (calcrete) displays a "poor fit" (displayed as shorter vectors, indicating lower degrees of correlative covariance), but plots close to CaO, which supports the petrographic observation of pervasive carbonate cement (likely responsible for CaO content). F7 (GB oncoids – discussed in Chapter 2) was found to have relatively high CaO content (Appendix; Table 5.3), but also displayed considerable values for LOI (up to 30% by wt.). F7 plots near LOI rather than CaO, but the length of the F7 vector indicates "poor fit".

3.4.4 Trace Element Geochemistry

Trace element analyses were performed on all siliceous rock types and their host sediments (Appendix; Tables 5.4 to 5.6). Trace element values were normalized to C1 chondrite (Taylor & MacLennan, 1985) to compare with the results of Owen *et al.* (2011, 2012). Each plot includes the trace element composition of the Magadi Trachyte for comparison (trachyte values are from le Roex *et al.,* 2001).

The depletion of constituents relative to the Magadi Trachyte is variable, and the trace element spider diagram patterns of the exposed cherts and sediments could potentially be used when trying to understand the origin of rock or sediment types in drill core, for example.

3.4.4.1 Trace element composition of magadiite, Magadi-type chert, and the High Magadi Beds

Magadiite and Magadi-type cherts have similar trace-element patterns (Fig. 3.8 (A, B)), implying little fractionation of trace elements during the alteration of magadiite to quartzose chert. The Eu anomaly is pronounced more negatively in these sediments than in the trachyte, which, according to Kerrich *et al.* (2002), may indicate oxidized interactive waters, as they are inhibitive to Eu^{2+} solubility. Magadiite and Magadi-type chert show variably positive Ce. The High Magadi Beds have a flatter REE pattern (Fig. 3.9(A)). Only the stratigraphically higher tuffaceous sediments (sample "SE Magadi 9") show a Eu anomaly, implying variations in redox conditions during deposition.

3.4.4.2 Trace element composition of Green Beds cherts and associated sediments

The cherts forming the dykes, attributed by Behr (2002), show the most unusual REE pattern (Fig. 3.8(E)), with relatively high La-to-Nd values, a strongly negative Eu anomaly, and variable Yb. The pattern of the pillow cherts is less pronounced, but also shows a negative Eu anomaly, whereas other constituents are variable (Fig. 3.8(C)). The trace element patterns seen for the pillow cherts of the Green Beds are variable from one sample to the next, and this patternicity could therefore never be utilized as an indicator.

The REE pattern of the upper and lower Green Beds sediments displays subtle excursions (Fig. 3.9(B,C)) showing a flat pattern from La to Nd, with a slight negative Nd excursion. Sm is

variably positive, while Eu is variably negative, however both excursions are slight. Tb is variably positive, and the remaining elements have a flat trend.

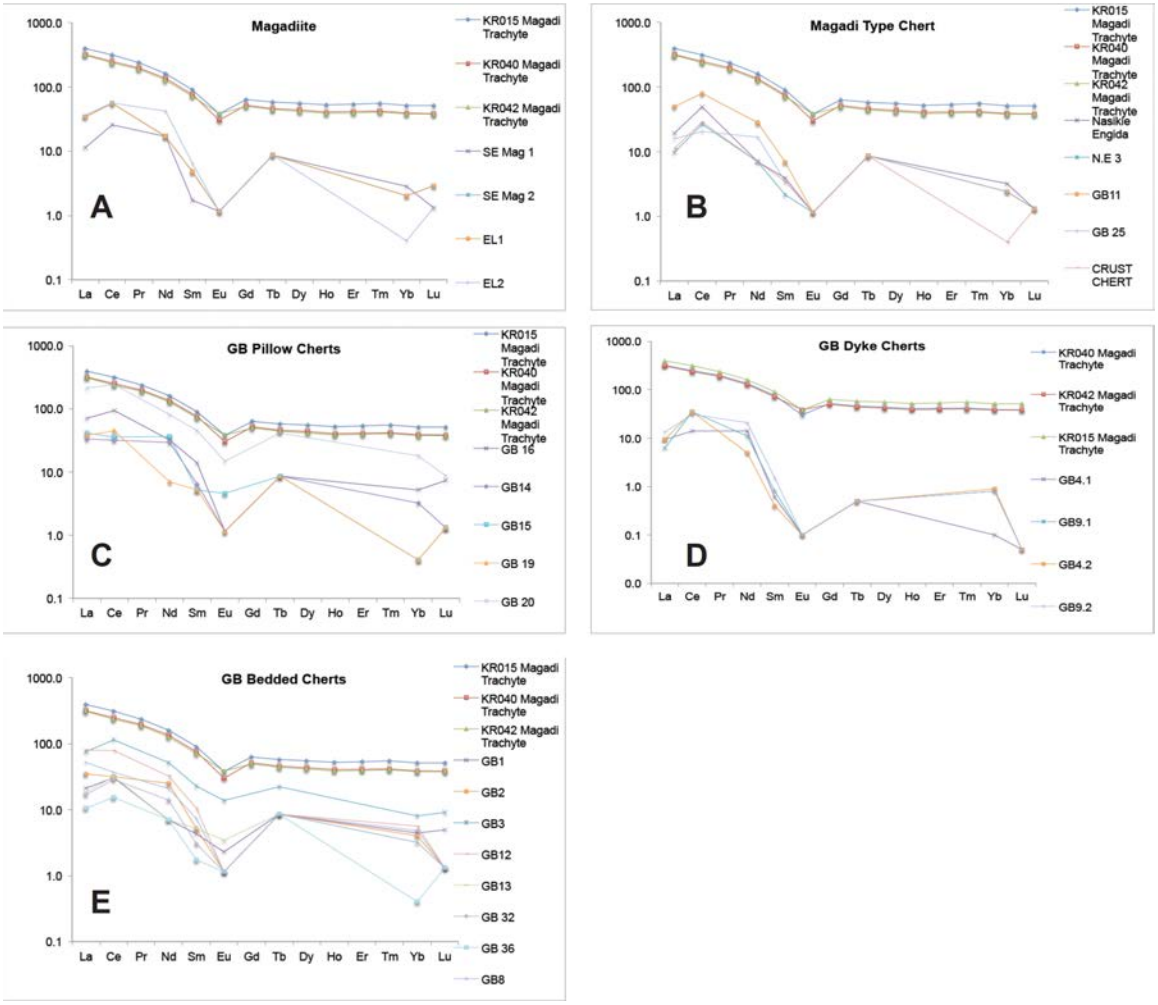

Figure 3.8 - Trace elements - siliceous sediments

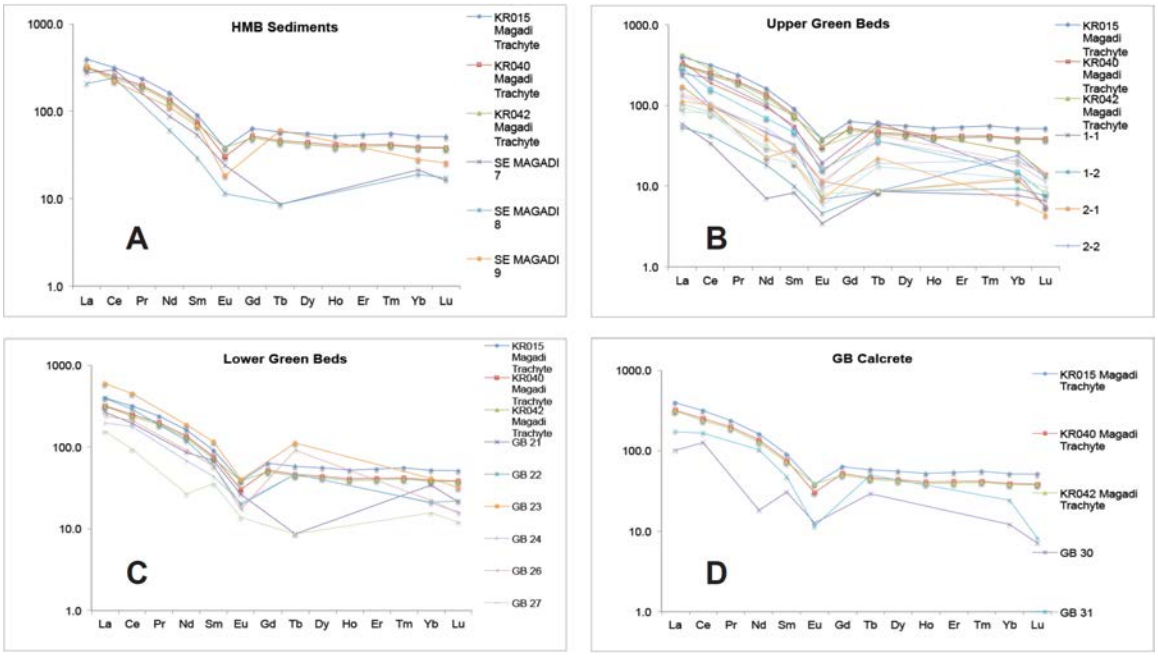

Figure 3.9 – Trace elements – host sediments

3.4.5 Multi-Element Geochemistry

"Multi-element" geochemical values for all sediments were normalized to continental crust (Taylor & MacLennan, 1985), to compare to the work of Kerrich *et al.* (2002) (Appendix; Tables 5.7 to 5.9). Patterns exhibited by magadiite, the dyke cherts and bedded cherts of the Green Beds, and the upper Green Beds sediments show strong coherence from one sample to the next (Fig. 3.10(A, D, E); Fig. 3.11(B)).

Most multi-element plots show the following characteristics, in varying degrees of prominence (Fig. 3.10; Fig. 3.11): High U contents, low Th contents, low Hf, high Zr, and high Ti. The resulting ratios of U/Th and Zr/Hf are high for all the cherts and sediments analysed.

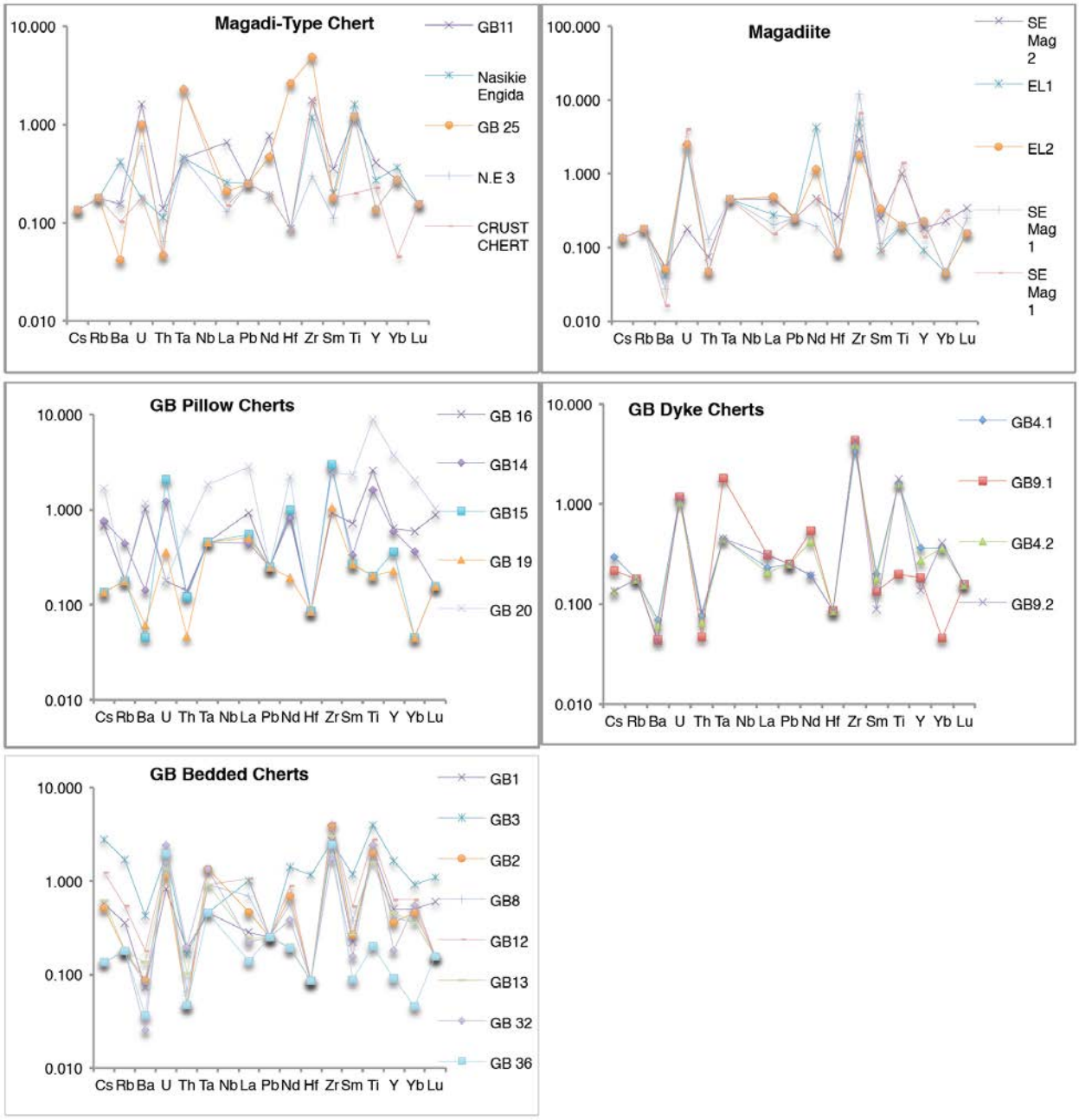

Figure 3.10 - Multi-element plots - siliceous sediments

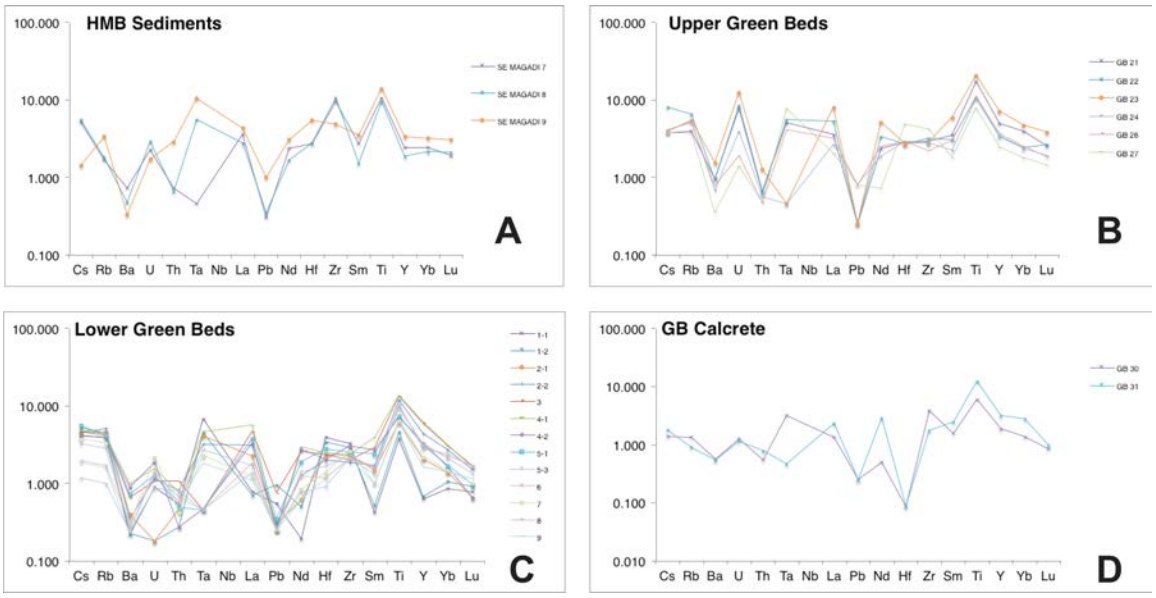

Figure 3.11 - Multi-element plots - host sediments

3.4.6 Transition Metal Geochemistry

Very general trends are observed in the transition metal plots for each sediment type (Fig. 3.12; Fig. 3.13) with no sharp peaks between Sc and Zn; a relative depletion of Cr; high Co in the lithified samples (cherts and silicified samples); and relatively high Ag in almost all samples.

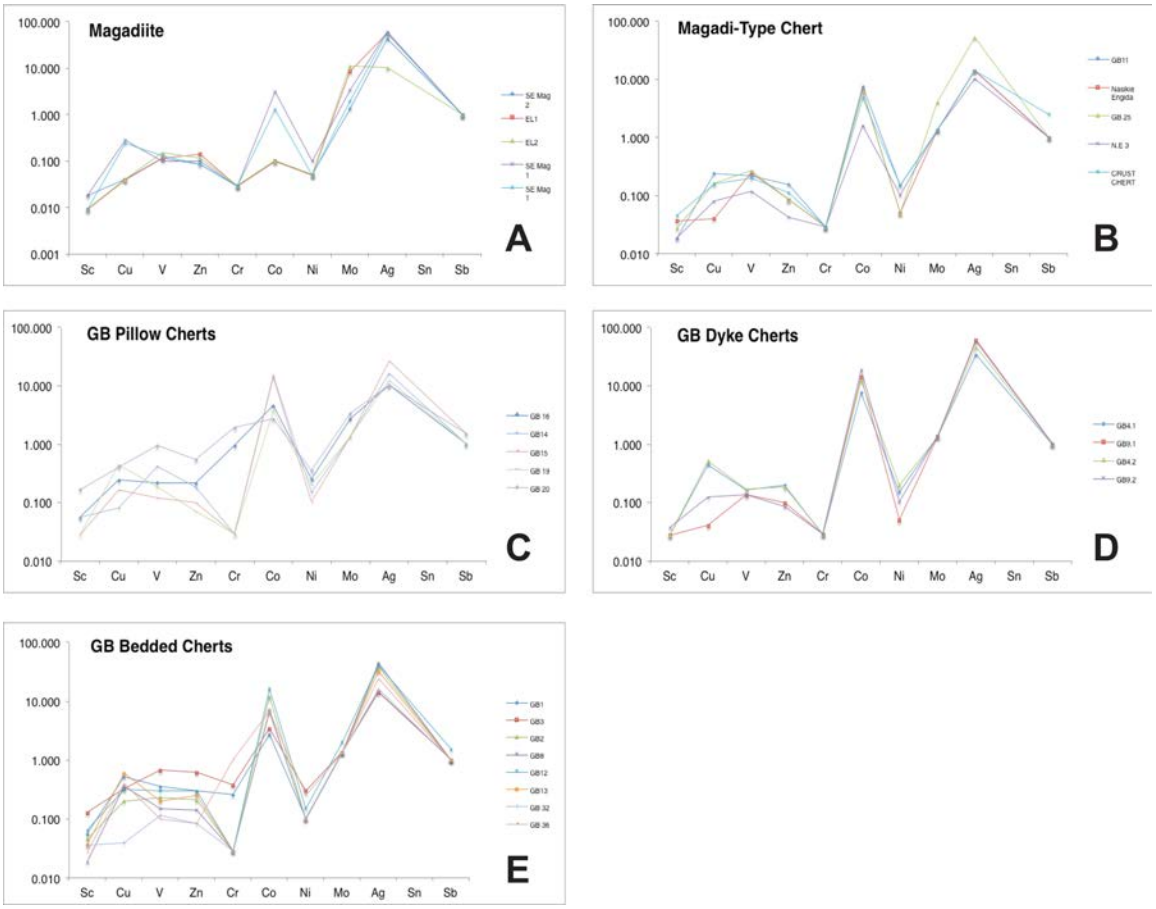

Figure 3.12 - Transition metals - siliceous sediments

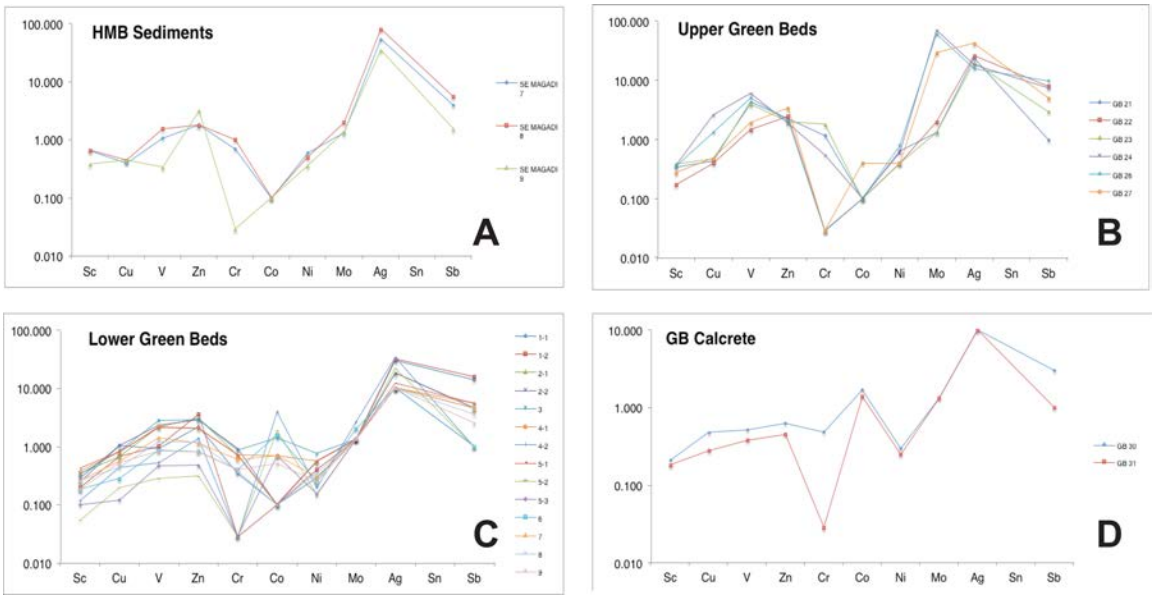

Figure 3.13 - Transition metals - host sediments

3.5 Discussion

The results of this study show element patterns similar to those reported by Kerrich *et al.* (2002) for alkaline lake cherts, and support their general conclusions. Advantages (or disadvantages) to using each plot type are discussed below.

3.5.1 Major Elements vs. TiO_2

These plots (Fig. 3.4; Fig. 3.5) show the relationship of common crustal elements in the studied sediments relative to their parent rock (Magadi Trachyte). TiO_2, a conservative oxide, has been observed to deplete to the same extent as the major element oxides, presumably from a dominance of chemical weathering.

The major elemental values of the trachyte plotted with those of the chert types often graphically displays linear dilution, indicating that the sediments gained or lost constituents relatively congruently, relative to the loss of TiO_2, often experiencing no particular elemental enrichments (other than with respect to SiO_2). Non-linear relationships between major elements and TiO_2 indicate an input or loss of an element from an additional source (i.e. magadiite and Magadi-type chert show relatively high Na contents (Na-silicate precipitated from a saline brine)); scattered CaO plot likely due to presence of secondary $CaCO_3$ as a pore lining or pore filling mineral, precipitated from dilute inflow or shallow dilute groundwater); or a more pronounced weathering of a constituent. Bedded and intrusive cherts from the Green Beds have the highest concentrations of K_2O, potentially from adsorption of K^+ onto gel surfaces (Röhricht, 1999), or relict from diagenetic alteration of trachytic glass to a soft, sodium aluminosilicate gel through interaction of the glass with a high pH brine (Eugster and Jones, 1968).

Major-element plots of the sediments in the Magadi basin show vague trends, if any, with slight gains and losses of constituents relative to the geochemical values of the Magadi Trachyte. The upper Green Beds are enriched in SiO_2, relative to the Magadi Trachyte, whereas the lower Green Beds and the High Magadi Beds show a relative depletion. This interpretation is supported by the presence of cherts at the top of the exposed Green Beds. CaO distribution in the host sediments of the Green Beds and the High Magadi Beds is quite variable. The lower Green Beds and part of the upper Green Beds are enriched in CaO relative to the Magadi Trachyte. This may have been due to fresher conditions at the onset of Green Beds deposition, which supplied Ca^{+} to the lake and precipitated $CaCO_3$ in pore spaces.

3.5.2 Tri-Plots (A-CN-K Diagrams)

Tri-plots commonly show the chemical changes between sediments and their inferred parent rocks after weathering, transport, deposition and diagenesis. These plots include common oxides in silicate rocks (K_2O, $CaO + Na_2O$, Al_2O_3), and show their relative gains and losses in those constituents, compared to their parent lithologies. Intensely altered sediments typically often shift towards the Al_2O_3 apex, as clay minerals are created during acid-silicate hydrolysis (e.g., gibbsite and kaolinite). Samples with compositions that plot near Magadi Trachyte have undergone the least chemical transformation, whereas those furthest from the volcanic parent rocks have experienced more alteration.

3.5.3 Principle Component Analysis (PCA) plot

These plots show relationships between chemical constituents, calculated through linear and orthogonal transitions of a data matrix to create eigenvectors, which depend on covariance of the elements and oxides in the samples examined. The focus of this study is chemical characterization of chert, so it was interesting to note a correlation with W and Co.

Unfortunately, those samples are assumed to have been contaminated during sample preparation in a tungsten-carbide swing mill.

The Principal Component Analysis plot (Fig. 3.7) showed relationships that support certain expectations (dense cherts strongly correlated to SiO_2; calcrete and CaO; magadiite between SiO_2 and Na_2O). The strong correlation between the F6 group (Green Beds sediments) and the chemically resistant oxides might also indicate that these Green Beds sediments underwent more chemical alteration during weathering and diagenesis than the High Magadi Beds, as inferred from the tri-plots.

3.5.4 Trace Element Geochemistry

Trace element plots of sediment geochemistry has been used to determine sediment provenance (e.g., Zhang *et al*., 2014; Owen *et al.,* 2011), and, according to Kerrich *et al.* (2002) help to distinguish the geodynamic and depositional setting of cherts (in marine sediments). The Magadi Trachyte is the dominant lithology that crops out in the Magadi basin, and the provenance of the later sediments is therefore predictable. Trace elements can be used to distinguish cherts deposited in alkaline lacustrine settings from marine cherts in the rock record.

Several geochemical characteristics separate alkaline cherts from marine cherts: (1) relatively flat, but negatively fractionated, REE patterns; and (2) positive Ce but negative Eu anomalies (Kerrich *et al.,* 2002). These trends are confirmed by the findings of this study. Positive Ce values reflect its higher solubility for Ce^{2+} than its trivalent neighbouring elements (Moller & Bau, 1993).

3.5.5 Multi-Element Geochemistry

Multi-element geochemical plots include elements beyond the REEs, and show, in this study, strong patterns that indicate characteristic compositions for alkaline volcanic sediments modified

by saline alkaline brines. Kerrich *et al.* (2002) also noted characteristics that may be inherited from a highly alkaline fluid. These include high absolute concentrations of U and Zr (as well as normalized enrichments of U and Zr in relation to REE); profound fractionations of U/Th and Zr/Hf. High alkalinity has been documented over the history of the basin from zeolitic evidence (Mariner and Surdam, 1970), and the increase in evaporite precipitation through the Holocene (Baker, 1958).

3.5.6 Transition Metal Geochemistry

Transition metal geochemical plots (Figs. 3.12, 3.13) show the relative abundance of transition metals in the sediments of Magadi basin, with only Co and Ag showing enrichment. As noted, these enrichments likely are due to contamination.

3.6 Conclusion

While the results of this study were unsuccessful in providing discernable geochemical differences, and reliable repeatable patterning, between the varieties of chert at Magadi, they helped to reinforce the findings of Kerrich *et al.* (2002), and the common characteristics of cherts formed in highly alkaline lacustrine environments.

Specific characteristics noted in this study include: (1) general weathering of Magadi trachyte (linear dilution patterns in major element plots, and a common trend in increasing $CaO + Na_2O$ [tri-plots]); (2) higher Na_2O contents in the "interbedded" sediments of the Green Beds (between chert layers -- especially the Upper Green Beds) than in the interbedded sediments of the High Magadi Beds; (3) greater REE fractionation in magadiite, Magadi-type chert, and the bedded cherts (compared to the Magadi trachyte), than in the intrusive cherts; (4) enriched U and Zr in relation to other REEs, for all sediment types; (5) generally high U/Th and Zr/Hf; (6) enrichments in Co and Ag in the cherts.

3.7 REFERENCES

Baker, B.H. (1958) Geology of the Magadi Area: Report. 42. Kenyan Government Printer, Nairobi, pp. 88.

Baker, B.H. (1986) Tectonics and volcanism of the southern Kenya Rift Valley and its influence on rift sedimentation. *Geol. Soc. London, Spec. Publ.* **25**, 45–57.

Behr, H.J. (2002) Magadiiite and Magadi Chert: A Critical Analysis of the Silica Sediments in the Lake Magadi Basin, Kenya. In: Sedimentation in Continental Rifts (Eds R.W. Renaut and G.M. Ashley)*, SEPM Special Publication,* 73*,* 257–273.

Behr, H.J., and **Röhricht, C.** (2000) Record of seismotectonic events in siliceous cyanobacterial sediments (Magadi cherts), Lake Magadi, Kenya. *Int. J. Earth Sci.,* **89**, 268–283.

Butzer, K.W., Isaac, G.L., Richardson, J.L., and **Washbourn-Kamau, C.** (1972) Radiocarbon Dating of East African Lake Levels. *Science,* **175**, 1069–1076.

Cohen, A.S. , Campisano, C., Arrowsmith, R., Asrat, A., Behrensmeyer, A.K., Deino, A., Feibel, C., Hill, A., Johnson, R., Kingston, J., Lamb, H., Lowenstein, T., Noren, A., Olago, D., Owen, R.B., Potts, R., Reed, K., Renaut, R., Schäbitz, F., Tiercelin, J.-J., Trauth, M.H., Wynn, J., Ivory, S., Brady, K., O'Grady, R., Rodysill, J., Githiri, J., Russell, J., Foerster, V., Dommain, R., Rucina, S., Deocampo, D., Russell, J., Billingsley, A., Beck, C., Dorenbeck, G., Dullo, L., Feary, D., Garello, D., Gromig, R., Johnson, T., Junginger, A., Karanja, M., Kimburi, E., Mbuthia, A., McCartney, T., McNulty, E., Muiruri, V., Nambiro,E., Negash, E.W., Njagi, D., Wilson, J.N.,

Rabideaux, N., Raub,T., Sier,M.J., Smith, P., Urban, J., Warren, M., Yadeta, M., Yost, C., and **Zinaye, B.** (2016). The Hominin Sites and Paleolakes Drilling Project: Inferring the Environmental Context of Human Evolution from Eastern African Rift Lake Deposits. *Scientific Drilling*, **21**, 1-16.

Eugster, H.P. (1967) Hydrous Sodium Silicates from Lake Magadi, Kenya: Precursors of Bedded Chert. *Science*, **157**, 1170–1180.

Eugster, H.P. (1969) Inorganic Bedded Cherts from the Magadi Area, Kenya. *Contrib. to Mineral. Petrol.,* **22**, 1–31.

Eugster, H.P. (1970) Chemistry and Origin of the Brines of Lake Magadi, Kenya. *Mineral. Soc. Am. Spec. Pap.,* **3**, 213–235.

Eugster, H.P. (1980) Lake Magadi, Kenya, and its Precursors, In: Hypersaline Brines and Evaporitic Environments. (Ed Nissenbaum, A.), Elsevier Scientific Publishing Company, Amsterdam, The Netherlands, pp. 195–232.

Eugster, H.P. (1986) Lake Magadi, Kenya: a model for rift valley hydrochemistry and sedimentation. *Geol. Soc. London, Spec. Publ.,* **25**, 177–189.

Eugster, H.P., and **Hardie, L.A. (**1978) Lakes: Chemistry, Geology, Physics. In: Lerman, A. (Ed.), Springer New York, New York, NY, pp. 237–293.

Eugster, H.P., and **Jones, B.F. (**1968) Gels Composed of Sodium-Aluminum Silicate, Lake Magadi, Kenya. *Science,* **161**, 160–163.

Eugster, H.P., and **Jones, B.F.** (1979) Behaviour of major solutes during closed-basin brine evolution. *Am. J. Sci.*, **279**, 609–631.

Fairhead, J.D., Mitchell, J.G., and **Williams, L.A.J.** (1972) New K/Ar Determinations on Rift Volcanics of S. Kenya and their Bearing on Age of Rift Faulting. *Nat. Phys. Sci.,* **238**, 66-69.

Goetz, C., and **Hillaire-Marcel, C.** (1992) U-series disequilibria in early diagenetic minerals from Lake Magadi sediments, Kenya: Dating potential. *Geochim. Cosmochim. Acta*, **56**, 1331–1341.

Hardie, L.A., and **Eugster, H.P.** (1980) Evaporation of seawater: calculated mineral sequences. *Science*, **208**, 498–500.

Hay, R.L. (1966) Zeolites and Zeolitic Reactions in Sedimentary Rocks. *Geological Society of America Special Papers*, **85**, 1-122.

Hay, R.L. (1968) Chert and its sodium-silicate precursors in sodium-carbonate lakes of East Africa. *Contrib. to Mineral. Petrol.,* **17**, 255–274.

Hillaire-Marcel, C., and **Casanova, J.** (1987) Isotopic Hydrology and Paleohydrology of the Magadi (Kenya)- Natron (Tanzania) Basin During the Late Quaternary. *Palaeogeography, Palaeoclimatology, Palaeoecology,* **58**, 155–181.

Jones, B.F., Eugster, H.P., and **Rettig, S.L.** (1977) Hydrochemistry of the Lake Magadi basin , Kenya. *Geochim. Cosmochim. Acta,* **41**, 53–72.

Jones, B.F., Rettig, S.L., and **Eugster, H.P.** (1964) Silica in Alkaline Brines. *Science,* **158**, 1310–1314.

Kerrich, R., Renaut, R.W., and **Bonli, T**. (2002) Trace Element Composition of Cherts from Alkaline Lakes in the East African Rift: A Probe for Ancient Counterparts. In: *Sedimentation in Continental Rifts* (Eds R.W. Renaut and G.M. Ashley)*, SEPM Special Publication,* **73***,* 275–294.

le Roex, A.P., Spath, A., and **Zartman, R.E.** (2001) Lithosheric thickness beneath the southern Kenyan Rift: implications from basalt geochemistry. *Contrib. Mineral Petrol.*, **142,** 89-106.

Moller, P. and **Bau, M.** (1993) Rare-earth patterns with positive cerium anomaly in alkaline waters from Lake Van, Turkey. *Earth and Planetary Science Letters*, **117**, 671-676.

ONeil, J.R. and **Hay, R.L**. (1973) $^{18}O/^{16}O$ Ratios in Cherts Associated with the Saline Lake Deposits of East Africa. *Earth and Planetary Science Reviews,* **19**, 257–266.

Owen, R.B., Lee, R., and **Renaut. R.W. (**2012) Early Pleistocene lacustrine sedimentation and diatom stratigraphy at Munya wa Gicheru, southern Kenya Rift Valley. *Palaeogeography, Palaeoclimatology, Palaeoecology,* **331-332**, 60-74.

Owen, R.B., Renaut, R.W, Potts, R. and **Behrensmeyer, A.K.** (2011) Geochemical trends through time and lateral variability of diatom floras in the Pleistocene Olorgesailie Formation, southern Kenya Rift Valley. *Quaternary Research,* **76,** 167-179.

Owen, R.B., Renaut, R.W., Behrensmeyer, A.K., and **Potts, R** (2014) Quaternary geochemical stratigraphy of the Kedong-Olorgesailie section of the southern Kenya Rift valley. *Palaeogeography, Palaeoclimatology, Palaeoecology,* **396,** 194-212.

Parkinson, J. (1914) East African Trough in the Neighbourhood of Soda Lakes. *The Geographical Journal,* **44**, 33–46.

Röhricht, C. (1999) Lithologie und Genese der Chertserien des Magadi Beckens, Lake Magadi, Kenia. Georg-August-Universitat zu Gottigen, Ph. D. Thesis, pp. 106.

Schubel, K.A., and **Simonson, B.M.** (1990) Petrography and Diagenesis of Cherts From Lake Magadi, Kenya. *J. Sediment. Petrol.,* **60**, 761–776.

Sheppard, R.A., and **Gude, A.J.** (1986) Magadi-Type Chert - A Distinctive Diagenetic Variety From Lacustrine Deposits. In: Studies in Diagenesis (Ed Mumpton, F.A.), *U.S. Geological Survey Bulletin,* **1578**, 335-345.

Surdam, R.C., and **Eugster, H.P.** (1976) Mineral reactions in the sedimentary deposits of the Lake Magadi region, *Kenya. Geol. Soc. Am. Bull.*, **87**, 1739–1752.

Taylor, S.R., and **McLennan, S.M.** (1985) The Continental Crust; Its composition and evolution; an examination of the geochemical record preserved in sedimentary rocks. *Blackwell, Oxford.* pp. 312.

Tichy, H. and **Seegers, L.** (1999) The Oreochromis alcalicus flock (Teleostei: Cichlidae) from lakes Natron and Magadi, Tanzania and Kenya: a model for the evolution of "new" species flocks in historical times. *Ichtyol. Explor. Freshwaters,* **10**, 147–174.

Williamson, D., Taieb, M., Damnati, B., Icole, M., and **Thouveny, N.** (1993) Equatorial extension of the younger Dryas event: rock magnetic evidence from Lake Magadi (Kenya). *Glob. Planet. Change,* **7**, 235–242.

Zhang, Y., Pe-Piper, G., and **Piper, D.J.W. (2014)** Sediment geochemistry as a provenance indicator: Unravelling the cryptic signatures of polycyclic sources, climate change, tectonism and volcanism. *Sedimentology*, **61**, 383-410.

CHAPTER 4

CONCLUSION

4.1 Overview

The Green Beds sediment unit shows indications of alternating lake conditions, from shallow and evaporative, to potentially hot-spring dominated, to periodic freshwater incursions. Alkaline spring- and lake-water reacting with trachytic debris allowed for siliceous gel formation, providing volumes of precursor material for chert formation. The combination of silica-rich spring water, evaporative conditions, seismic activity, and a highly productive microbial community allowed for the passive silicification and chert formation in the Green Beds unit. Microbial mats are considered to have been a fundamental component in chert formation, providing protection for the gels, as well as a moisture wicking surface. The lack of geochemical patterning omits this method as a means of chert-type identification, without sedimentological context (e.g., drillcore).

4.2 Future work

Sediment cores extracted from Lake Magadi during the summer of 2014 will reveal the nature of the Green Beds and other sedimentary units encountered at depth (Cohen *et al*., 2016). The findings presented in this study will be used in conjuction with drill core observations to aid in paleoenvironmental reconstruction.

4.3 Broader implications

The superficial resemblance of the Magadi cherts to Archean cherts raises significant questions about their mode of occurrence, and the depositional environment of ancient chert deposits. It is possible that certain processes responsible for Magadi's cherts might also be relevant to Archean chert formation. Eugster & Chou (1973) once considered magadiite to be a

possible precursor to chert in Precambrian banded iron formations. Here, it is suggested that Magadi cherts may be analogous to ancient stromatolites.

Schopf (1987, 1993) made observations of Early Archean bedded and stromatolitic cherts, found in Western Australia, believed to host some of the oldest evidence of microbial life. Brasier (2004, 2011) questioned this evidence for early life, highlighting insufficiencies in biological classification, and providing an alternative explanation for measured carbon content (hydrothermal graphite). More recently, Van Kranendonk (2011) used macro-observations of stromatolitic characteristics to determine biogenicity.

While this controversy persists, and is of utmost importance, the environment in which these cherts formed has also been considered and reconsidered many times. From evidence within these Western Australian cherts, the proposed paleoenvironments for stromatolite/microbial mat formation include: (1) shallow evaporative lagoon (Groves *et al.,* 1981; Walter *et al.,* 1980); (2) marine sandstone (Schopf, 1993); (3) shallow marine sabkha (Lowe, 1980; 1983); (4) submarine pillow basalt (Banerjee *et al.,* 2007; Furnes *et al.,* 2007); (5) chemotrophic community with a hydrothermal vent association (Rasmussen, 2000); (6) sediment-hosted microbes with hydrothermal influence (Duck *et al.,* 2007).

From a strictly morphological standpoint, it is reasonable to compare the stromatolitic textures of the Magadi cherts (Plates 2.3, 2.4 & 2.5), to the Apex cherts in Western Australia (Fig. 4.1). With this, it may be of interest to consider a hydrothermally-influenced soda lake as a potential paleoenvironment for Early Archean cherts. Primary silicification may also be a consideration.

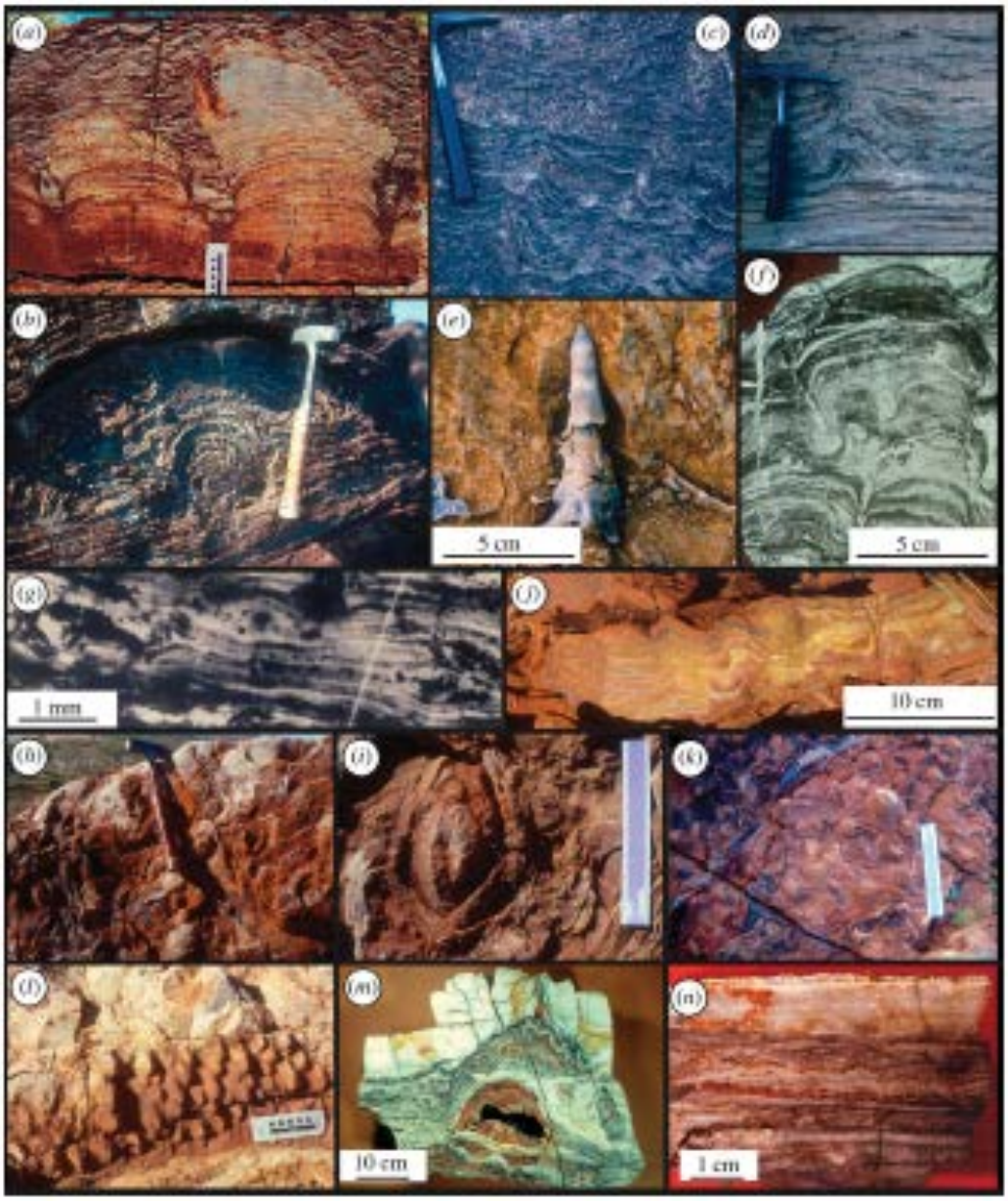

Figure 4.1 - From Schopf (2006); stomatolitic textures observed in Archean rocks

4.4 REFERENCES

Banerjee, N.R., Simonnetti, A., Furnes, H., Muehlenbachs, K., Staudigel, H., Heaman, L., and **Van Kranendonk, M.J.** (2007) Direct dating of Archean microbial ichnofossils. *Geology,* **35**, 487–490.

Brasier, M.D., Green, O.R., Jephcoat, A.P., Kleppe, A.K., Van Kranendonk, M.J., Lindsay, J.F., Steele, A. and **Grassineauk, N.V.** (2002) Questioning the evidence for Earth's oldest fossils. *Nature*, 416, 76-81.

Brasier, M.D., Green, O.R., Lindsay, J.F., McLoughlin, N., Stoakes, C.A., Brasier, A.T., and Wacey, D. (2011) Geology and putative microfossil assemblage of the c. 3460 Ma 'Apex chert', Western Australia – a field and petrographic guide. *Geologic Survey of Western Australia*, Record 2011/7, pp. 60.

Cohen, A.S. , Campisano, C., Arrowsmith, R., Asrat, A., Behrensmeyer, A.K., Deino, A., Feibel, C., Hill, A., Johnson, R., Kingston, J., Lamb, H., Lowenstein, T., Noren, A., Olago, D., Owen, R.B., Potts, R., Reed, K., Renaut, R., Schäbitz, F., Tiercelin, J.-J., Trauth, M.H., Wynn, J., Ivory, S., Brady, K., O'Grady, R., Rodysill, J., Githiri, J., Russell, J., Foerster, V., Dommain, R., Rucina, S., Deocampo, D., Russell, J., Billingsley, A., Beck, C., Dorenbeck, G., Dullo, L., Feary, D., Garello, D., Gromig, R., Johnson, T., Junginger, A., Karanja, M., Kimburi, E., Mbuthia, A., McCartney, T., McNulty, E., Muiruri, V., Nambiro,E., Negash, E.W., Njagi, D., Wilson, J.N., Rabideaux, N., Raub,T., Sier,M.J., Smith, P., Urban, J., Warren, M., Yadeta, M., Yost, C., and **Zinaye, B.** (2016). The Hominin Sites and Paleolakes Drilling Project: Inferring the

Environmental Context of Human Evolution from Eastern African Rift Lake Deposits. *Scientific Drilling*, **21**, 1-16.

Duck, L.J., Glikson, M., Golding, S.D., and **Webb, R.E.** (2007) Microbial remains and other carbonaceous forms form the 3.24 Ga Sulphur Springs black smoker deposit, Western Australia. *Precambrian Research,* **154**, 205–220.

Eugster, H.P., and **Chou, I.M.** (1973) The depositional environments of Precambrian banded iron-formations. *Economic Geology*, **86**, 1144-1168.

Furnes, H., Banerjee, N.R., Staudigel, H., Muehlenbachs, K., de Wit, M., and **Van Kranendonk, M.J.** (2007) Comparing petrographic signatures of bioalteration in recent to Mesoarchean pillow lavas: Tracing subsurface life in oceanic igneous rocks. *Precambrian Research,* **158**, 156–176.

Groves, D.I., Dunlop, J.S.R., and **Buick, R.** (1981) An early habitat of life. *Scientific American,* **245**, 64–73.

Lowe, D.R. (1980) Stromatolites 3,400-Myr old from the Archaean of Western Australia. *Nature* **284**, 441–443.

Lowe, D.R. (1983) Restricted shallow-water sedimentation of Early Archean stromatolitic and evaporitic strata of the Strelley Pool Chert, Pilbara Block, Western Australia. *Precambrian Research,* **19**, 239–283.

Rasmussen, B. (2000) Filamentous microfossils in a 3,235-million-year-old volcanogenic massive sulphide deposit. *Nature*, **405**, 676–679.

Walter, M.R., Buick, R., and **Dunlop, J.S.R.** (1980) Stromatolites, 3,400–3,500 Myr old from the North Pole area, Western Australia. Nature, **284**, 443–445.

Schopf, J. W. and **Packer, B. M.** (1987) Early Archean (3.3 billion to 3.5 billion-year-old) microfossils from Warrawoona Group, Australia. *Science,* **237**, 70-73.

Schopf, J. W. (1993) Microfossils of the Early Archean Apex Chert: new evidence of the antiquity of life. *Science,* **260**, 640-646.

Schopf, J. W. (2006) Fossil evidence of Archaean life. *Phil. Trans. R. Soc. B*, **361**, 869–885.

Van Kranendonk, M.J. (2011) Morphology as an Indictor of Biogenicity for 3.5–3.2 Ga Fossil Stromatolites from the Pilbara Craton, Western Australia, *Advances in Stromatolite Geobiology*, pp. 537-554.

CHAPTER 5

APPENDIX

Table 5.1 – Major Element Composition of Magadiite

Analyte Symbol		SiO2	Al2O3	Fe2O3(T)	MnO	MgO	CaO	Na2O	K2O	TiO2	P2O5	LOI	Total
Detection Limit		0.01	0.01	0.01	0.01	0.01	0.01	0.01	0.01	0.005	0.01		0.01
Analysis Method		FUS-ICP	FUS-ICP	FUS-ICP	FUS-ICP	FUS-ICP	FUS-ICP	FUS-ICP	FUS-ICP	FUS-ICP	FUS-ICP	FUS-ICP	FUS-ICP
Sample Type	Sample Name	%	%	%	%	%	%	%	%	%	%	%	%
Magadiite	EL1	56.97	0.31	0.16	0.01	0.06	0.04	6.19	0.68	0.019	0.02	34.09	98.54
	EL2	36.77	0.35	0.19	0.01	0.04	0.38	22.03	0.41	0.022	0.04	39.07	99.31
	SE Mag 1.1	79.83	0.2	0.1	0.01	0.01	0.04	5.52	0.07	0.08	0.01	13.83	99.7
	SE Mag 1.2	86.23	0.18	0.13	0.01	0.02	0.05	3.67	0.08	0.051	0.01	10.55	101
	SE Mag 2	76.47	0.31	0.18	0.01	0.04	0.27	5.69	0.13	0.021	0.01	15.06	98.17

Table 5.2 - Major Element Composition of Various Chert Types

Analyte Symbol		SiO2	Al2O3	Fe2O3(T)	MnO	MgO	CaO	Na2O	K2O	TiO2	P2O5	LOI	Total
Detection Limit		0.01	0.01	0.01	0.01	0.01	0.01	0.01	0.01	0.005	0.01		0.01
Analysis Method		FUS-ICP	FUS-ICP	FUS-ICP	FUS-ICP	FUS-ICP	FUS-ICP	FUS-ICP	FUS-ICP	FUS-ICP	FUS-ICP	FUS-ICP	FUS-ICP
Sample Type	Sample Name	%	%	%	%	%	%	%	%	%	%	%	%
Magadi-type chert	NE 1	93.65	0.16	0.1	0.01	0.06	1.06	0.36	0.11	0.011	0.01	2.65	98.17
	NE 3	92.81	0.1	0.07	0.01	0.03	1.9	0.34	0.05	0.007	0.01	4.42	99.75
	EL 3	93.78	0.16	0.27	0.01	0.03	0.33	1.74	0.18	0.034	0.02	4.27	100.8
	CRUST CHERT	94.55	0.29	0.67	0.01	0.09	1.09	0.42	0.16	0.022	0.01	2.96	100.3
	GB 11	97.24	0.16	0.32	0.01	0.05	0.73	0.45	0.12	0.037	0.01	1.57	100.7
	GB 25	96.76	0.32	0.31	0.01	0.1	0.1	0.75	0.24	0.018	0.01	2.31	100.9
Bedded Chert	GB 1	94.51	0.95	0.78	0.02	0.3	0.7	0.48	0.6	0.086	0.02	2.37	100.8
	GB 3	89.39	2.15	1.51	0.05	1.19	0.65	0.95	1.86	0.157	0.02	3.05	101
	GB 2	93.87	0.71	0.44	0.01	0.26	0.51	0.61	0.38	0.048	0.03	2.46	99.33
	GB 8	96.43	0.24	0.47	0.01	0.05	0.27	0.37	0.15	0.047	0.01	1.57	99.61
	GB 12	93.89	1.04	0.72	0.02	0.43	0.25	0.74	0.56	0.065	0.01	2.67	100.4
	GB 13	96	0.7	0.59	0.01	0.22	0.25	0.64	0.41	0.05	0.01	2.05	100.9
	GB 32	97.58	0.17	0.19	0.01	0.04	0.19	0.52	0.15	0.018	0.01	1.8	100.7
	GB 36	97.07	0.2	0.48	0.01	0.03	0.14	0.29	0.13	0.014	0.01	1.45	99.81
Chert Dyke	GB 4.1	94.12	0.39	0.51	0.01	0.11	0.65	0.35	0.24	0.034	0.01	2.1	98.53
	GB 4.2	95.61	0.36	0.51	0.01	0.09	0.53	0.37	0.19	0.03	0.02	1.92	99.63
	GB 9.1	95.08	0.26	0.2	0.01	0.11	0.22	0.62	0.2	0.027	0.01	2.16	98.9
	GB 9.2	97	0.24	0.15	0.01	0.11	0.13	0.67	0.18	0.021	0.01	2.09	100.6
Pillow Chert	GB 16	96.34	0.44	0.71	0.02	0.09	0.63	0.3	0.23	0.034	0.07	2.1	100.9
	GB 14	95.19	0.43	0.37	0.02	0.16	0.69	0.35	0.29	0.036	0.02	2.47	100
	GB 15	97.22	0.21	0.19	0.03	0.07	0.27	0.32	0.15	0.021	0.02	1.91	100.4
	GB 19	96.98	0.12	0.77	0.01	0.03	0.44	0.34	0.11	0.011	0.01	2.01	100.8
	GB 20	81.52	2.62	1.5	0.05	0.46	4.83	1.35	0.97	0.111	0.05	7.48	100.9

Table 5.3 - Major Element Composition of Various Sediments

Analyte Symbol		SiO2	Al2O3	Fe2O3	MnO	MgO	CaO	Na2O	K2O	TiO2	P2O5	LOI	Total
Detection Limit		0.01	0.01	0.01	0.01	0.01	0.01	0.01	0.01	0.005	0.01		0.01
Analysis Method		FUS-ICP	FUS-ICP	FUS-ICP	FUS-ICP	FUS-ICP	FUS-ICP	FUS-ICP	FUS-ICP	FUS-ICP	FUS-ICP	FUS-ICP	FUS-ICP
Sample Types	Sample Name	%	%	%	%	%	%	%	%	%	%	%	%
High Magadi Beds Sediments	SE MAG 7	40.33	2.53	1.46	0.05	0.58	28.84	1.14	1.31	0.198	0.09	24.37	100.9
	SE MAG 8	58.78	10.46	5.82	0.19	1	2.47	5.79	4	0.675	0.09	9.09	98.35
	SE MAG 9	60.88	9.27	5.53	0.18	1.04	2.38	5.89	3.51	0.632	0.06	10.43	99.8
Green Beds Sediments	GB 21	56.43	12.87	6.9	0.25	0.56	2.19	5.15	4.02	0.626	0.07	10.14	99.19
	GB 22	52.53	9.38	6	0.25	4.72	3.83	4.47	5.52	0.486	0.1	11.62	98.9
	GB 23	54.55	11.49	6.66	0.15	1.62	2.67	5.26	5.62	0.26	0.05	11.03	99.36
	GB 24	49.76	8.65	6.05	0.2	4.57	7.21	4.34	5.42	0.473	0.15	12.01	98.84
	GB 26	49.27	8.98	6.71	0.18	4.86	3.07	4.16	4.99	0.471	0.08	15.11	97.9
	GB 27	47.89	9.72	5.99	0.16	3.21	4.32	4.64	4.33	0.488	0.07	17.06	97.86
	1.1	52.22	11.72	6.79	0.15	1.26	2	5.48	5.27	0.451	0.06	12.95	98.34
	1.2	52.92	11.89	9.82	0.11	0.89	0.21	5.51	4.98	0.478	0.03	13.51	100.3
	2.1	50.98	11.9	6.99	0.09	0.81	0.19	8.33	4.75	0.39	0.02	15.43	99.88
	2.2	51.89	10.7	5.94	0.18	2.65	2.2	5.9	4.98	0.459	0.04	15.89	100.8
	3	47.97	9.5	5.31	0.2	3.09	5.3	5.98	4.51	0.436	0.06	18.34	100.7
	4.1	49.03	9.58	5.49	0.16	2.67	6.25	4.56	4.63	0.437	0.07	16.27	99.16
	4.2	49.03	9.16	5.81	0.22	3.49	6.43	4.9	4.83	0.543	0.09	15.34	99.84
	5.1	58.41	13.13	3.27	0.06	0.53	0.96	5.65	4.82	0.16	0.03	12.53	99.54
	5.2	52.67	10.18	6.12	0.16	3.5	2.73	4.47	5.44	0.625	0.09	12.38	98.36
	5.3	88.14	1.03	0.86	0.03	0.41	0.98	2.32	0.56	0.066	0.01	5.4	99.81
	6	73.55	2.58	1.38	0.04	0.67	9.76	0.77	1.81	0.133	0.02	10.25	101
	7	70.84	4.28	2.61	0.07	1.2	4.42	3.53	2.99	0.262	0.04	9.5	99.74
	8	68.61	5.74	4.07	0.08	2.13	2.62	3.26	4.76	0.34	0.06	9.14	100.8
	9	66.69	4.98	3.89	0.1	1.84	3.69	2.9	3.94	0.303	0.03	10.6	98.95
Green Beds Oncoids	GB 28	75.75	3.98	2.4	0.06	1.19	2.31	2.93	2.89	0.23	0.02	7.67	99.43
	GB 18	30.51	0.08	0.1	0.09	0.45	37.28	0.23	0.06	0.01	0.04	30.34	99.19
Green Beds Calcrete	GB 30	74.22	0.11	0.51	0.01	0.16	16.89	0.53	0.12	0.011	0.16	6.22	98.93
	GB 31	81.92	4.91	2.25	0.07	0.86	2.3	2.26	1.91	0.272	0.09	4.01	100.8

Table 5.4 - Trace Element Composition of Magadiite

Analyte Symbol		La	Ce	Pr	Nd	Sm	Eu	Gd	Tb	Dy	Ho	Er	Tm	Yb	Lu
Detection Limit		**0.2**	**3**		**5**	**0.1**	**0.1**		**0.5**					**0.1**	**0.05**
Analysis Method		**INAA**	**INAA**		**INAA**	**INAA**	**INAA**		**INAA**					**INAA**	**INAA**
Sample Type	**Sample Name**	**ppm**	**ppm**		**ppm**	**ppm**	**ppm**		**ppm**					**ppm**	**ppm**
Magadiite	EL1	8.3	59		110	0.4	0.1		0.5					0.1	0.05
	EL 2	14.5	55		30	1.5	0.1		0.5					0.1	0.05
	SE Mag 1.1	6.1	30		5	0.5	0.1		0.5					0.1	0.08
	SE Mag 1.2	4.5	25		12	0.4	0.1		0.5					0.7	0.05
	SE Mag 2	13.5	54		12	1.1	0.1		0.5					0.5	0.11

Table 5.5 - Trace Element Composition of Various Chert Types

Analyte Symbol		La	Ce	Pr	Nd	Sm	Eu	Gd	Tb	Dy	Ho	Er	Tm	Yb	Lu
Detection Limit		**0.2**	**3**		**5**	**0.1**	**0.1**		**0.5**					**0.1**	**0.05**
Analysis Method		**INAA**	**INAA**		**INAA**	**INAA**	**INAA**		**INAA**					**INAA**	**INAA**
Sample Type	**Sample Name**	**ppm**	**ppm**		**ppm**	**ppm**	**ppm**		**ppm**					**ppm**	**ppm**
Magadi-Type Chert	NE 1	7.7	48		5	0.9	0.1		0.5					0.8	0.05
	NE 3	3.9	26		5	0.5	0.1		0.5					0.6	0.05
	EL 3	30.5	209		28	3	0.1		0.5					1	0.17
	CRUST CHERT	4.5	28		5	0.8	0.1		0.5					0.1	0.05
	GB 11	19.7	78		20	1.6	0.1		0.5					0.6	0.05
	GB 25	6.3	20		12	0.8	0.1		0.5					0.6	0.05
Bedded Cherts	GB 1	8.4	30		5	1	0.2		0.5					1.1	0.19
	GB 3	30.3	112		37	5.3	1.2		1.3					2	0.35
	GB 2	14	31		18	1.2	0.1		0.5					1	0.05
	GB 8	20.8	36		15	1.7	0.1		0.5					0.8	0.05
	GB 12	31.9	78		23	2.4	0.1		0.5					1.4	0.05
	GB 13	7.3	31		5	1.2	0.3		0.5					0.8	0.05
	GB 32	6.7	28		10	0.7	0.1		0.5					1.2	0.05
	GB 36	4.2	15		5	0.4	0.1		0.5					0.1	0.05
Chert Dyke	GB 4.1	6.9	46		5	0.9	0.1		0.5					0.8	0.05
	GB 9.1	9.4	14		14	0.6	0.1		0.5					0.1	0.05
	GB 4.2	6.2	35		11	0.8	0.1		0.5					0.8	0.05
	GB 9.2	9.3	35		5	0.4	0.1		0.5					0.9	0.05
Pillow Chert	GB 14	13.3	31		21	1.5	0.1		0.5					0.8	0.05
	GB 15	16.5	35		26	1.2	0.4		0.5					0.1	0.05
	GB 16	28	92		23	3.2	0.1		0.5					1.3	0.28
	GB 19	15.2	44		5	1.2	0.1		0.5					0.1	0.05
	GB 20	84.8	237		58	10.5	1.3		2.4					4.5	0.33

Table 5.6 - Trace Element Composition of Various Sediments

Analyte Symbol		La	Ce	Pr	Nd	Sm	Eu	Gd	Tb	Dy	Ho	Er	Tm	Yb	Lu
Detection Limit		**0.2**	**3**		**5**	**0.1**	**0.1**		**0.5**					**0.1**	**0.05**
Analysis Method		**INAA**	**INAA**		**INAA**	**INAA**	**INAA**		**INAA**					**INAA**	**INAA**
Sample Type	**Sample Name**	**ppm**	**ppm**		**ppm**	**ppm**	**ppm**		**ppm**					**ppm**	**ppm**
High Magadi Beds Sediments	SE Mag 7	109	291		62	12.3	2.1		0.5					5.3	0.61
	SE Mag 8	82.6	235		43	6.7	1		0.5					4.7	0.66
	SE Mag 9	131	214		79	15.7	1.6		3.5					7	0.98
Green Beds Sediments	GB 21	106	189		61	15.7	2.3		0.5					8.5	0.81
	GB 22	156	282		85	13.4	1.7		2.7					5.2	0.83
	GB 23	237	436		133	26.6	3.5		6.5					10.2	1.21
	GB 24	78.1	173		48	10.1	1.8		2.7					5.1	0.61
	GB 26	95.3	206		65	13.4	1.5		5.3					5.5	0.59
	GB 27	61.2	91		19	8.2	1.2		0.5					3.9	0.46
	1.1	23.3	33		5	1.9	0.3		0.5					1.9	0.25
	1.2	21.1	41		13	2.3	0.4		0.5					2.3	0.29
	2.1	67.9	91		16	6.6	1		0.5					3	0.21
	2.2	92.7	98		33	7.6	0.6		0.5					5.9	0.49
	3	140	183		67	13	1.3		3.2					6.6	0.54
	4.1	170	275		77	17.3	2.7		3.1					6.7	0.51
	4.2	98.8	212		71	12	1.7		3.6					3.5	0.21
	5.1	114	153		49	10.7	1.4		2.1					3.7	0.31
	5.2	45.1	97		28	4.5	0.6		1.3					1.6	0.17
	5.3	41.3	81		20	5.9	0.8		1.1					5.2	0.53
	6	54.3	104		32	7.2	0.9		2.5					4.9	0.54
	7	37	75		22	4.5	0.7		0.5					3.2	0.32
	8	50.9	97		37	7.2	1		2.1					4.6	0.43
	9	32.8	78		16	4.4	0.5		1					3.1	0.37
Green Beds Oncoids	GB 28	230	437		173	47.2	4.4		9.6					16.8	1.12
	GB 18	98.5	238		91	15	1.7		3.4					5	0.28
Green Beds Calcrete	GB 30	40	123		13	7.1	1.1		1.7					3	0.27
	GB 31	68.7	161		73	10.9	1		2.9					6	0.31

Table 5.7 - Multi-Element Composition of Magadiite

Analyte Symbol		Cs	Rb	Ba	U	Th	Ta	Nb	La	Pb	Nd	Hf	Zr	Sm	Ti	Y	Yb	Lu
Detection Limit		0.5	20	3	0.5	0.5	1		0.2	5	5	0.5	2	0.1	0.005	1	0.1	0.05
Analysis Method		INAA	INAA	INAA/ FUSICP	INAA	INAA	INAA		INAA	TD-ICP	INAA	INAA	FUS-ICP	INAA	FUS-ICP	FUS-ICP	INAA	INAA
Sample Type	Sample Name	ppm	ppm	ppm	ppm	ppm	ppm		ppm	ppm	ppm	ppm	ppm	ppm	%	ppm	ppm	ppm
Magadiite	EL 1	0.5	20	23	6.1	0.5	1		8.3	5	110	0.5	950	0.4	0.060	2	0.1	0.05
	EL 2	0.5	20	28	7	0.5	1		14.5	5	30	0.5	343	1.5	0.060	5	0.1	0.05
	SE Mag 1.1	0.5	20	15	5.9	1.4	1		6.1	5	5	0.5	2308	0.5	0.060	5	0.1	0.08
	SE Mag 1.2	0.5	20	9	11.1	0.5	1		4.5	5	12	0.5	1262	0.4	0.420	3	0.7	0.05
	SE Mag 2	0.5	20	29	0.5	0.8	1		13.5	5	12	1.5	569	1.1	0.300	4	0.5	0.11

Table 5.8 - Multi-Element Composition of Various Chert Types

Analyte Symbol		Cs	Rb	Ba	U	Th	Ta	Nb	La	Pb	Nd	Hf	Zr	Sm	Ti	Y	Yb	Lu
Detection Limit		0.5	20	3	0.5	0.5	1		0.2	5	5	0.5	2	0.1	0.005	1	0.1	0.05
Analysis Method		INAA	INAA	INAA/ FUSICP	INAA	INAA	INAA		INAA	TD-ICP	INAA	INAA	FUS-ICP	INAA	FUS-ICP	FUS-ICP	INAA	INAA
Sample Type	Sample Name	ppm	ppm	ppm	ppm	ppm	ppm		ppm	ppm	ppm	ppm	ppm	ppm	%	ppm	ppm	ppm
Magadi-Type Chert	NE 1	0.5	20	227	0.5	1.2	1		7.7	5	5	0.5	224	0.9	0.479	6	0.8	0.05
	NE 3	0.5	20	84	1.7	0.7	1		3.9	5	5	0.5	57	0.5	0.360	3	0.6	0.05
	EL 3	0.5	20	45	2.5	2.3	1		30.5	6	28	3.1	1245	3	0.599	11	1	0.17
	CRUST CHERT	0.5	20	56	0.5	0.5	5		4.5	5	5	0.5	344	0.8	0.060	5	0.1	0.05
	GB 11	0.5	20	85	4.5	1.5	1		19.7	5	20	0.5	333	1.6	0.360	9	0.6	0.05
	GB 25	0.5	20	23	2.8	0.5	5		6.3	5	12	15.2	919	0.8	0.360	3	0.6	0.05
Bedded Chert	GB 1	2.1	40	40	2.3	2	1		8.4	5	5	0.5	513	1	0.659	11	1.1	0.19
	GB 3	10.3	190	235	5.4	1.8	1		30.3	5	37	6.7	503	5.3	1.199	36	2	0.35
	GB 2	1.9	20	48	3.2	0.5	3		14	5	18	0.5	749	1.2	0.599	8	1	0.05
	GB 8	0.5	20	43	4.2	0.7	2		20.8	5	15	0.5	776	1.7	0.479	9	0.8	0.05
	GB 12	4.6	60	98	4.5	0.5	2		31.9	5	23	0.5	798	2.4	0.839	14	1.4	0.05
	GB 13	2.3	20	74	3.8	1.1	2		7.3	5	5	0.5	576	1.2	0.479	10	0.8	0.05
	GB 32	0.5	20	14	6.7	2.1	3		6.7	5	10	0.5	325	0.7	0.719	4	1.2	0.05
	GB 36	0.5	20	20	5.5	0.5	1		4.2	5	5	0.5	463	0.4	0.060	2	0.1	0.05
Chert Dyke	GB 4.1	1.1	20	38	3.3	0.8	1		6.9	5	5	0.5	642	0.9	0.479	8	0.8	0.05
	GB 9.1	0.8	20	24	3.3	0.5	4		9.4	5	14	0.5	830	0.6	0.060	4	0.1	0.05
	GB 4.2	0.5	20	33	2.9	0.7	1		6.2	5	11	0.5	747	0.8	0.479	6	0.8	0.05
	GB 9.2	0.5	20	23	3.2	0.9	1		9.3	5	5	0.5	813	0.4	0.539	3	0.9	0.05
Pillow Chert	GB 14	2.8	50	78	3.4	1.4	1		13.3	5	21	0.5	528	1.5	0.479	13	0.8	0.05
	GB 15	0.5	20	25	5.8	1.3	1		16.5	5	26	0.5	570	1.2	0.060	8	0.1	0.05
	GB 16	2.5	20	564	0.5	1.5	1		28	5	23	0.5	177	3.2	0.779	14	1.3	0.28
	GB 19	0.5	20	34	1	0.5	1		15.2	5	5	0.5	201	1.2	0.060	5	0.1	0.05
	GB 20	6.2	20	647	0.5	6.7	4		84.8	5	58	0.5	468	10.5	2.697	81	4.5	0.33

Table 5.9 - Multi-Element Composition of Various Sediments

Analyte Symbol		Cs	Rb	Ba	U	Th	Ta	Nb	La	Pb	Nd	Hf	Zr	Sm	Ti	Y	Yb	Lu
Detection Limit		0.5	20	3	0.5	0.5	1		0.2	5	5	0.5	2	0.1	0.005	1	0.1	0.05
Analysis Method		INAA	INAA	MULT INAA/ FUSICP	INAA	INAA	INAA		INAA	TD-ICP	INAA	INAA	FUS-ICP	INAA	FUS-ICP	FUS-ICP	INAA	INAA
Sample Type	Sample Name	ppm	ppm	ppm	ppm	ppm	ppm		ppm	ppm	ppm	ppm	ppm	ppm	%	ppm	ppm	ppm
High Magadi Beds Sediments	SE Mag 7	19.3	190	399	6.4	7.8	1		109	6	62	15.9	1828	12.3	3.18	54	5.3	0.61
	SE Mag 8	20.4	200	260	8	7	12		82.6	7	43	16	1978	6.7	2.82	41	4.7	0.66
	SE Mag 9	5.3	380	183	4.8	31	23		131	20	79	31.5	925	15.7	4.20	74	7	0.98
Green Beds Sediments	GB 21	13.7	440	525	21.6	6.7	11		106	5	61	16.3	545	15.7	5.09	107	8.5	0.81
	GB 22	29.2	730	513	23.3	6.9	12		156	5	85	15.5	600	13.4	3.12	74	5.2	0.83
	GB 23	14.5	600	845	34.6	13.5	1		237	5	133	15.4	537	26.6	6.11	155	10.2	1.21
	GB 24	14.4	590	372	10.8	6	1		78.1	16	48	16.9	519	10.1	3.06	73	5.1	0.61
	GB 26	15.2	570	425	5.3	5	9		95.3	16	65	16.7	418	13.4	3.30	81	5.5	0.59
	GB 27	13.8	420	196	3.9	5.1	17		61.2	16	19	28	809	8.2	2.34	54	3.9	0.46
	1.1	15.2	440	119	2.5	5.8	15		23.3	11	5	22.8	626	1.9	1.14	14	1.9	0.25
	1.2	19	510	124	0.5	2.9	10		21.1	19	13	19.7	547	2.3	1.38	15	2.3	0.29
	2.1	16.8	510	218	0.5	4.9	9		67.9	6	16	13.6	437	6.6	1.80	45	3	0.21
	2.2	17	570	189	3.2	8.6	7		92.7	6	33	11.5	354	7.6	3.54	96	5.9	0.49
	3	16.9	470	360	3	11.4	1		140	15	67	13.5	377	13	3.96	131	6.6	0.54
	4.1	17.5	470	546	4.3	8.2	10		170	5	77	14	438	17.3	4.02	135	6.7	0.51
	4.2	15.1	430	487	5.2	2.9	1		98.8	5	71	11.8	573	12	2.10	73	3.5	0.21
	5.1	20.7	470	400	3.6	5.2	1		114	7	49	16.2	476	10.7	2.22	68	3.7	0.31
	5.2	2.2	20	161	4	3.2	1		45.1	5	28	4.5	467	4.5	0.96	30	1.6	0.17
	5.3	4.3	110	129	2.4	8.4	1		41.3	5	20	5.2	398	5.9	3.12	61	5.2	0.53
	6	7.2	190	182	3.9	7.1	1		54.3	5	32	6.8	402	7.2	2.94	67	4.9	0.54
	7	13.7	370	160	6.1	4.5	5		37	5	22	7.9	497	4.5	1.92	48	3.2	0.32
	8	12	320	150	3.6	5.9	6		50.9	5	37	9.8	437	7.2	2.76	72	4.6	0.43
	9	6.9	180	125	4.1	6.1	4		32.8	5	16	6.9	398	4.4	1.86	36	3.1	0.37
Green Beds Oncoids	GB 28	0.5	20	1500	2.5	12.8	1		230	5	173	0.5	88	47.2	10.07	269	16.8	1.12
	GB 18	3.7	20	305	4.1	6.5	1		98.5	5	91	0.5	248	15	3.00	203	5	0.28
Green Beds Calcrete	GB 30	5.1	150	309	3.5	5.9	7		40	5	13	0.5	738	7.1	1.80	41	3	0.27
	GB 31	6.7	100	296	3.2	8.3	1		68.7	5	73	0.5	328	10.9	3.60	68	6	0.31

Table 5.10 - Transition Metal Composition for Magadiite

Analyte Symbol		Sc	Cu	V	Zn	Cr	Co	Ni	Mo	Ag	Sn	Sb
Detection Limit		0.1	1	5	1	1	1	1	2	0.5		0.2
Analysis Method		INAA	TD-ICP	FUS-ICP	TD-ICP	INAA	INAA	TD-ICP	TD-ICP	MULT INAA / TD-ICP		INAA
Sample Type	Sample Name	ppm	ppm	ppm	ppm	ppm	ppm	ppm	ppm	ppm		ppm
Magadiite	EL1	0.1	1	7	10	1	1	1	13	2.8		0.2
	EL2	0.1	1	9	8	1	1	1	16	0.5		0.2
	SE Mag 1.1	0.2	7	6	7	1	31	2	5	3		0.2
	SE Mag 1.1	0.1	6	8	6	1	13	1	3	2.8		0.2
	SE Mag 2	0.2	1	7	6	1	1	1	2	2.1		0.2

Table 5.11 - Transition Metal Composition for Various Chert Types

Analyte Symbol		Sc	Cu	V	Zn	Cr	Co	Ni	Mo	Ag	Sn	Sb
Detection Limit		0.1	1	5	1	1	1	1	2	0.5		0.2
Analysis Method		INAA	TD-ICP	FUS-ICP	TD-ICP	INAA	INAA	TD-ICP	TD-ICP	MULT INAA / TD-ICP		INAA
Sample Type	Sample Name	ppm	ppm	ppm	ppm	ppm	ppm	ppm	ppm	ppm		ppm
Magadi-Type Chert	NE 1	0.4	1	15	6	1	65	1	2	0.7		0.2
	NE 3	0.2	2	7	3	1	16	2	2	0.5		0.2
	EL 3	0.6	6	13	15	33	45	5	4	0.5		0.2
	CRUST CHERT	0.5	4	12	8	1	48	3	2	0.7		0.5
	GB11	0.2	6	13	11	1	76	3	2	0.7		0.2
	GB 25	0.3	4	16	6	1	62	1	6	2.6		0.2
Bedded Chert	GB1	0.6	13	21	21	9	27	2	2	0.7		0.2
	GB3	1.4	8	40	44	13	34	6	2	0.7		0.2
	GB2	0.5	5	14	15	1	120	2	2	1.9		0.2
	GB8	0.2	9	9	10	1	65	2	2	2.2		0.2
	GB12	0.7	8	18	21	1	161	3	3	2		0.3
	GB13	0.4	15	12	18	1	70	2	2	1.6		0.2
	GB 32	0.4	1	7	6	1	72	2	2	0.8		0.2
	GB 36	0.3	10	6	6	36	68	5	2	1.2		0.2
Chert Dyke	GB 4.1	0.3	11	10	14	1	76	3	2	1.7		0.2
	GB 9.1	0.3	1	8	7	1	143	1	2	3		0.2
	GB 4.2	0.3	13	10	13	1	125	4	2	2.3		0.2
	GB 9.1	0.4	3	8	6	1	184	2	2	2.8		0.2
Pillow Chert	GB 14	0.6	2	25	13	1	150	3	2	0.8		0.2
	GB 15	0.3	4	7	7	1	139	2	2	1.3		0.3
	GB 16	0.5	14	6	30	7	19	1	2	3.7		0.7
	GB 19	0.3	11	11	5	1	37	4	2	0.6		0.2
	GB 20	1.8	10	56	38	66	27	7	5	0.5		0.3

Table 5.12 - Transition Metal Composition for Various Sediments

Analyte Symbol		Sc	Cu	V	Zn	Cr	Co	Ni	Mo	Ag	Sn	Sb
Detection Limit		0.1	1	5	1	1	1	1	2	0.5		0.2
Analysis Method		INAA	TD-ICP	FUS-ICP	TD-ICP	INAA	INAA	TD-ICP	TD-ICP	MULT INAA / TD-ICP		INAA
Sample Type	Sample Name	ppm	ppm	ppm	ppm	ppm	ppm	ppm	ppm	ppm		ppm
High Magadi Beds	SE MAGADI 7	7.2	10	65	131	24	1	12	2	2.7		0.8
	SE MAGADI 8	7.3	11	92	127	35	1	10	3	4		1.1
	SE MAGADI 9	4.1	11	20	222	1	1	7	2	1.7		0.3
Green Beds Sediments	GB 21	3.8	11	262	160	41	1	13	2	1.2		0.2
	GB 22	1.9	10	88	177	1	1	8	3	1.3		1.6
	GB 23	4.3	12	239	144	64	1	8	2	1		0.6
	GB 24	3.9	64	360	133	19	1	12	104	0.9		1.5
	GB 26	3.9	33	313	153	1	1	16	92	0.8		2
	GB 27	3	12	115	242	1	4	8	44	2.1		1
	1-1	2.7	26	56	157	12	1	6	2	1.5		2.8
	1-2	2.2	17	61	260	1	1	8	2	1.6		3.2
	2-1	3.7	17	132	213	24	1	11	2	0.9		0.9
	2-2	3.1	26	137	201	32	1	11	2	0.9		0.9
	3	3.6	21	169	206	30	14	15	2	0.5		0.9
	4-1	4.1	20	132	146	25	7	11	2	0.5		1.1
	4-2	1.3	11	32	100	1	40	4	4	1.7		0.2
	5-1	4.6	20	126	142	25	1	11	2	0.6		1.1
	5-2	0.6	5	17	22	1	19	3	2	1.1		0.2
	5-3	1.1	3	28	34	1	7	3	2	0.5		0.2
	6	2	7	52	58	14	16	5	3	0.5		0.2
	7	2.8	14	85	80	21	7	6	2	0.5		0.9
	8	2.8	11	73	84	13	1	7	2	0.5		0.7
	9	2	13	50	58	14	5	5	2	0.5		0.5
Green Beds Oncoids	GB 28	0.6	2	13	4	1	28	2	2	0.5		0.2
	GB 18	0.4	4	12	5	1	16	3	2	0.5		0.2
Green Beds Calcrete	GB 30	2.3	12	31	45	17	17	6	2	0.5		0.6
	GB 31	2	7	23	32	1	14	5	2	0.5		0.2

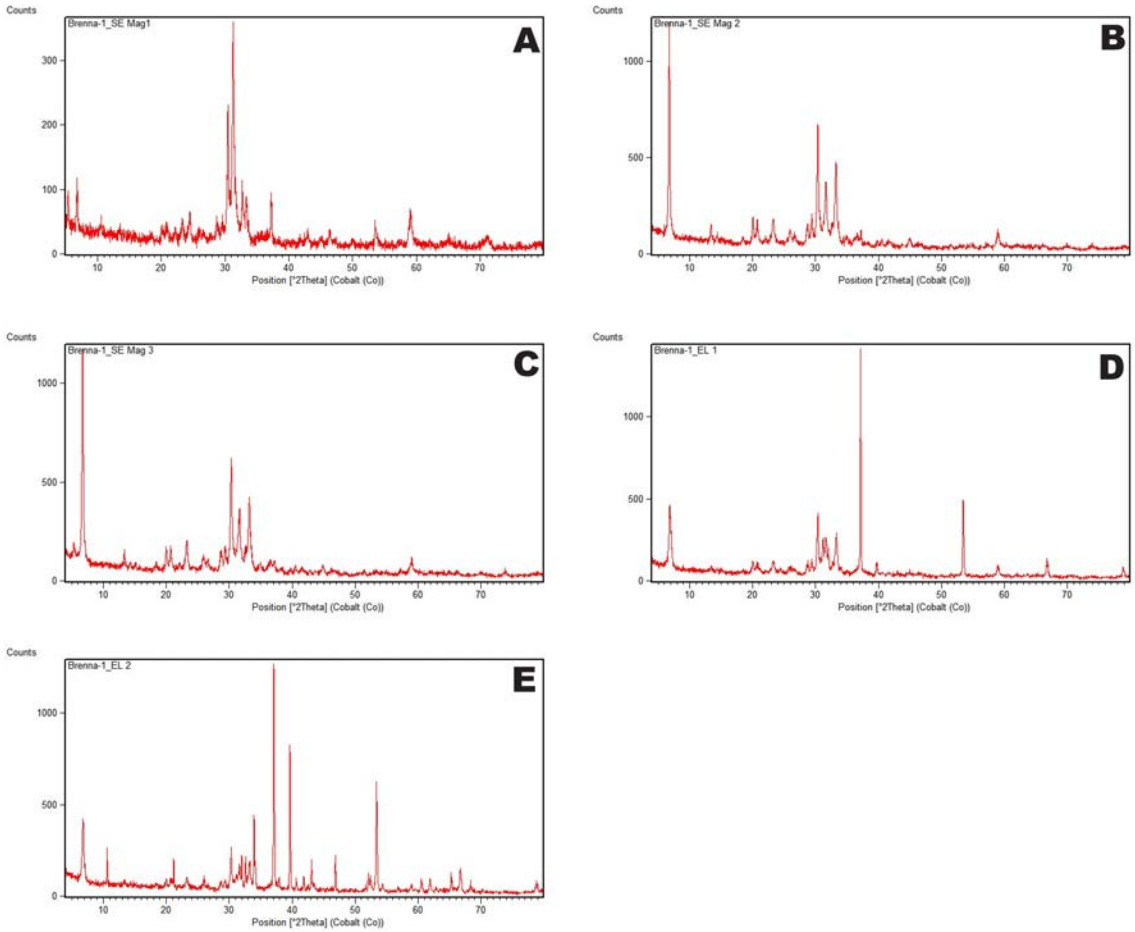

Figure 5.1 - XRD – Magadiite

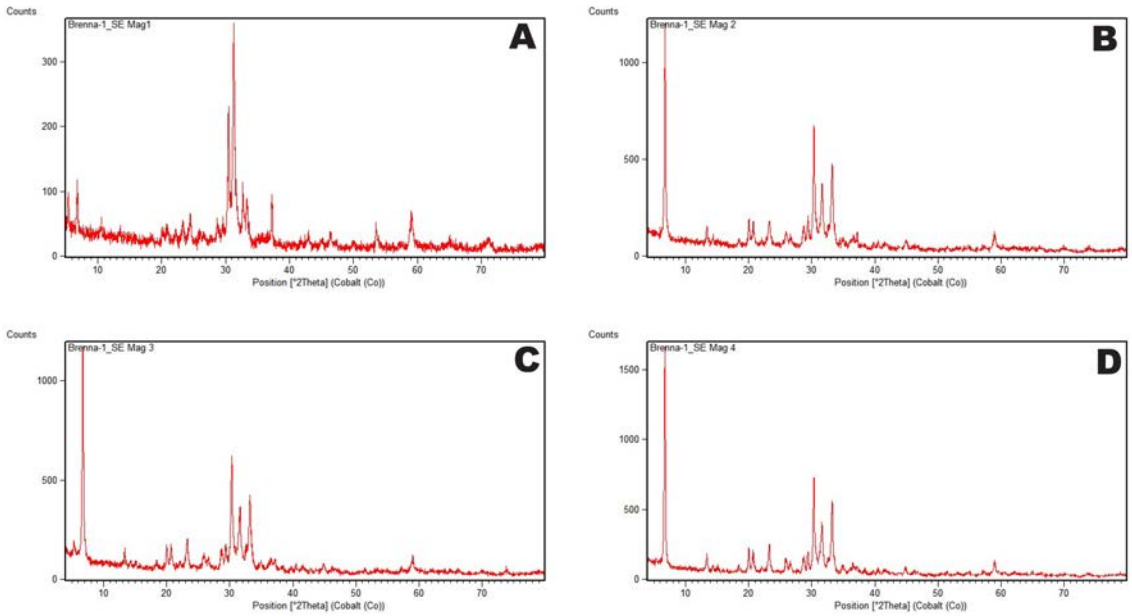

Figure 5.2 - XRD plots - Hardened magadiite samples

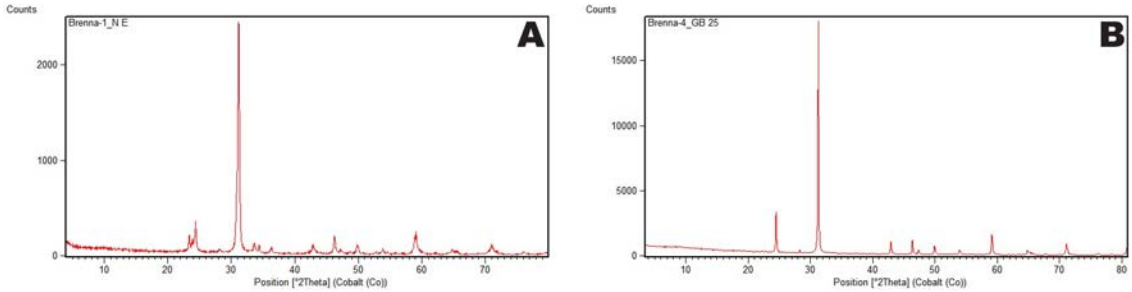

Figure 5.3 - XRD plots - Magadi-type chert samples

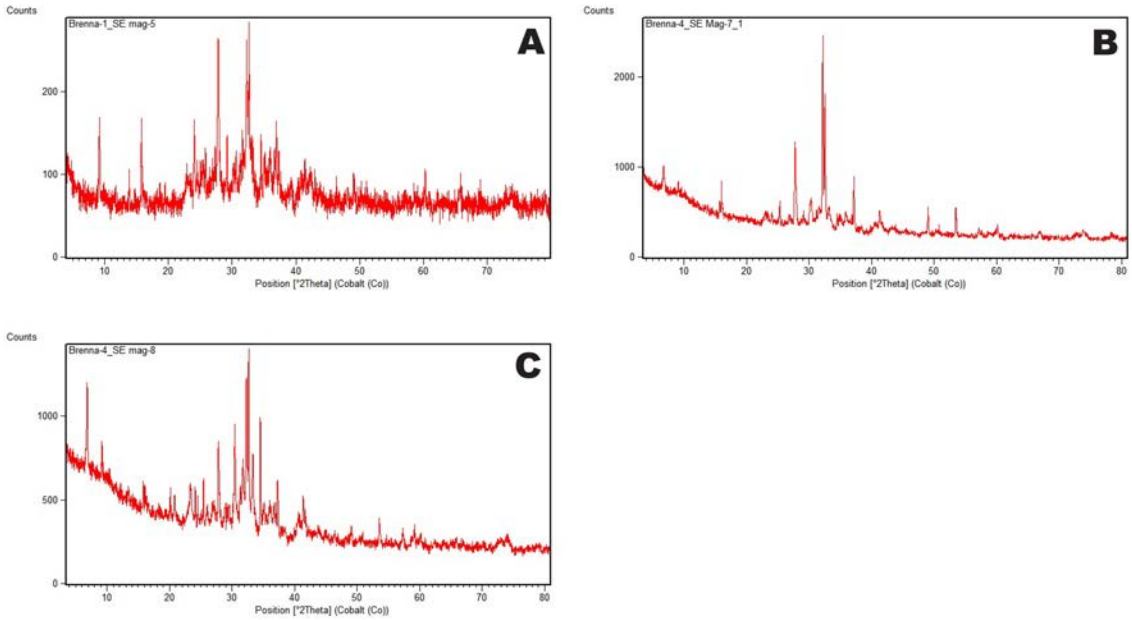

Figure 5.4 - XRD - HMB host sediments (tuffs)

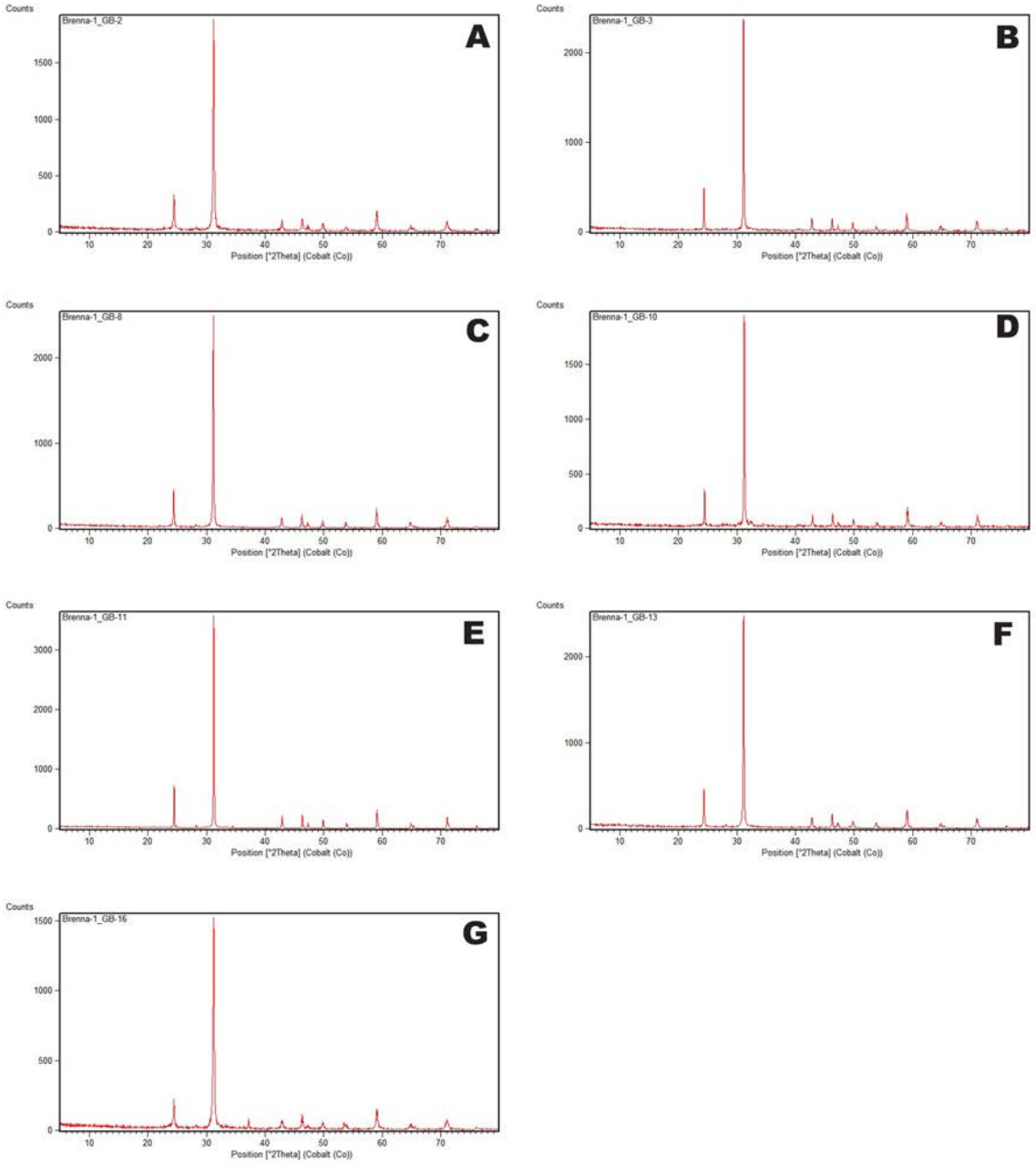

Figure 5.5 - XRD - Green Beds chert samples

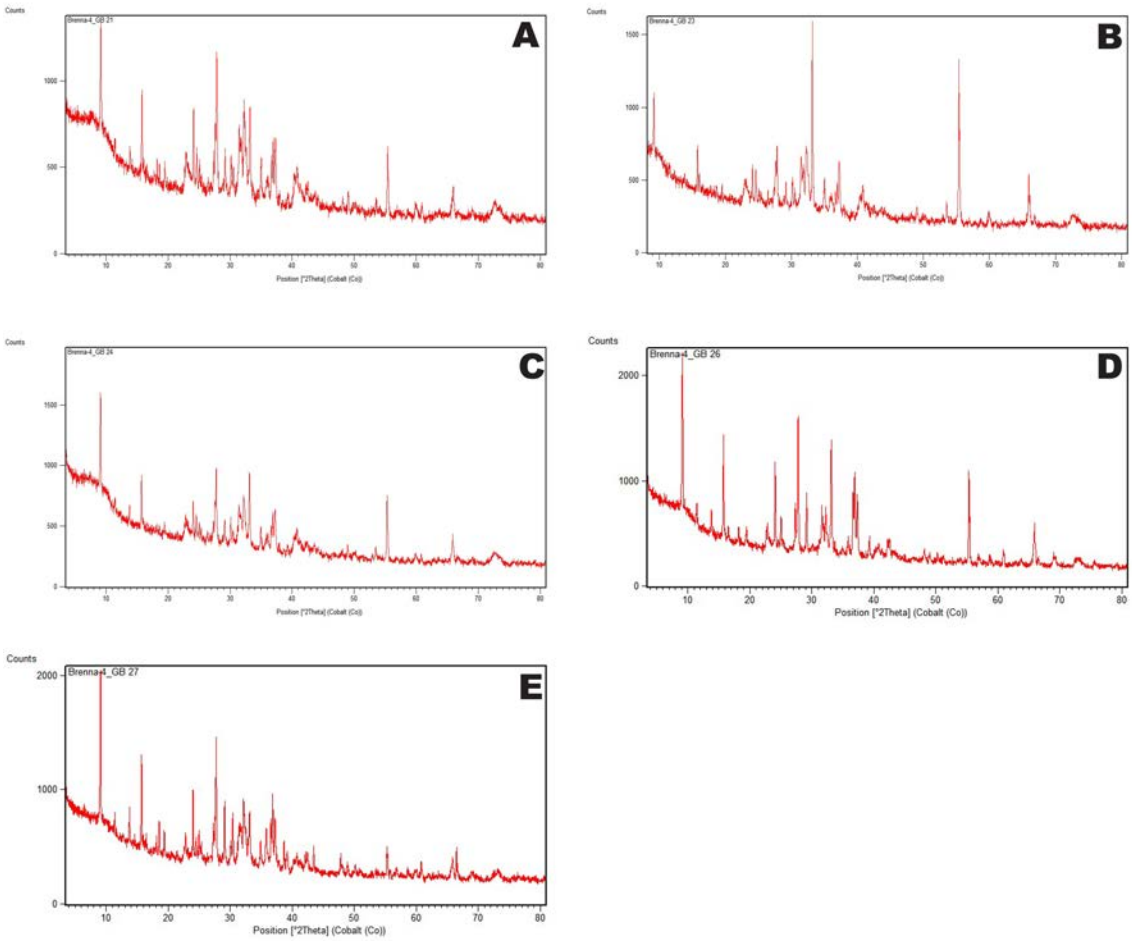

Figure 5.6 - XRD - Green Beds host sediments (tuffs and silts)

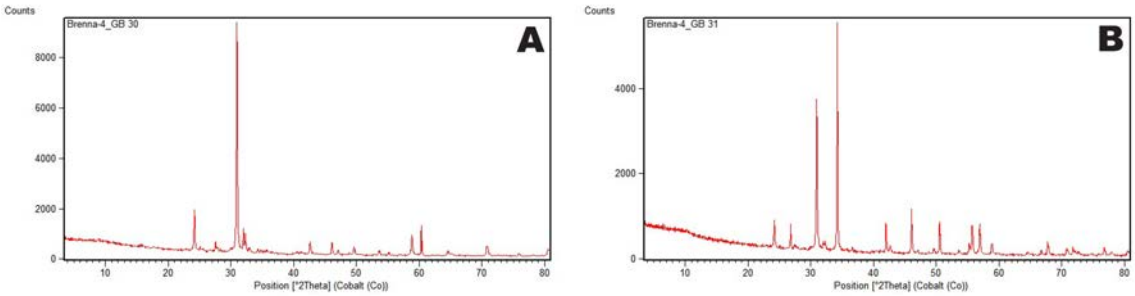

Figure 5.7 - XRD - Green Beds calcrete

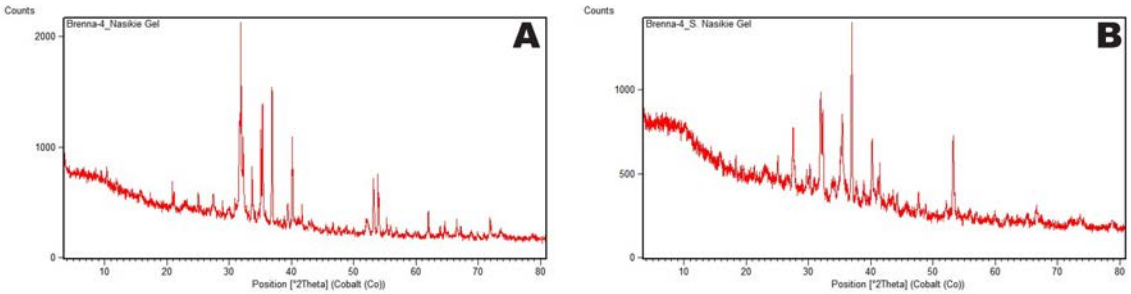

Figure 5.8 - XRD – Green Beds oncoids

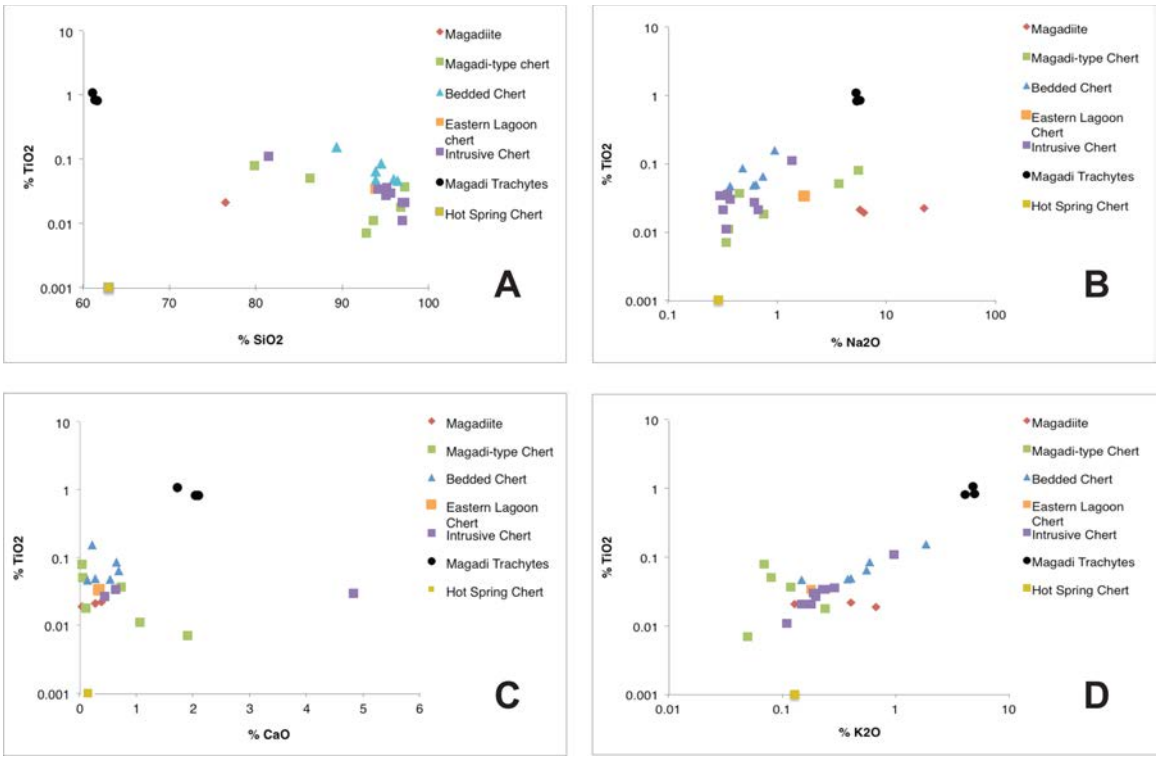

Figure 5.9 - Major elements – siliceous sediments

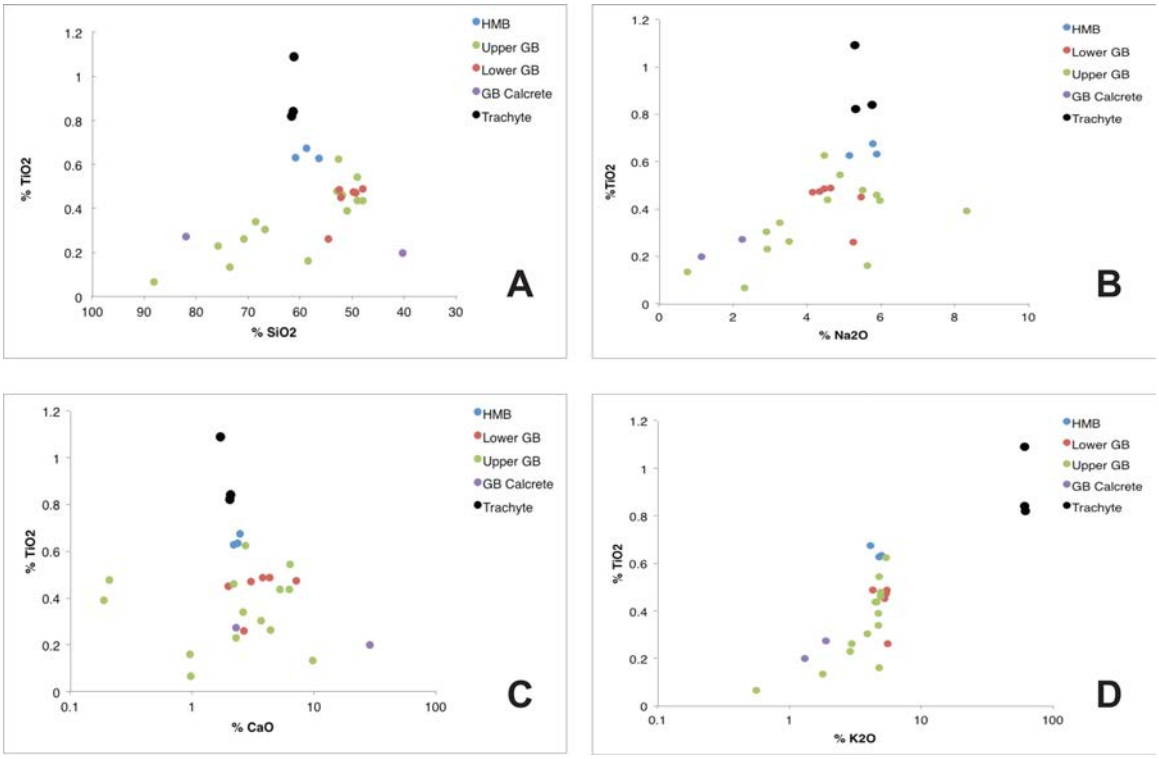

Figure 5.10 - Major elements – host sediments

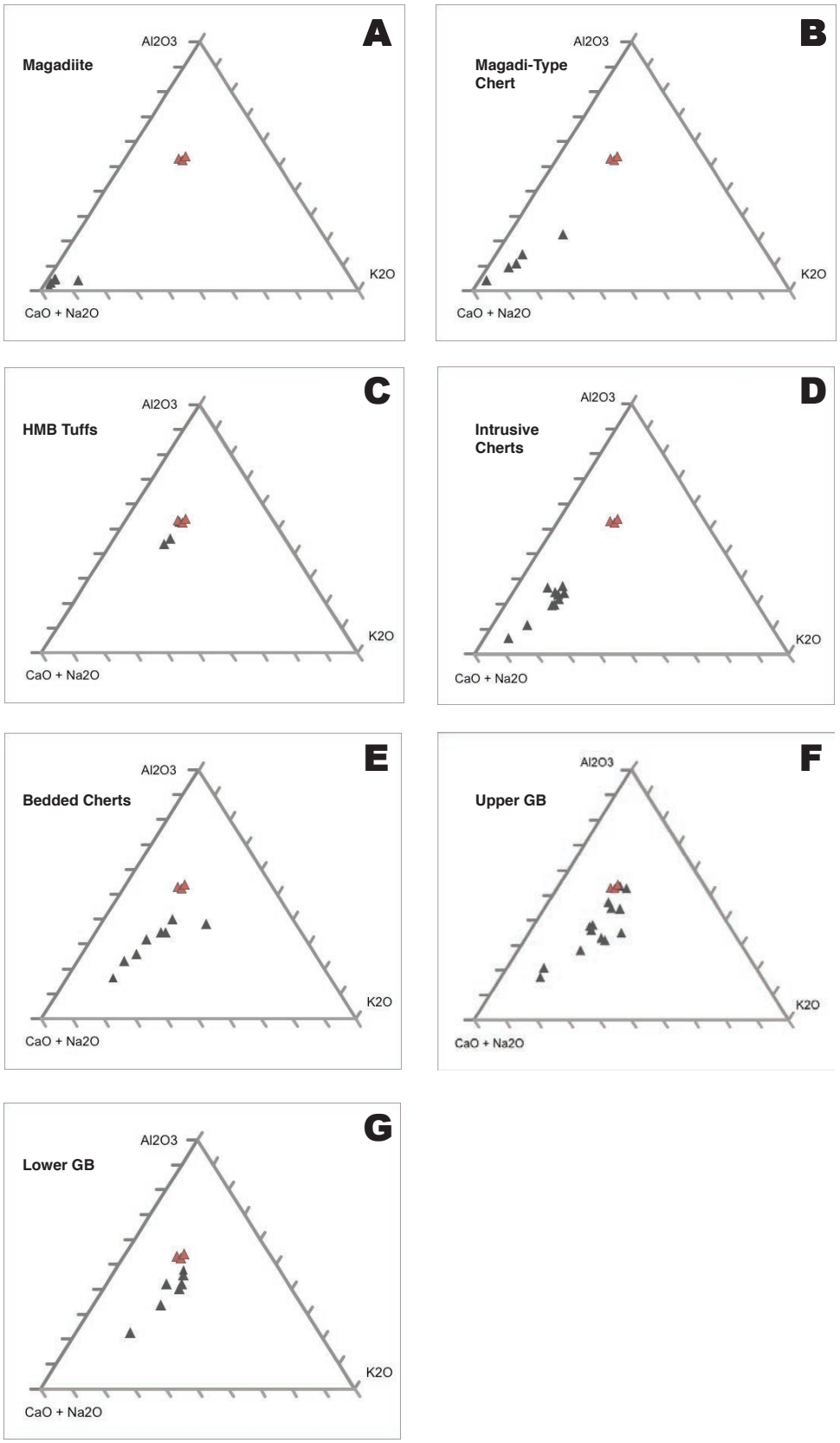

Figure 5.11 - A-CN-K diagram (Magadi Trachyte in red)

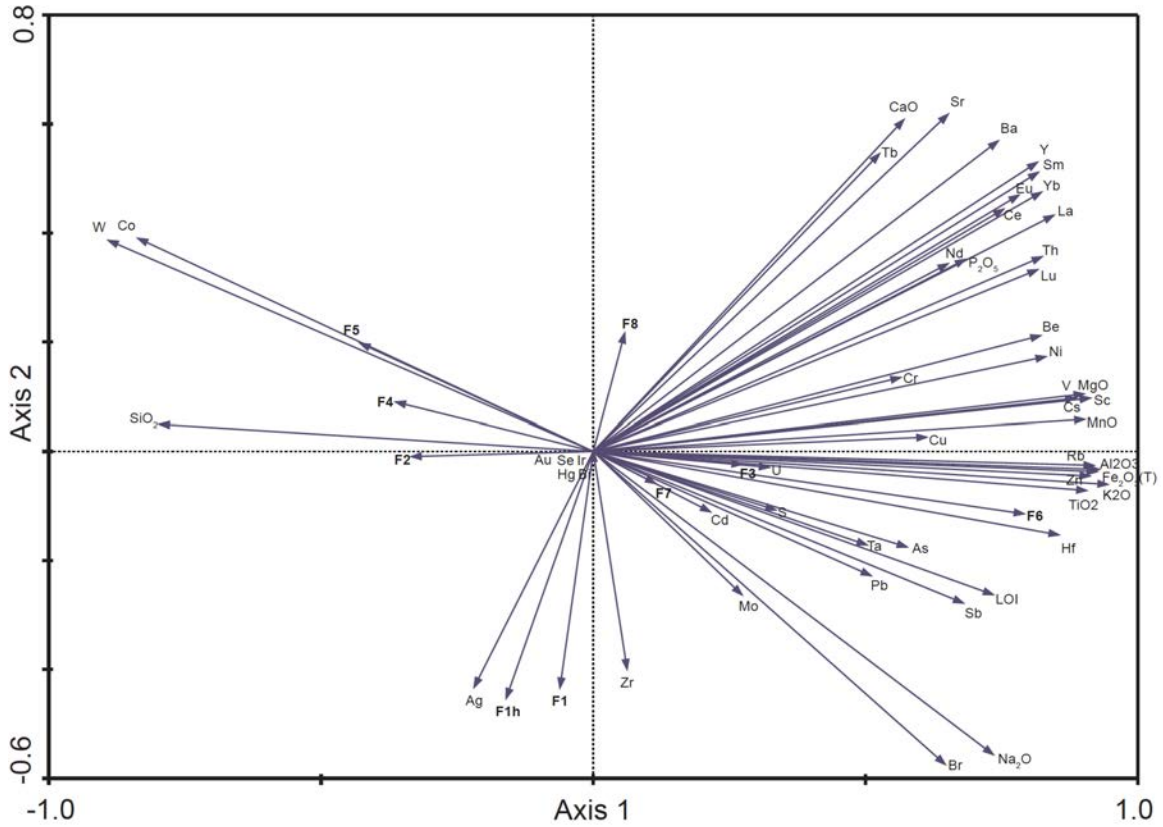

Figure 5.12 - Principle Component Analysis (PCA) plot

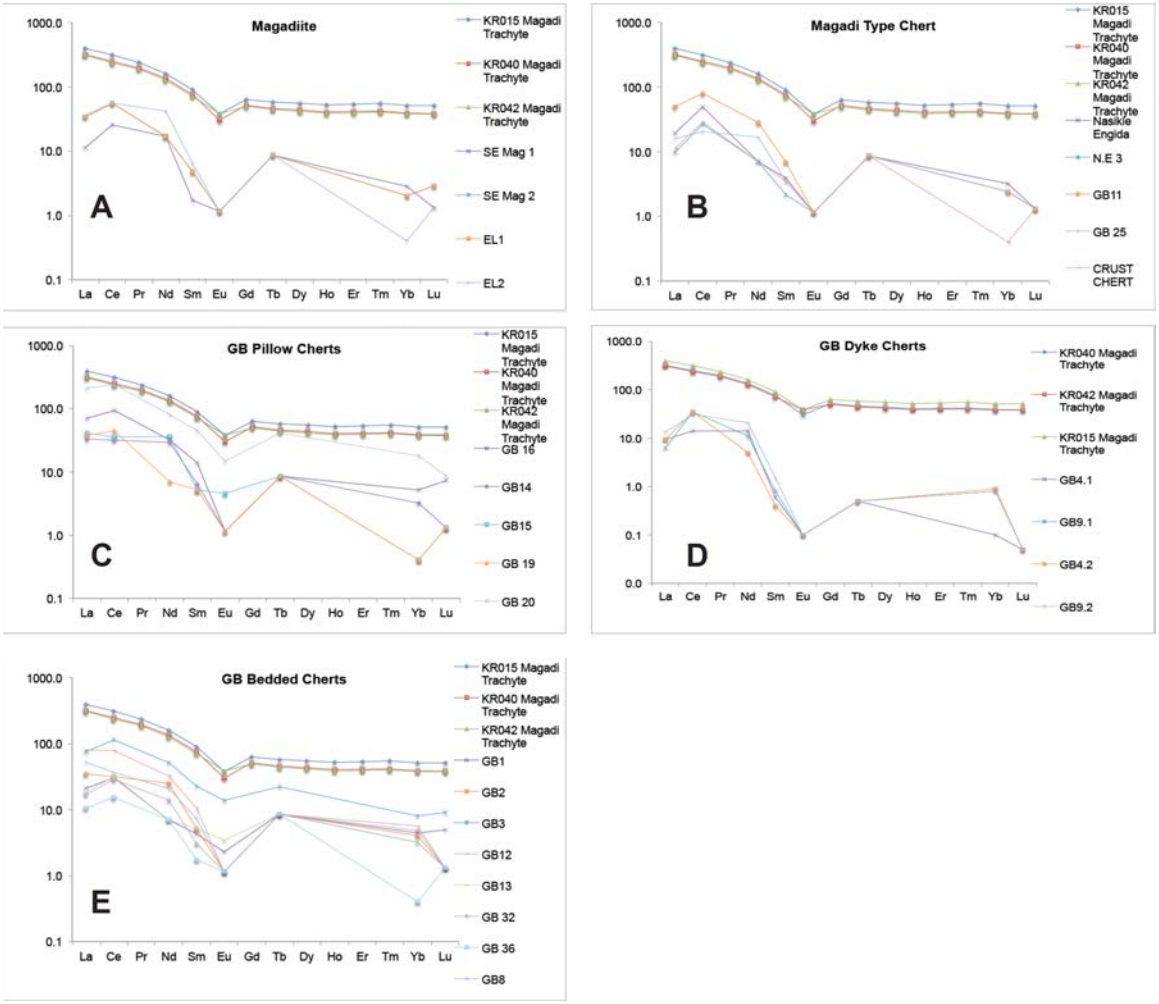

Figure 5.13 - Trace elements - siliceous sediments

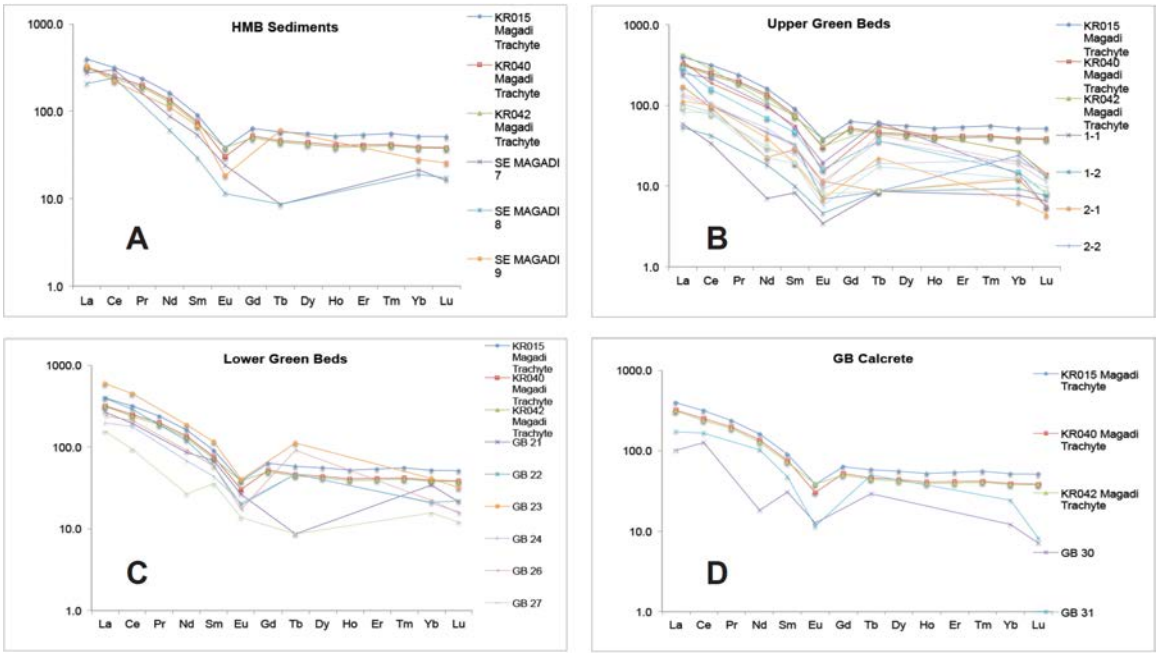

Figure 5.14 – Trace elements – host sediments

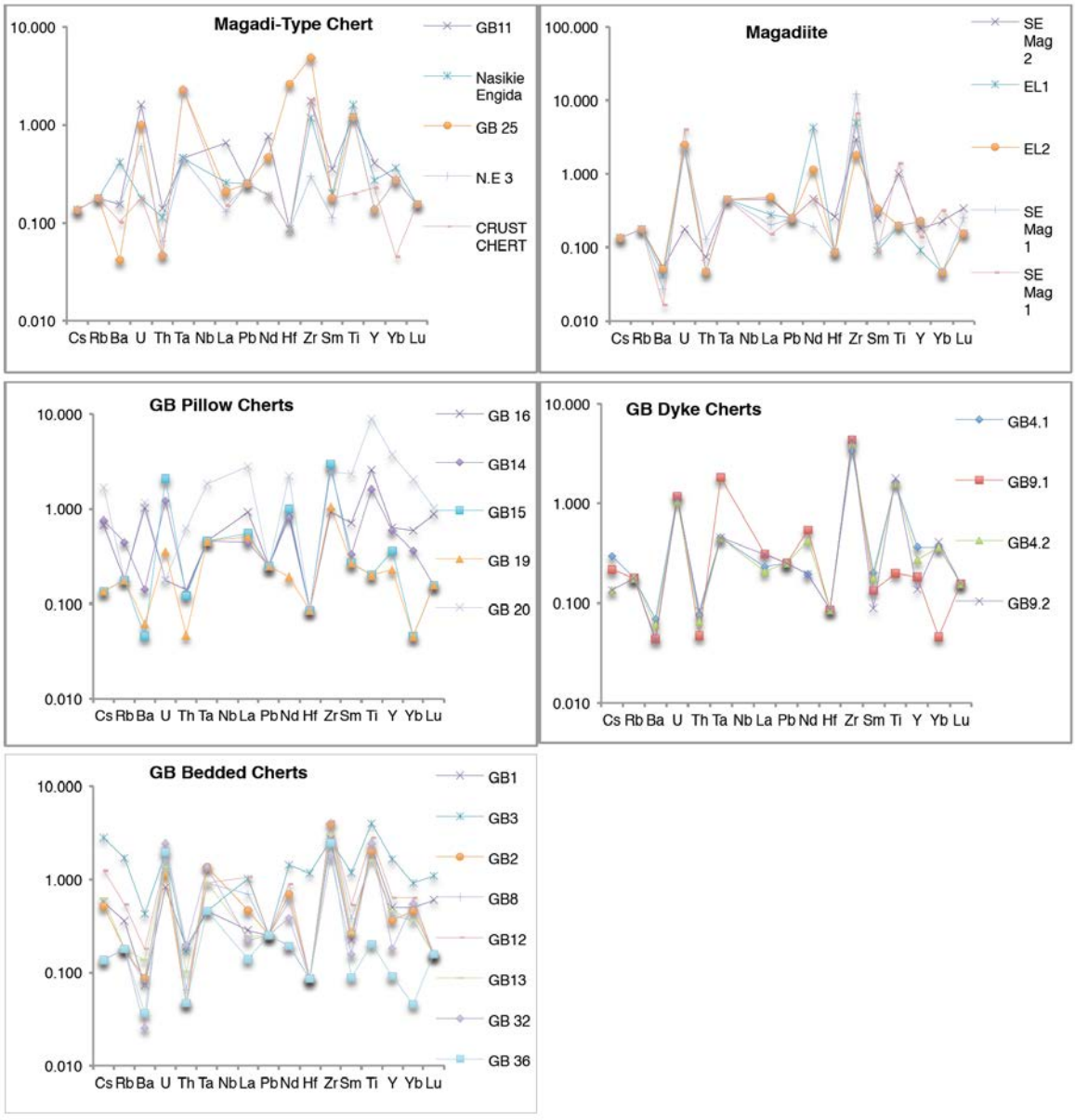

Figure 5.15 - Multi-element plots - siliceous sediments

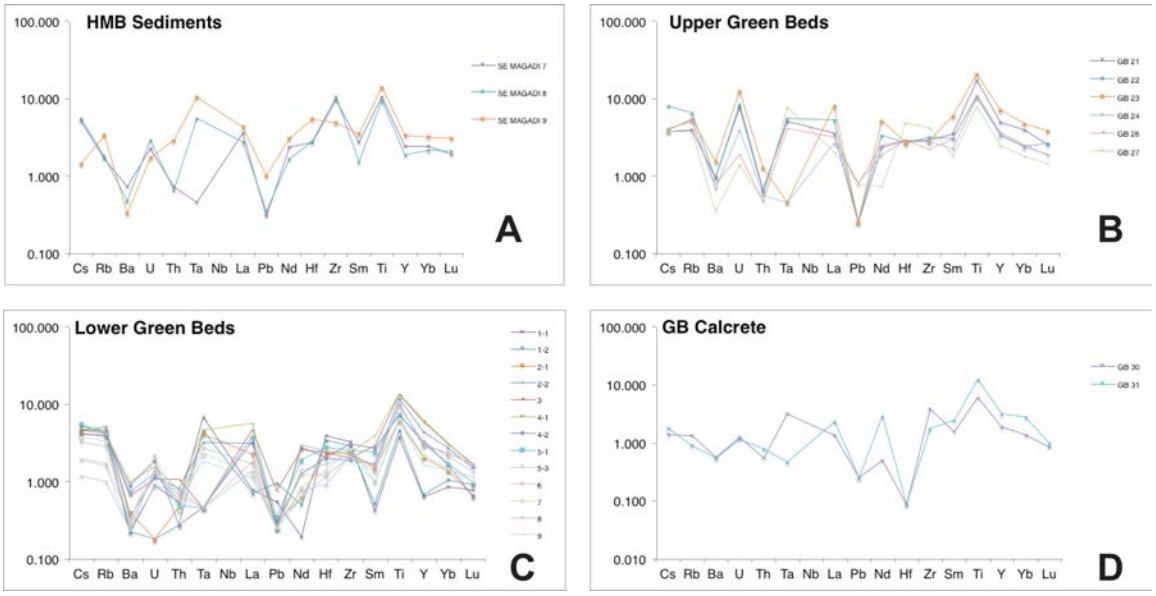

Figure 5.16 - Multi-element plots - host sediments

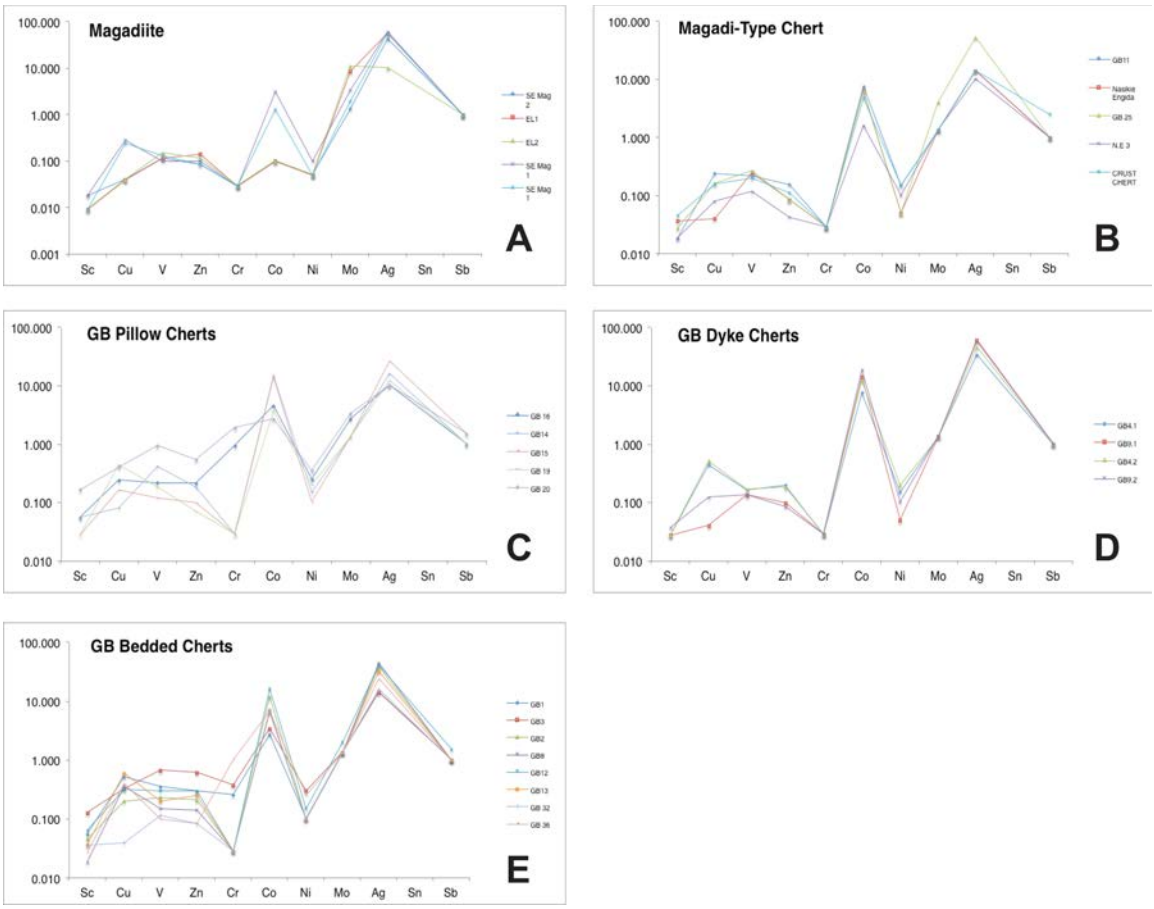

Figure 5.17 - Transition metals - siliceous sediments

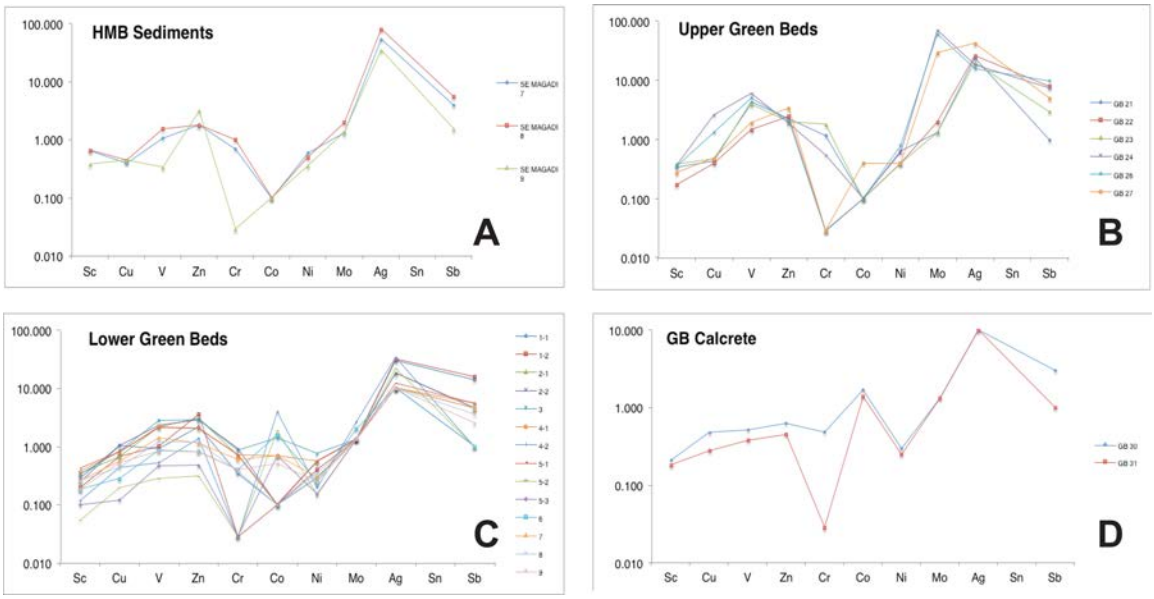

Figure 5.18 - Transition metals - host sediments